Investigating the Causes of the Lower Electroluminescence Stability of OLEDs with Solution-Coated versus Vacuum-Deposited Host:Guest Systems

by

Fatemeh Samaeifar

A thesis

presented to the University of Waterloo

in fulfillment of the

thesis requirement for the degree of

Doctor of Philosophy

in

Electrical and Computer Engineering (Nanotechnology)

Waterloo, Ontario, Canada, 2023

Examining Committee Membership

The following served on the Examining Committee for this thesis. The decision of the Examining Committee is by majority vote.

External Examiner   Jun Gao
Professor, Dept. of Physics, Engineering Physics & Astronomy,
Queen's University

Supervisor   Hany Aziz
Professor, Dept. of Electrical & Computer Engineering,
University of Waterloo

Internal Member   Bo Cui
Professor, Dept. of Electrical & Computer Engineering,
University of Waterloo

Internal Member   Mahla Poudineh
Assistant Professor, Dept. of Electrical & Computer Engineering,
University of Waterloo

Internal-external Member   Yuning Li
Professor, Dept. of Chemical Engineering,
University of Waterloo

Author's Declaration

I hereby declare that I am the sole author of this thesis. This is a true copy of the thesis, including any required final revisions, as accepted by my examiners.

I understand that my thesis may be made electronically available to the public.

Abstract

Organic light-emitting devices (OLEDs) are increasingly being used in commercial flat display products from mobile phones and smart watches to televisions. Although OLEDs have become a recognizable product to consumers only recently, their exceptional potential over competing display technologies – liquid crystal displays (LCDs) primarily – has been demonstrated for decades. While LCDs use backlighting, OLEDs are self-emissive, making it possible for each pixel to be turned on and off individually, resulting in lower power draw and deeper black levels. Perhaps one of the most unique properties of OLEDs arises from the low-temperature fabrication process as this allows for the use of flexible plastic substrates and thus inexpensive large scale processing. Further down the line, the possibility of fabrication of OLEDs via a solution-coating process presents an opportunity for lower cost applications, especially solid-state lighting products.

From a fabrication standpoint, OLEDs can be made via one of two approaches: vacuum-deposition or solution-coating. Vacuum-deposition is currently the main one used in the manufacturing of commercial OLED products since it allows for complicated multiple-layer devices and gives excellent device performance. However, this method has major drawbacks such as inefficient utilization of materials, high equipment cost, high vacuum requirements, and complicated color patterning processes. Solution-coating, in contrast, provides significant advantages in terms of material utilization and fabrication costs, especially for large-area products. It also allows using inkjet printing for color patterning, offering additional advantages in reducing fabrication costs. However, the EL stability of solution-coated (SOL) OLEDs continues to be significantly lower in comparison to their vacuum-deposited (VAC) counterparts. The short lifetime is currently the main obstacle preventing the commercialization of low-cost OLEDs via solution-coating.

While several studies have investigated degradation mechanisms in SOL OLEDs and identified excitons and polarons to be leading culprits, the root causes underlying the relatively faster degradation in these systems are still not clearly understood. Moreover, most of those investigations have focused on neat SOL layer systems comprised of only a single material, and host:guest (H:G) systems, typically used in the light-emitting layer (EML) of phosphorescent OLEDs, have not been adequately investigated. In addition, the studies have paid little attention to the role of guest molecules in the lower stability of SOL devices, focusing instead on the host materials. Moreover, it is necessary to find new

approaches to improve the stability of SOL OLEDs and surmount this long-standing challenge for SOL OLED technology. Therefore, the main focus of this work is to (i) understand the role of host-to-guest (H → G) energy transfer and guest materials in the lower stability of SOL versus VAC phosphorescent OLEDs, and (ii) explore approaches to increase SOL device stability. This study led to a number of new findings.

First, our studies indicated that the faster degradation of SOL EML devices relative to their VAC EML counterparts under electrical stress is due – at least in part – to the less efficient H → G energy transfer in these systems, which accelerates molecular aggregation in the EML. Interactions between excitons and polarons in the EMLs induce this aggregation phenomenon which occurs more strongly in the case of SOL EMLs compared to their VAC counterparts because of the higher host exciton concentration in the former as a result of the less efficient H → G energy transfer.

In addition, our results demonstrated that emitter guests aggregate as a result of electrical stress, giving rise to the emergence of new longer-wavelength bands in the EL spectra of devices after prolonged operation. However, the intensity of these aggregation emission bands is much stronger in the case of SOL H:G systems than their VAC counterparts, indicating that guest aggregation occurs much faster in the former. Results also showed that the differences in behavior arise from differences in the initial film morphologies, and are likely associated with the solvent used in the solution-coating process. Moreover, although excitons can drive this aggregation in the case of SOL EML devices, the coexistence of excitons and polarons accelerates this phenomenon significantly in these devices, possibly through exciton-polaron-induced aggregation (EPIA).

Next, a co-doped system was introduced as a novel approach for enhancing the lifetime of SOL phosphorescent OLEDs. The findings revealed that the intensity of guest aggregation emission bands is much stronger in devices with a single dopant compared to their co-doped counterparts, indicating a faster occurrence of guest aggregation in the former. Moreover, devices utilizing the co-doped system exhibit a 3× longer half-life (LT50) than devices with a single dopant.

Finally, the improvement of SOL OLED lifetime was presented using increasing the guest concentrations. To achieve this, thermally-activated delayed fluorescence (TADF) emitters, capable of being incorporated into the EML at a relatively high concentration, were doped into the host material at varying concentrations. The results showed that increasing guest concentration from 10 wt. % to 30 wt. % in H:G systems leads to a more efficient H → G energy transfer, resulting in a longer LT50.

Acknowledgements

The journey of completing my PhD has been profoundly rewarding, filled with exhilarating challenges at every turn. Although there were moments of frustration when it seemed that obstacles were insurmountable, in retrospect, those experiences have played a pivotal role in shaping my character, fostering patience, and refining my research skills. Throughout this entire endeavor, I have been fortunate to have Professor Hany Aziz as my supervisor, who has been more than I could have ever asked for. His guidance, compassion, invaluable knowledge, and profound insights have not only inspired me to become a better researcher but also a better individual.

I would like to acknowledge my advisory committee, Professor Bo Cui, Professor Mahla Poudineh, and Professor Yuning Li for reviewing my work and their valuable comments and suggestions. I would also like to thank Professor Jun Gao for accepting the role as my external PhD examiner.

I would like to thank Richard Barber and Czang-Ho Lee for their technical assistance and for making the Giga-to-Nano lab facilities a great working environment.

I would also like to thank my mom and dad; my siblings, Zahra and Mohammad Reza; and all the rest of my extended family and friends for their love and support. I would not have been able to do it without you all.

Last but not least, I want to express my heartfelt gratitude to Saeed Moghadam, my best friend, soul mate, and loving husband. His love and encouragement have been the driving force behind my accomplishments, and I am forever indebted to him for his unwavering support. Thank you, Saeed, for being my rock and my inspiration.

Table of Contents

List of Figures

List of Tables

Chapter 1 - Introduction

Organic light-emitting devices (OLEDs) are based on thin-film electroluminescent technology utilizing organic semiconductors. Light emission from organic semiconductors was first discovered in the 1960s, when electroluminescence was observed in large (3 mm thick) anthracene single crystals with liquid electrodes, however, these early devices required high driving voltages, exceeding 100 V [1]. Subsequently, electroluminescence from anthracene films (500-3000 nm thick) deposited by vacuum deposition and solid-state electrodes was achieved with a more reasonable driving voltage of 30 V [2]. Nonetheless, the most significant breakthrough occurred with the advent of the bilayer OLED in 1987 by Tang and Van Slyke, which exhibited a high brightness of 1000 cd m^{-2} at driving voltages < 10 V [3]. Since this breakthrough, OLED technology has attracted significant research interest and has emerged as a multi-billion dollar industry. OLEDs offer several advantages over their inorganic counterparts, including the potential for printable, large-area panels utilizing ultra-low cost roll-to-roll manufacturing on flexible substrates [4].

In this chapter, section 1.1 introduces OLED structure and explains the working principle of OLED. Section 1.2 discusses the electrical and physical properties of organic semiconductors to better understand and study OLEDs. Section 1.3 explains host-guest systems. Section 1.4 addresses OLED fabrication processes. Section 1.5 explains the performance metrics of OLEDs, and section 1.6 discusses the stability gap between solution-coated (SOL) and vacuum-deposited (VAC) OLEDs.

1.1 OLED structure and operation

The state-of-the-art OLED structure widely adopted today is a multi-layer structure, as shown in **Figure 1.1**. The substrate is used to support the device and can be made from a variety of different materials, including glass, paper, plastic, or metal foil. Two electrodes are conductive materials (metals, carbon nanotubes, etc.), and one of them must be transparent/semi-transparent, such as indium tin oxide

(ITO), to allow for light transmission. Electron/Hole injection layers (EIL/HIL) are buffer layers typically made of inorganic materials used to modify the work function of an electrode to enhance carrier injection into a device. To facilitate the transport of injected electrons and holes to the emissive layer (EML) in a balanced way, organic materials with good electron/hole transport properties are used as electron/hole transport layers (ETL/HTL) between a charge injection layer and the EML.

An EML usually consists of a guest:host (H:G) system in which guest molecules (or emitters) are sparsely dispersed (or doped) in a host matrix through a co-deposition process. The color of the light emission from an OLED is largely determined by the guest material, while the host material is primarily used to reduce aggregation between guest molecules and thus decrease fluorescence/phosphorescence quenching and improve device efficiency. The doping concentration of the guest materials in the system can vary from a low weight percentage of <1 wt. % to blends of guest and host materials (>20 wt. %) or even 100 wt. %, where the guest material is exclusively used as a neat-film EML.
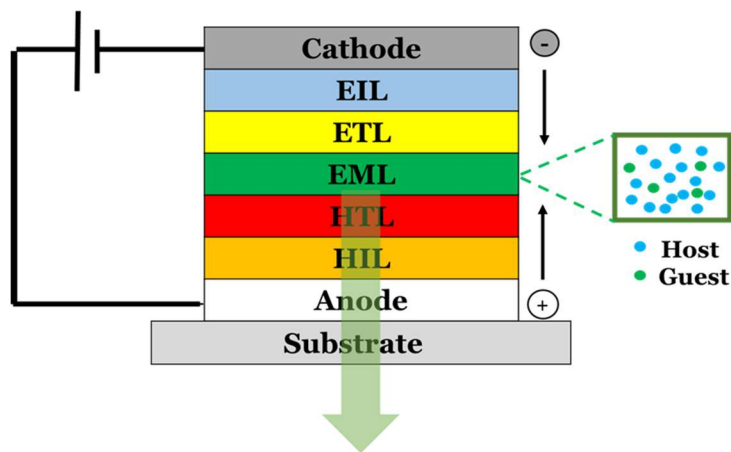
Figure 1.1. Multi-layer OLED structure

The operation principle of an OLED can be illustrated in a device as shown in **Figure 1.2**. The physical operation can be divided into four main steps: (1) A forward voltage bias is applied across the OLED, and electrons and holes are injected into the organic layers from the cathode and anode, respectively; (2) electrons and holes are transported in the organic layers via a "hopping" process between localized states and/or traps; (3) the electrons and holes meet and form electron-hole pairs bound by Coulomb interactions known as excitons; (4) the excitons decay to release energy in the form of light emission or heat.

2
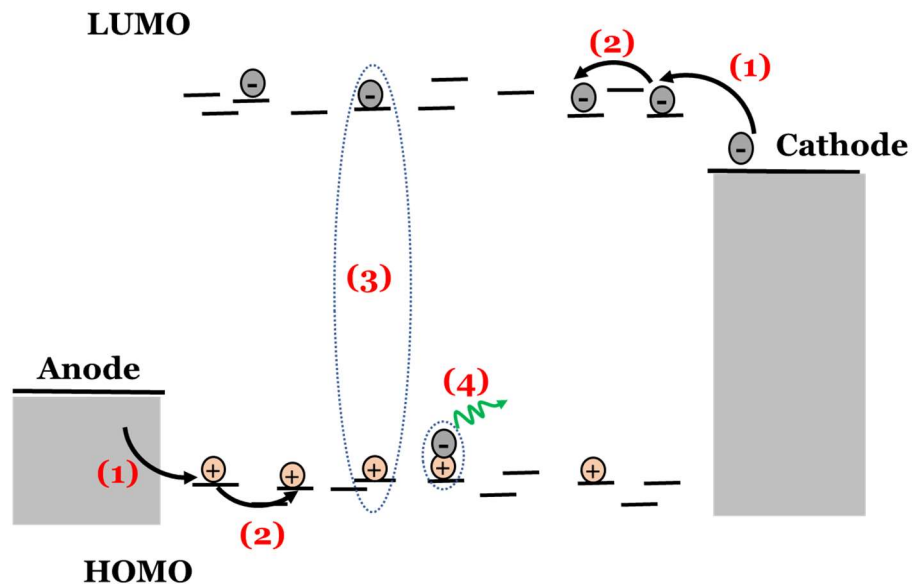
Figure 1.2. Working principle of an OLED: (1) charge injection, (2) charge transport, (3) exciton formation, (4) exciton decay

An OLED typically consists of multiple layers of organic materials, and the device performance is highly dependent on the energy-level alignment of highest occupied molecular orbital (HOMO)/ lowest unoccupied molecular orbital (LUMO) levels between two adjacent materials. **Figure 1.3** shows typical HOMO/LUMO levels of materials used in different layers of an OLED, which are measured from isolated materials.

The electrons and holes need to overcome energy barriers that exist in the multiple interfaces to enter the EML. To achieve highly-efficient devices, the energy difference between HOMO levels of the HIL, HTL, and EML should be small to allow for efficient hole injection into the EML. Similarly, the LUMO levels of the EIL, ETL, and EML need to align well for efficient electron injection into the EML. In the design of OLED architectures, these energy barriers at interfaces need to be well controlled by selecting appropriate materials so that the recombination zone can be positioned in the middle of the EML.
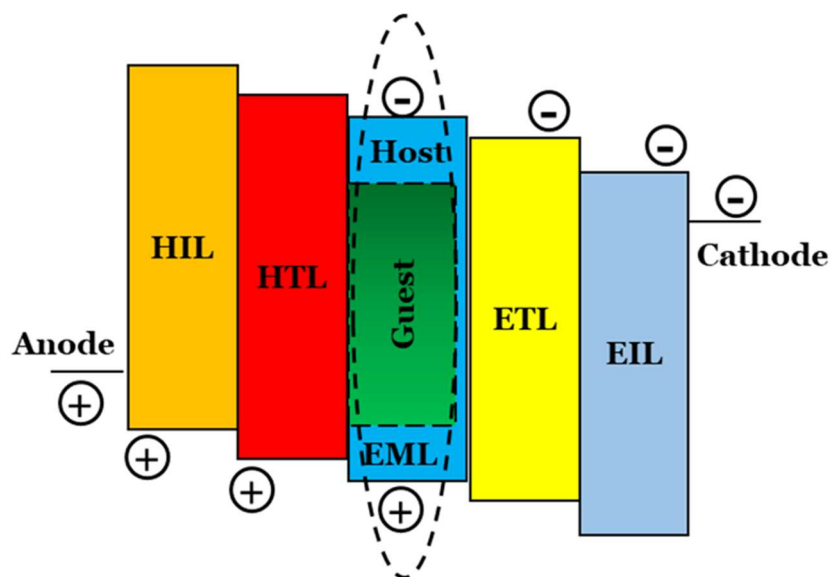
Figure 1.3. Energy level diagram of the materials used in an OLED stack. Relative energies are shown for individual materials, not considering interactions at interfaces between adjacent materials. The EML is a H:G system.

1.2 Fundamentals of organic semiconductors

Organic molecules are held together intra-molecularly by covalent bonds and inter-molecularly by transient dipole van der Waals forces [4]. However, in highly conjugated small molecules and polymers – ones with alternating single and double bonds – there is a notable delocalization of π orbital electrons. This delocalization arises from the overlap in the electron wave-functions [5].

In molecular bonding, the overlap between two atomic orbitals creates bonding (σ, π) and anti-bonding (σ^*, π^*) orbitals with lower energy and higher energy compared to the initial orbital energy, respectively. As the number of bonds increases, the number of orbital energy levels also increases, leading to sufficient energy splitting to be considered an approximation of the equivalent band structure in crystalline semiconductors in some respects.

In the context of organic semiconductors, the HOMO can be considered as the valence band equivalent, hosting the highest energy bound electrons. These electrons can be excited to the LUMO, which can be considered as the conduction band equivalent [5]. As conjugation increases in a molecule,

the number of both high and low energy orbitals increases, leading to a decrease in the effective band gap of the molecule, as seen in **Figure 1.4** [4].

The HOMO energy level can be measured by finding the ionization potential (IP) of electrons located in the HOMO. This measurement can be carried out using techniques such as photoelectron spectroscopy or electrochemical oxidation potentials [4]. Similarly, the energy levels of the LUMO can be determined by measuring the electron affinity (EA) of the material, which can be achieved through electrochemical reduction potentials [4]. A range of possible values can be calculated for these energy levels depending on the type of measurement chosen, which leads to the discrepancies in HOMOs and LUMOs reported in literature for the same molecule.
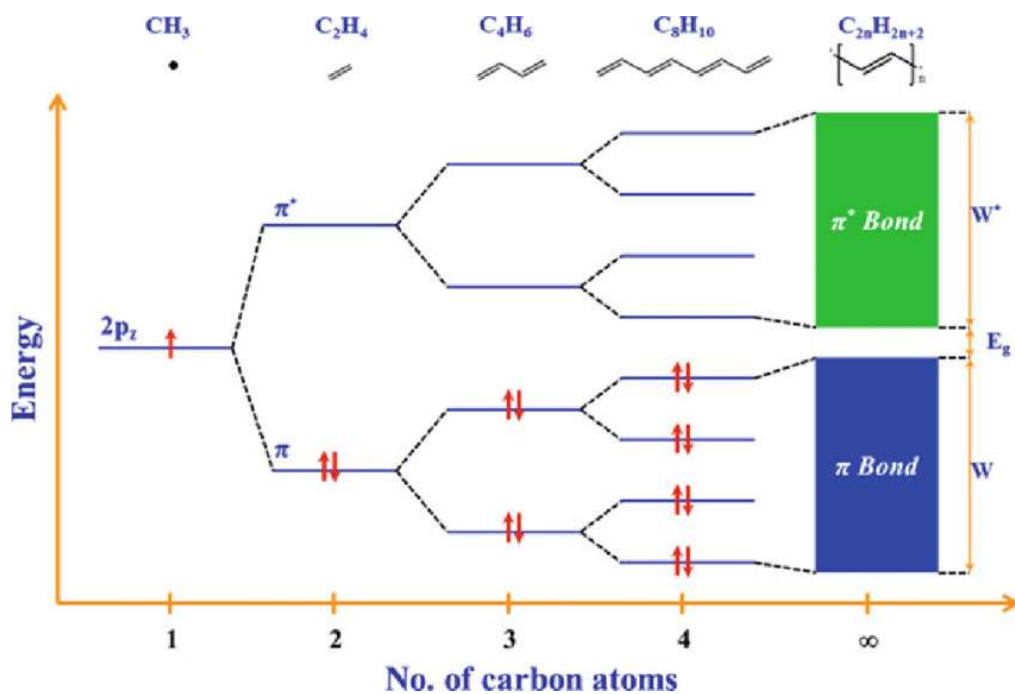
Figure 1.4. Energy band formation in conjugated molecules [6]

1.2.1 Electronic conduction in organic semiconductors

Due to the absence of continuous bands for the HOMO and LUMO and the prevalent amorphous nature of organic semiconducting thin films, the movement of charge carriers differs significantly from that observed in crystalline semiconductors. In band transport, the very small interatomic distances (<3Å) and strong molecular interactions between atoms form a continuous conduction and valance

band as illustrated in **Figure 1.5 (a)**. This allows charge carriers to move relatively freely between atoms, with electron (μ_e) and hole (μ_h) mobility values typically exceeding than 100 cm^2/Vs, primarily governed by various carrier scattering mechanisms.

In contrast, amorphous films exhibit molecular disorder, a range of intermolecular bond strengths, and limited wave-function overlap. Consequently, the density of states in these films follows a Gaussian distribution, leading to a hopping transport mechanism between molecules instead of band transport, as illustrated in **Figure 1.5 (b)** [5]. Here, hopping is essentially the tunneling of charge carriers between molecules with a Gaussian distribution of energy levels as described by the following Gaussian disorder model equation:

$$\mu(F,T) = \mu_\infty \exp\left[-\left(\frac{2\sigma}{3k_BT}\right)^2\right]\exp(\beta\sqrt{F}) \qquad (1.1)$$

$$\beta = C\left[\left(\frac{\sigma}{k_BT}\right)^2 - \Sigma^2\right] \qquad (1.2)$$

Where T is the absolute temperature, F is the electric field over the space of interest, k_B is the Boltzmann constant, μ_∞ is the high temperature limit of mobility, and the constant C is 2.9×10^{-4} $(\frac{cm}{V})^{1/2}$ [9]. The material dependent variables in the equation are the positional disorder (Σ) of the molecules in the amorphous thin film and the disorder in energy levels (σ), which can be rationalized as the width of the Gaussian distribution of states. The hopping transport mechanism is inherently much slower than band transport, with typical good amorphous materials exhibiting carrier transport values on the order of 10^{-3} cm^2/Vs [5].
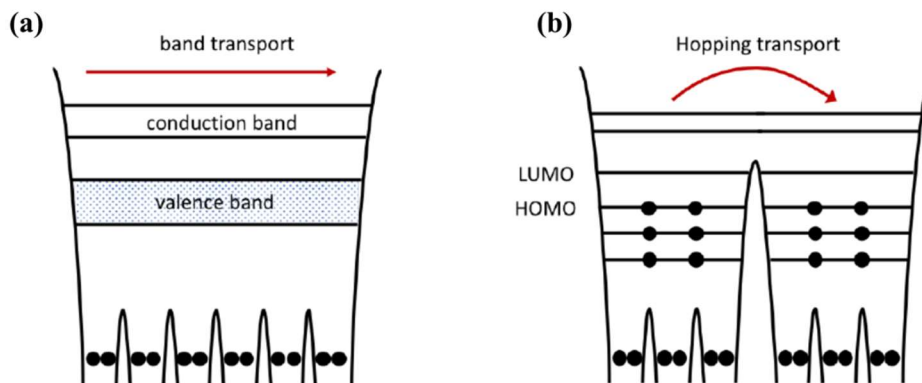
Figure 1.5. Electronic structure for (a) inorganic semiconductors and (b) organic semiconductors. Band transport occurs within the continuous conduction band (CB) in (a), whereas hopping transport occurs between two adjacent molecules in (b).

1.2.2 Excited states in organic semiconductors

Excitons can be formed in organic materials through photoexcitation or electrical excitation. In optical excitation, the absorption of light promotes an electron from the HOMO to the LUMO, thus creating an exciton. In electrical excitation, an electron is injected from the cathode into the LUMO, while another electron is extracted from the HOMO by the anode, resulting in the creation of a hole. These charges then undergo hopping within the organic solid until they become bound by Coulomb interaction and form an exciton.

In quantum mechanics, an electron possesses a spin of either S= 1/2 or S= -1/2, represented by the symbols of ↑ and ↓, respectively. In a two-electron system, there are four eigenstates, and the spin wavefunction of each eigenstate can be expressed as a function of the one-electron spin state:

$$|S = 0\rangle = \frac{1}{\sqrt{2}}\{|\uparrow\downarrow\rangle - |\downarrow\uparrow\rangle\}$$

$$|S = 1\rangle = |\uparrow\uparrow\rangle$$

$$|S = -1\rangle = |\downarrow\downarrow\rangle$$

$$|S = 1\rangle = \frac{1}{\sqrt{2}}\{|\uparrow\downarrow\rangle + |\downarrow\uparrow\rangle\}$$

In these four states, the total spin of the system, S, can be either 0 or 1. The spin wavefunction with S = 0 is referred to as a singlet excited state of the system, while the other three spin wavefunctions with S = 1 are referred to as triplet excited states due to the triple degeneracy of S. Unlike photoexcitation, which preserves spin and only generates singlet excitons, electrical excitation of organic semiconductors creates both singlet and triplet excited states, with a statistically ratio of 1:3.

The ground state is a singlet state and is commonly denoted as S_0. The first excited singlet state above S_0 is denoted as S_1, while the first triplet state above S_0 is denoted as T_1. According to selection rules, transitions are allowed from singlet to singlet states or from triplet to triplet states, while transitions from a singlet state to a triplet state are forbidden. However, an increased contribution from the opposite state results in a mixture of states, allowing for permissible singlet $\rightarrow$ triplet transitions. There are two ways to achieve this: by increasing the spin-orbit coupling integral or by reducing the energy gap between singlet and triplet states. PHOLED emitters containing heavy metals take advantage of the increased spin-orbit coupling integral, as it depends on Z^4 [7].

On the other hand, thermally activated delayed fluorescence (TADF) OLEDs are completely organic but capable of singlet $\rightarrow$ triplet transitions by minimizing the disparity in state energies. According to Hund's rule, the triplet state typically possesses lower energy than the singlet state. However, it is possible to manipulate the molecular structure of organic materials to separate the electron density wave-functions of the HOMO and LUMO. This separation results in a smaller gap between singlet and triplet energy states. The original energy gap, which would typically be around $0.5-1.0$ eV, is now reduced to approximately $0.1 eV$ or less, which can be overcome by the thermal energy of the electron [8].

The Jablonski diagram in **Figure 1.6** shows how the energy of an excited state will change for a given process. Radiative transitions, represented by straight lines in Jablonski diagrams, involve fluorescence ($S_1 \rightarrow S_0$ transition), which occurs rapidly with a rate constant $k_f \sim 10^6 - 10^9$ s^{-1}, and phosphorescence ($T_1 \rightarrow S_0$ transition), which is significantly slower with a rate constant $k_p \sim 10^{-2} - 10^4$ s^{-1} due to its forbidden nature, and likewise for delayed fluorescence.

On the other hand, radiationless transitions, indicated by wavy lines in Jablonski diagrams, occur between electronic states with degenerate energy levels, where energy is not dissipated through photon emission. Internal conversion refers to a non-radiative transition between states with the same spin, while intersystem crossing describes a radiationless transition between states with opposite spins. After

undergoing a transition, an electron is likely not be in the ground state and will release any excess energy through vibrational relaxation. Quenching is a detrimental process that competes with radiative transitions and can be triggered by various sources, typically impurities. This process invariably results in the loss of energy from the excited state through non-radiative dissipation [7].
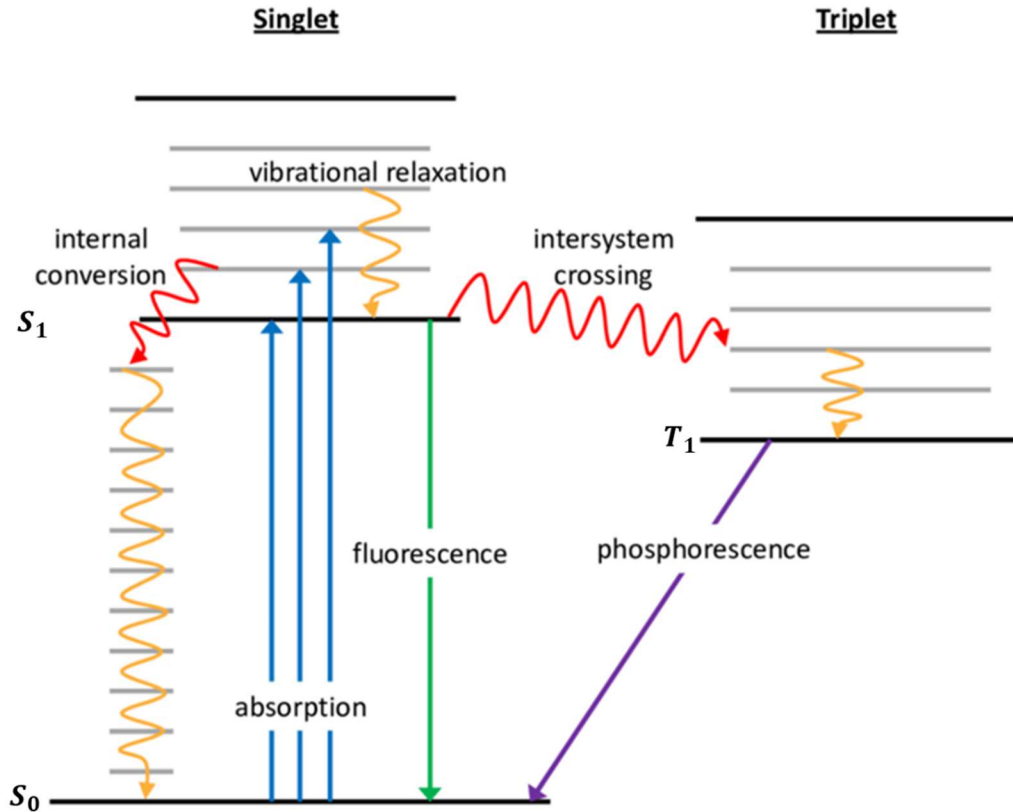
Figure 1.6. A Jablonski diagram illustrating the mechanism of the dissipative pathways. Wavy lines indicate non-radiative transitions whereas straight lines indicate transitions that either absorb or emit a photon. S_0 = ground state singlet, S_1 = excited state singlet, T_1 = excited state triplet, T_2 = second lowest energy excited state triplet [9].

1.3 Emitter generations

As mentioned, the ratio of generated singlet excitons to triplet excitons in OLED devices is typically around 25% to 75%. To achieve satisfying device performance with high EQEs, it is crucial to focus

on the development and design of light-emitting materials that can effectively harvest both singlet and triplet excitons.

OLED devices have evolved through three generations of emitter materials, each employing different mechanisms of light emission. These generations include fluorescence (first generation), phosphorescence (second generation), and TADF (third generation) [10]. In the following section, a detailed description of each of these generations and their respective contributions to OLED technology is provided.

1.3.1 Fluorescent emitters

In the early development of OLEDs, conventional fluorescent emitters were used in EMLs. To reduce fluorescence quenching, the EML is designed as a host-guest system, where the emitters are sparsely doped (1 to 5 wt. %) in a host matrix. The exciton energy transfer mechanism in the host-guest system is shown in **Figure 1.7**. Under electrical excitation, excitons are first formed on host materials with a singlet-to-triplet ratio of 1:3. Through Förster and Dexter energy transfer processes, these excitons are then transferred to the singlet and triplet excited states of guest molecules, respectively. On the guest molecule, singlet excitons at S_1 decay rapidly from S_1 to S_0 and emit fluorescence; while triplet excitons at T_1 can only decay non-radiatively to S_0 due to a forbidden transition, which results in a 75% emission loss in the EML. The lifetime of fluorescence excitons is in the range of nanoseconds [11].

Using these emitters, an OLED can achieve a maximum internal quantum efficiency (IQE) of 25%, which leads to a maximum external quantum efficiency (EQE) of ~5% considering a typical light out-coupling efficiency of ~20%. Despite low EQEs, the device stability and lifetime of these OLEDs are superior to that of phosphorescent- and TADF- emitter based OLEDs, a behavior that is mainly attributed to the short lifetime of the singlet excited states in these materials.
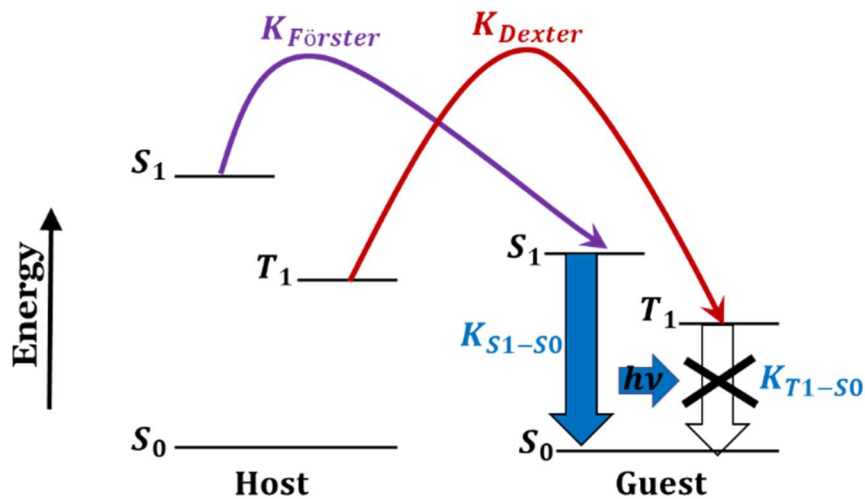
Figure 1.7. Exciton energy transfer mechanism in host-guest EMLs using conventional fluorescent emitters as guests.

1.3.2 Phosphorescent emitters

Phosphorescent emitters are typically organometallic complexes including heavy metals such as platinum (Pt), iridium (Ir), osmium (Os), and ruthenium (Ru). The incorporation of these heavy metals significantly enhances spin-orbit coupling, leading to increased singlet-triplet-mixing according to first-order perturbation theory. Therefore, the electronic transition from S_1 to T_1 becomes possible through fast intersystem crossing (ISC). Furthermore, the strong coupling between T_1 and S_0 states facilitates radiative decay, producing photons in the form of phosphorescence, with an exciton lifetime typically in the range of microseconds.

The energy transfer processes in the H:G system using phosphorescent emitters as guests are shown in **Figure 1.8**. Using this type of emitter, both singlet and triplet excitons can be harvested for phosphorescent emission in OLEDs. In these devices, an IQE of 100% can be achieved, and the EQEs can approach 40% without using any external light extraction methods [12, 13]. Phosphorescent emitters are widely used in today's OLED display technology since its first commercialization in 2003 [14]. It should be noted that, while phosphorescence OLEDs can achieve high efficiencies, the rare heavy metal used in the emitters can lead to higher cost and environment issues. Moreover, the device

stability and lifetime for blue emitting devices are not as good as conventional fluorescent emitters and require further improvement.
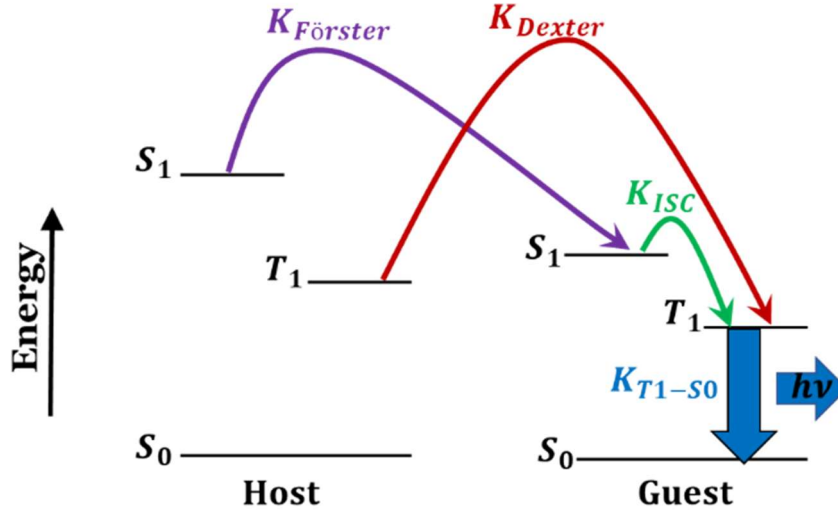
Figure 1.8. Emission mechanism of phosphorescent emitters in a host-guest EML system.

1.3.3 TADF emitters

TADF emitters are metal-free organic materials capable of harvesting non-radiative triplet excitons to achieve an IQE of 100%.

First-order perturbation theory ($\lambda \propto \frac{H_{SO}}{\Delta E_{ST}}$) demonstrates that singlet-triplet-mixing (λ) increases with enhanced spin-orbit coupling (H_{SO}) and decreased S-T energy gap (ΔE_{ST}). To achieve a large mixing coefficient, it is not necessary to enhance the spin-orbit coupling through the heavy atom effect, if the molecule has a sufficiently small ΔE_{ST}. A TADF molecule is designed with a ΔE_{ST} value negligibly small (<100 meV). Due to a strong singlet-triplet mixing, the triplets in the T_1 state can be thermally up-converted to the S_1 state through a fast reverse intersystem crossing (RISC) process, leading to the emission of delayed fluorescence [8]. The energy transfer processes occurring in a TADF emitter are shown in **Figure 1.9**.

In the molecule design of TADF, it is necessary to spatially separate the HOMO and LUMO of the molecule as much as possible to reduce ΔE_{ST}. A common strategy to increase the separation is by

introducing a steric hindrance structure or a donor-acceptor (D-A) system with twist/spiro/bulky connections [8].

In recent years, TADF OLEDs have attracted huge interest, and considerable efforts have been dedicated to developing new TADF molecules with various emission colors. Some of the most promising candidates exhibit small ΔE_{ST} values close to zero, high PLQYs approcaing 100%, and short exciton lifetimes of less than 5 μs, all of which contribute to high-efficiency performance in OLEDs [15-17]. However, TADF emitters, particulalrly blue-emitting TADF emitters, face challenges regarding short lifetime and efficiency roll-off. In fact, in theory, the lifetime of a TADF device is unlikely to significantly exceed that of a phosphorescent device. This is because the lifetime of triplet excited states in TADF emitters is comparable to that of phosphorescent emitters, typically in the range of microseconds. These long-lived excited states also play a crucial role in causing significant EQE roll-off in OLEDs. As the current density increases in a device, the density of long-lived triplet excitons increases, leading to a higher probability of annihilation processes such as triplet-triplet annihilation (TTA), triplet-polaron quenching (TPQ), and other non-radiative processes, which result in efficiency roll-off. In addition, the energy dissipated through these exciton-quenching reactions can be substantial enough to irreversibly damage certain bonds in organic molecules, leading to rapid device degradation [18, 19].
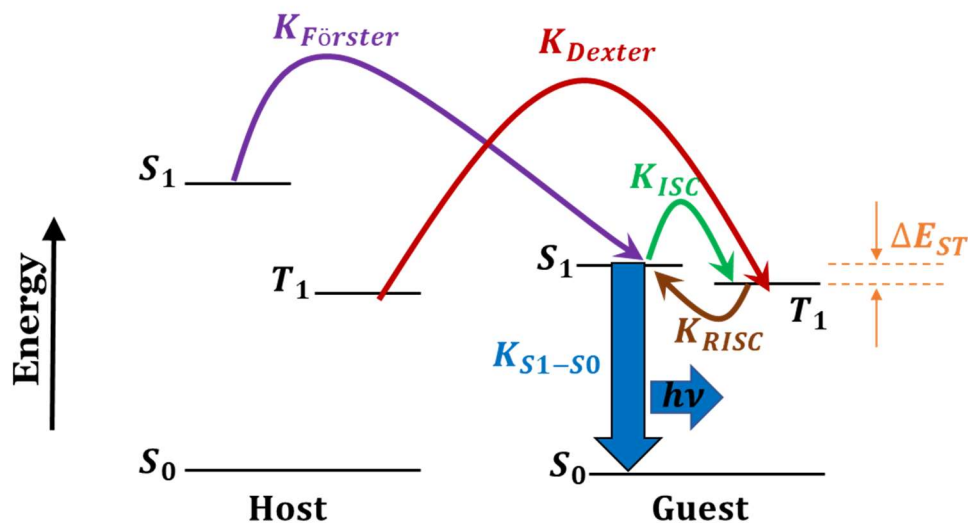
Figure 1.9. Emission mechanism of TADF emitters in a host-guest system.

1.4 OLED Fabrication processes

In general, the organic layers of an OLED can be fabricated by one of two fabrication approaches: vacuum-deposition or solution-coating. The standard method for fabricating organic films for most commercialized OLEDs based on small molecules is the vacuum-deposition of materials. Meanwhile, the organic films can potentially be deposited by solution-coating processes, since the materials can generally be dissolved in certain organic solvents. The two processes are discussed below.

1.4.1 Vacuum deposition

Vacuum thermal evaporation is the most commonly used fabrication technique for OLEDs in both research and industry production. In this technique, purified organic materials are evaporated from crucibles using thermal energy. The crucibles are electrically heated by resistive metal coils, and the heating temperature is controlled by the thermocouple underneath the crucible and a PID control system. The evaporation rate of a material can be controlled by adjusting the heating power of the crucible. When the evaporation sources are heated up and reach the evaporation temperature (typically <300 ℃ for small molecules) of the organic materials, the material vapor will propagate along a direct path to the substrate and form a thin film patterned by the shadow mask. The film thickness is monitored by a sensor known as a quartz crystal monitor (QCM). The QCM vibrates in the deposition flux and the material will accumulate on the crystal, leading to resonant frequency shifts. The frequency shift can be used to calculate the accumulated mass of the material and its deposition rate.

One of the greatest advantages of vacuum-deposition is that it enables the fabrication of multilayer devices in a single deposition procedure. Using fine metal masks as shadow masks, RGB OLEDs can be fabricated on the same substrate, which is necessary for full-color OLED displays.

It is worth noting that vacuum deposition is specifically suitable for organic small molecules rather than polymers due to their high molecular weight [20]. However, this is not considered a significant concern because to date, small molecule-based OLEDs have demonstrated superior performance compared to their polymer counterparts [21]. High vacuum is required to minimize the mean free path (i.e.: the distance traveled by a particle in a medium before colliding with another particle) of the sublimed organic molecules to ensure that they do not collide with impurity species as they make their way to the substrate. The higher the vacuum, the greater the mean free path, hence the stringent

requirement for high vacuum in this process. This results in very high manufacturing costs and constitutes the main drawback of vacuum deposition [22].

1.4.2 Solution-coating

Solution coating, in principle, provides a low-cost approach to fabricate devices because it does not require high vacuum and thus costly equipment. It also allows more efficient utilization of materials and easier scalability for the mass production of large-area devices.

In order to fabricate SOL OLEDs, organic material needs first to be dissolved into the appropriate solvent to form solutions (usually assisted with stirring or moderate heating to accelerate the dissolving process). Organic films are deposited from the solution precursors onto a substrate by additive methods such as gravure printing, screen printing, inkjet printing, blade coating, and spin coating. Among the above processes, spin coating is the most widely used for research purposes.

In a spin-coating process, the solution is first applied onto the surface of a substrate, which is fixed on a rotation stage by vacuum pump. When the rotation stage starts to spin and accelerates to a preset spin-speed, the solution rapidly spreads on the surface and expands onto the entire substrate, while any excess solution is ejected off the edge. The film thickness is determined by the viscosity of the solvent, solution density, angular velocity of the spinning, and the spinning time [23]. However, it may not be suitable for large-area applications or for patterning RGB structures for full-color displays.

On the other hand, inkjet printing is considered an alternative process for large-area OLEDs. During printing, the ink can be locally deposited on the substrate and then dried. The film thickness is controlled by the flow rate of the ink and the scan speed of the printer. By applying different layers of inks with various functional materials, complex patterns can be printed.

Nonetheless, solution-coating processes present significant difficulties. First, they limit device design possibilities due to the need for orthogonal solvents. During solution coating of one organic layer on top of another, the solvent may dissolve or even remove the underlying layer because most of the small molecules have low molecular weights and do not adhere strongly to the underlying layer. In other words, each layer cannot use a solvent that dissolves the underlying layers. This fact significantly limits the total number of organic layers, making it difficult to fabricate multilayer structures, which are usually required for good exciton confinement and, therefore, high efficiency.

Another challenge in SOL OLEDs is choosing an appropriate organic material which have adequate solubility in organic solvents. For example, Tris(8-hydroxyquinoline)aluminum(III) (Alq$_3$) has very limited solubility in organic solvents. Some materials, therefore, need to be modified to become more soluble and stable. However, increasing material solubility while maintaining its photophysical and charge transport properties is not straightforward. Moreover, the relatively low operational lifetime of SOL OLEDs is an issue for their commercialization in the display and general lighting markets.

1.5 Performance metrics

In general, the performance of OLEDs is quantified by a number of metrics, including the EQE, power conversion, current efficiency, and operational stability.

1.5.1 EQE

The most important efficiency aspect is EQE (or η_{ext}), which is defined as the ratio of the number of emitted photons to the number of injected electrons. The EQE can be described as the product of IQE (or η_{int}) and the light out-coupling efficiency (η_{out}) as shown in equation (1-3).

$$\eta_{ext} = \eta_{out}\, \eta_{int} \tag{1-3}$$

η_{out} represents the fraction of light coupled out of the device, which depends on the orientation of the transition dipole moment of the emitter molecules as well as the geometry of the device. Since thin layers in an OLED have different refractive index values, total internal reflection causes a fraction of light to ultimately exit the device through a surface-escape cone formed by critical angles. Using a simple model based on Snell's law (assuming isotropic light emission and neglecting interference effects), η_{out} can be estimated as $\eta_{out} = \frac{1}{2n^2}$ [24], where n is the refractive index of the organic layer. With typical refractive index values for organic materials ranging from 1.6 to 1.8, the light out-coupling efficiency is roughly estimated to be 15% to 20%.

η_{int} of an OLED is defined as the ratio of the number of internally generated photons within the EML of a device to the total number of injected electrons, and it can be expressed by the product of the three terms as shown in equation (1-4).

$$\eta_{int} = \# \ of \ photons = \eta_{e/h} \ \eta_{exci} \ \eta_{PL} \tag{1-4}$$

$\eta_{e/h}$ is the carrier balance factor that describes the probability of one type of injected carriers combining with the opposite type to form excitons. By using an ETL and HTL with comparable charge motilities and optimized thicknesses, inserting charge blocking layers, or using bipolar host materials in the EML, the electrons and holes in a device can be well-balanced, and the value of $\eta_{e/h}$ can be very close to 1.

η_{exci} is the singlet–triplet factor, which represents the fraction of excitons that have the potential to decay radiatively and emit light. For conventional fluorescent emitters, the η_{exci} value has an upper limit of 25% due to the forbidden radiative transition process from T_1 to S_0. However, for phosphorescent and TADF emitters, the non-emissive triplets can be fully utilized for radiative decay, and the η_{exci} values can be close to 100%.

η_{PL} is the effective quantum yield, which depends on the photoluminescence quantum yield (PLQY) of the EML. It is the ratio of the number of absorbed photons to the number of emitted photons. To increase the η_{PL} value, non-radiative decay processes such as fluorescence quenching should be minimized. One commonly adopted method to achieve this is by employing a host-guest system in the EML.

1.5.2 Current efficacy and power efficacy

Besides EQE, there are other metrics that are widely used to evaluate the efficiency of OLEDs in different applications.

Current efficacy (η_c) is mostly used for OLEDs in display applications. It is defined as the ratio of luminance (L) to current density (J) as:

$$\eta_c = \frac{L}{J} \tag{1-5}$$

With the unit of cd/A. It is very useful for quantifying the current efficacy of OLEDs in display applications, since the luminance of each pixel is directly determined by the current passing through the OLED. The current needs to be well-controlled by multiple thin-film transistors and capacitors in an AMOLED pixel to ensure stable OLED performance [25].

Power efficacy (Ks) is mostly used for OLEDs in solid-state-lighting applications. It measures the amount of luminous flux produced by a light source at a given electrical input power. It is defined as

$$K_S = \frac{L_v}{J.V}$$
(1-6)

With the unit of lm/W as well.

1.5.3 Operational Stability

During the operation of OLEDs, the luminance gradually decreases, influenced by various distinct degradation phenomena. The following chapter delves into the examination of different degradation mechanisms. Device stability is typically quantified using a lifetime parameter LT X, which indicates the time elapsed for device luminance to degrade from its initial value (L_0) to X% under continuous electrical driving. Often, the lifetime of OLEDs is defined as half-lifetime (LT50). OLED degradation is a complex issue, and device stability generally depends on the choice of materials, device structure, fabrication process, and operation and storage conditions.

1.6 The stability gap between SOL vs VAC OLEDs

Due to the significant progress and advancements made in the development of SOL OLEDs over the last decade, small-molecule OLEDs with very impressive efficiencies, made by solution-coating, are now possible [26-31]. Despite this progress, the EL stability of SOL OLEDs continues to be significantly lower in comparison to their VAC counterparts [21, 26, 29, 32-37]. The short lifetime is currently the main obstacle preventing the commercialization of low-cost OLEDs via solution-coating.

Degradation mechanisms in VAC small-molecule OLEDs are fairly well studied, with polarons and excitons known to be two major culprits limiting OLED stability [38-44]. The co-existence of high densities of polarons and excitons can drive various bimolecular chemical reactions that lead to material decomposition or quenching byproducts. In addition to chemical degradation pathways, it has recently been found that interactions between excitons and polarons can drive molecular aggregation [38-41].

While also a number of studies have investigated degradation mechanisms in SOL OLEDs [36, 45-48] and identified excitons and polarons to be leading culprits, the root causes underlying the relatively faster degradation in these systems compared to VAC counterparts are still not clearly understood. Moreover, the means to enhance the stability of SOL OLEDs remains unknown.

Therefore the primary objective of this research is to investigate the factors behind the limited EL lifetime of SOL OLEDs. Furthermore, this study explores various approaches to extend the operational lifetimes of SOL OLEDs, aiming to overcome this persistent challenge in SOL OLED technology.

1.7 Thesis Outline

The thesis is organized into seven chapters. Chapter 1 provides an introduction. Chapter 2 gives a literature review of root causes of the limited EL stability of SOL vs VAC OLEDs. Chapter 3 proposes the objectives of this study and presents the methodology regarding materials, device configuration, and characterization techniques used in this study. Chapters 4-6 are the main body of the thesis. Chapter 4 discusses the role of $H \rightarrow G$ energy transfer, and chapter 5 examines the impact of guest materials on the lower stability of SOL versus VAC phosphorescent OLEDs. Chapter 6 explores approaches to increase SOL device stability. Finally, chapter 7 summarizes the main findings of this work along with the recommendation for future work.

Chapter 2 - Literature Review: Root Causes of the Limited EL Stability of SOL vs VAC OLEDs

The material in this chapter is reprinted with permission from F.Samaeifar and H. Aziz, "The root causes of the limited electroluminescence stability of solution-coated versus vacuum-deposited small-molecule OLEDs: a mini-review", Frontiers in Chemistry journal, vol. 10, 857551, 2022 |

This chapter briefly reviews and summarizes some of the work that has been done to-date directed at elucidating the root causes of the shorter operational lifetime of SOL OLEDs, giving a special attention to studies that perform side-by-side comparisons of SOL versus VAC devices made of the same materials and thus allow for more reliable conclusions about the specific effects of the solution-coating process on device stability to be made. The first part reviews some of the work that has been done towards understanding and addressing extrinsic factors and covers solvent damage of pre-coated layers (in section 2.2.1) and chemical impurities (in section 2.2.2) whereas the second part covers some of the work directed towards investigating the intrinsic factors, covering the morphological and chemical stability differences between the SOL and VAC OLEDs (in sections 2.3.1 and 2.3.2 respectively).

2.1 Introduction

In general failure in OLEDs is caused by various degradation mechanisms that can be classified into two categories: ambient induced- and electrical stress induced-degradation mechanisms [49, 50]. Ambient induced-degradation appears in the formation of localized defects, induced by various ambient-driven reactions, that lead to the growth of non-emissive areas in the device (i.e. dark spots) over time, often also leading to electrical shorts [51, 52]. Electrical stress induced-degradation, in contrast, appears in the form of a gradual decrease in the internal quantum efficiency (IQE) of the devices without any visible defects. The behavior is caused by various physical and chemical changes that take place in the materials under electrical stress induced by the flow of charges or by the resulting excitons. These changes can be influenced by factors including device architecture and fabrication

process [38-42, 49, 53-61]. While degradation mechanisms in OLEDs have been extensively studied and are relatively well understood, the root causes of the lower stability of SOL OLEDs relative to their VAC counterparts remain largely unclear at this time. Closing this knowledge gap is critical for successfully surmounting the poor stability challenge of SOL OLEDs and propelling the technology towards commercialization.

There are several factors that uniquely affect SOL OLEDs and may contribute to their lower stability. These factors can generally be divided into two extrinsic and intrinsic factors. Extrinsic factors can be broadly defined as factors that are *external* to the specific material(s) or layer(s) being coated by the solution-coating process. Such factors include i) the negative effects of the solvents used in the layer(s) being coated on other device layers, especially pre-coated ones, and ii) the unintentional introduction of impurities into the device from either the solvents or the coating environment. Intrinsic factors, in contrast, can be defined as factors that are *inherent* to the nature of the layer(s) made by solution-coating such as specific characteristics in their i) morphologies and ii) chemical reactivity that may lead to a lower device stability. **Figure 2.1** shows the extrinsic and intrinsic factors behind the lower EL stability in SOL vs VAC OLEDs.
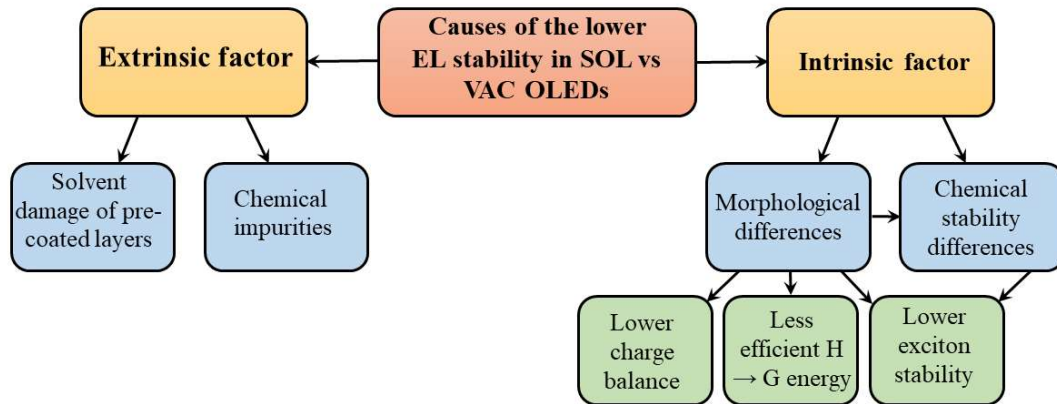
Figure 2.1. Extrinsic and intrinsic factors behind the lower EL stability in SOL vs VAC OLEDs

2.2 Extrinsic factors

2.2.1 Solvent damage of the pre-coated layers

Unlike in the case of the vacuum-deposition where the coating of one layer does not significantly disturb other pre-coated layers, solution-coating involves coating the layer from a liquid solution of the material in a solvent which makes it easier to disturb or alter other pre-coated layers. The solvent can penetrate into the underlying layers causing swelling and/or morphological changes in them, or even their partial (or complete) removal. Significant mixing along the boundary between the layers can also occur. Such changes to the underlying layers would obviously negatively affect device performance and contribute to the lower stability as was reported by [62-64].

One approach to avoid or mitigate the effects of damage to the underlying layers by the solvents is to use chemically cross-linkable materials in these layers, utilizing thermal or photochemical cross-linkers [65-71]. Using cross-linkable 4,4′,4″-tris-(N-carbazolyl)-triphenlyamine (TCTA) derivatives, Liu et al. showed that the current efficiency of devices with the SOL hole transport layer (HTL) could be preserved [72]. A similar observation was reported by Niu et al. [73]. While photo cross-linking is generally more efficient and can be used for creating more robust layers more quickly, its reliance on the use of photoacids makes it inevitable for a residual amount of side products or initiators to remain in the final layer which might impair device efficiency and stability. Thermal cross-linking is therefore considered to be a better option especially for device stability [74, 75]. Using PLEXCORE®, a thermally cross-linked HTL, Xiang et al. demonstrated OLEDs with efficiency and stability comparable to those with a VAC 4,4′-bis[N-(1-naphthyl)-N-phenylamino]biphenyl (NPB)-based HTL [76]. The light emission layer (EML) of these devices was however made by vacuum-deposition in both cases. A similar effect was observed in devices with a thermally cross-linked 9,9-Bis[4-[(4-ethenylphenyl)methoxy]phenyl]-N2,N7-di-1-naphthalenyl-N2,N7-diphenyl-9H-Fluorene-2,7-diamine (VB-FNPD) HTLs, where exposing the layers to solvents was found to have no detrimental effect on device efficiency or stability [77].

Another approach for avoiding solvent damage of underlying layers is to use, in the different layers, materials that are only soluble in orthogonal solvents [71, 78-80]. The search for suitable pairs of solvents can be aided by determining their Hansen solubility parameters [81]. However, recent work showed that even nonsolvents (i.e., solvents which can dissolve only insignificant amounts of the layers underneath) could still change the surface of the substrate on which the layers were coated and affected

22

interlayer interfaces [82, 83]. In fact other work has shown that even in cases where the underlying layers remained intact, the exposure to solvents may still alter their surface properties such as work function, sheet resistance and roughness [84-86]. While the exact implications of these phenomena on the performance of SOL OLEDs however remain to be worked out, one could expect changes at the interlayer interfaces to affect charge injection or transport, and, as a result, charge balance, and therefore stability [53, 83, 87, 88].

2.2.2 Chemical impurities

By virtue of their nature, the low pressure environments used in vacuum-deposition naturally allow for a better avoidance of unintentional contaminants that may get introduced in the materials during OLED fabrication and negatively affect efficiency and stability [89-91]. Also, many OLEDs materials are sensitive to oxygen and moisture and, while inert gas environments can be used to provide some protection, the lower pressure environments of the alternative are more effective for avoiding ambient species [92-94]. High vacuum environments also help minimize particle contamination, the latter caused by the movement of gases in the solution-coating environment during device fabrication [95]. Such particle contamination, which is more common in solution-coating processes, can induce undesired pathways for current leakage, causing device efficiency to deteriorate over time [67, 96]. Such leakage currents also facilitate the formation of microscopic shorts in the devices when under electrical stress, resulting in hot spots, possibly leading catastrophic device failure [97]. Controlling the impurity and particle levels in the solution-coating environment is therefore critical for improving SOL OLEDs' performance and stability. Another source of impurities in SOL OLEDs could be the solvents.[4]. Therefore, special attention needs to be paid not only to the solubility and purity of the OLED materials [21, 98], but also to the purity of the solvents used for the solution-coating. Liu et al. revealed that impurities in the solvents used in preparing the SOL emissive layers (EMLs) may have a leading role in the short operational lifetime of these devices. Therefore, in order to fabricate SOL OLEDs with longer operational lifetime, solvents with ultra-high purity levels are necessary [48].

2.3 Intrinsic factors

2.3.1 Morphological factors

Several studies have investigated the differences between small-molecule SOL and VAC films in regards to density, molecular orientation, and glass transition temperature. Kim et al. reported that SOL films of the N,N'-Di(1-naphthyl)-N,N'-diphenyl-(1,1'-biphenyl)-4,4'-diamine (NPB):2,2',2"-(1,3,5-benzenetriyl)-tris[1-phenyl-1H-benzimidazole] (TPBi):tris(1-phenylisoquinoline)iridium (Irpiq)$_3$ composite had a lower refractive index than their VAC counterparts, an effect that was attributed to the lower molecular packing density in the former, which was also believed to be the cause of the higher driving voltage of these devices [99]. Similarly, Lee et al. showed that the densities of 2-(t-butyl)-9,10-bis(20-naphthyl)anthracene (TBADN) doped with 4,4'-bis[2-[4-(N,N-diphenylamino)phenyl]vinyl] (DPAVBi) films processed from toluene and chlorobenzene solutions were much lower than VAC films of the same materials [33]. Xing et al. showed that VAC TCTA films had a highly oriented molecular arrangement with face-to-face $\pi-\pi$ stacking, whereas SOL films had a much more random molecular morphology [46]. In a systematic study covering a large number of small molecular materials, Shibata et al. found that film density, glass transition temperature, and degree of horizontal molecular orientation were lower in SOL films than the corresponding VAC ones. They also showed that the glass transition temperature and molecular orientation of SOL films of glassy materials were identical to those of ''deteriorated'' VAC films that experienced a transition induced by heating [100].

The lower glass transition temperature of solution coated systems can be expected to directly lead to a lower thermal and temporal morphological stability in these systems [101]. Naturally, any morphological changes that occur in device layers after fabrication can negatively affect device performance as they would lead to structural defects and non-homogeneities in charge transport that can in turn accelerate degradation processes. Therefore, a conclusion may be drawn that the lower EL stability of devices made by solution-coating may–at least in part–be due to a reduced morphological stability in these systems [102].

Aside from morphological instabilities, differences in film density and molecular orientation can also expectedly affect intermolecular charge transport and energy transfer in these systems[103], which would in turn affect device stability [54, 55]. While SOL TCTA films were shown to have lower hole transport mobility compared with their VAC counterparts [46], an opposite effect was observed in SOL N,N'-bis(3-methylphenyl)-N,N'-diphenyl-[1,1'-biphenyl]-4,4'-diamine (TPD) films. OLEDs

utilizing a SOL TPD layer as a HTL showed significantly higher currents and luminance levels at any given voltage relative to devices with a VAC TPD layer [45]. A similar observation was reported by Ishihara et al. in OLEDs with SOL TPD or N,N'-di(p-biphenyl-4-yl)-N,N'-diphenyl-[1,1'-biphenyl]-4,4'-diamine (p-BPD) HTLs [104]. Despite some variations in the observations [105-110], there is a broad agreement that SOL and VAC films exhibit significant differences in their charge transport characteristics.

Liu et al. investigated the degradation mechanisms in small molecule phosphorescent OLEDs with SOL versus VAC EMLs and found that the SOL EML devices were more prone to hole-induced degradation especially in the presence of excitons. They also found that the degradation rate in SOL devices depended on the initial hole injection/transport properties. Follow-up studies revealed that good hole injection and transport properties were required in SOL OLEDs to suppress interfacial degradation [48]. However, Lee at al. suggested that using materials with enhanced hole-blocking and electron-transporting properties was essential for improving the efficiency and stability in SOL EML devices in order to offset the higher hole mobility and electron trapping characteristics in these layers relative to VAC systems [33].

The degradation mechanisms in single organic layer devices were studied and found that SOL layers had more charge traps. With a higher concentration of charge traps, exciton−polaron interactions and exciton quenching by polarons become more efficient, which accelerates the deterioration in device EL output. SOL layers were also found to exhibit more significant electromer formation. The increased formation of electromers points to increased morphological and structural defects in these films relative to that in their VAC counterparts, possibly arising from non-homogeneities in the extent of intermolecular interactions and/or molecular packing density from one location to another within the film [36].

While differences in the initial morphology in SOL versus VAC films are believed to play a role in the lower stability of the former, other studies showed that SOL films may also be more susceptible to aggregation while under electrical stress, driven primarily by exciton-polaron interactions [35]. The phenomenon is facilitated by the relatively lower molecular packing density and larger free volume in SOL films which allow for a less-restricted molecular reorganization and mobility. Further work showed that exciton stress led to larger loses in PL quantum yield in host-to-guest (H $\rightarrow$ G) energy transfer in host:guest EML systems fabricated by solution-coating. An easier H:G phase separation in

25

these systems was found to play a key role in this behavior. Photoluminescence images showing the increased H:G phase separation and aggregation in 4,4′-bis-(carbazol-9-yl)biphenyl (CBP) films doped with various phosphorescent dopants–from that work [111]–are reproduced in **Figure 2.2(a)**. The findings revealed the influence of the initial film morphologies produced by the different fabrication methods on energy transfer and material stability under exciton stress. More recently, it was found that the less efficient H → G energy transfer in these systems can also be detected in their EL characteristics (some of those observations are reproduced in **Figure 2.2(b)**) and that the phenomenon plays a direct role in the lower stability of phosphorescent OLEDs based on H:G systems made by solution-coating. The observations again pointed to differences in molecular distribution or morphology in case of SOL layers, with more H:G phase separation compared to their VAC counterparts. Solubility limitations could be playing a role in this increased H:G phase separation resulting in the less efficient H → G energy transfer in these systems [77].

While a significant amount of effort has been devoted to studying and comparing morphology in solution coated versus vacuum deposited films, and its effect on differences in charge transport and exciton dynamics between these systems, it should be noted that in many cases the findings are material- and process-dependent [105-110]. For example, although several studies reported that SOL films have lower density and glass transition temperature, Feng et al. observed that SOL TPD films were more compact and had higher density than their VAC counterparts [45]. Similarly Kuznetsov et al. found that the density of tta: 2-thenoyltrifluoroacetone, DPPZ: dipyrido[3,2-a:2'c,3'c-c]phenazine (Eu(tta)$_3$DPPZ): CBP films made by solution-coating was higher than that of obtained with vacuum-deposition [105]. These observations show what while there may be some morphological commonalities between SOL films, the strong dependence of the morphology on the specific materials and process conditions makes it difficult to generalize phenomena observed in one material system to another without direct verification.
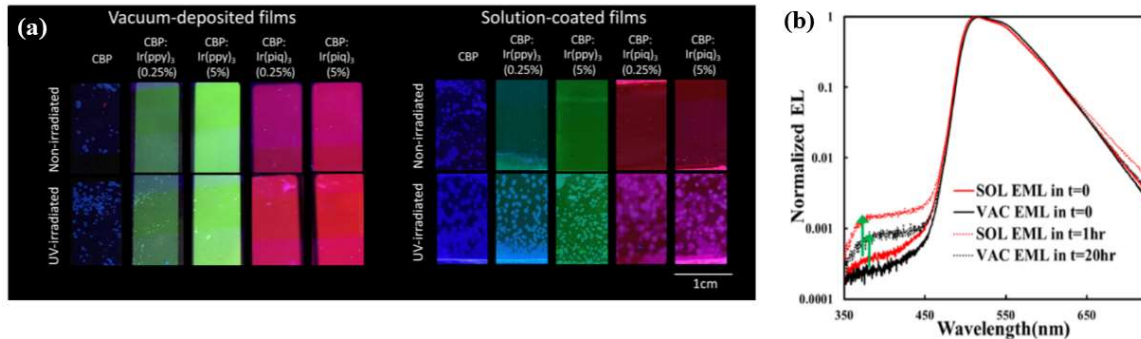
Figure 2.2. (a) Fluorescence microscopy images of neat and guest-doped CBP films subjected to UV irradiation for 18 h and of non-irradiated control films. 2,2′,2″-(1,3,5-benzinetriyl)tris(1-phe-nyl-1H-benzimidazole) (Ir(ppy)$_3$) and tris(1-phenylisoquinoline)iridium (Ir(piq)$_3$) used as guests. All films were thermally annealed at 100°C for 10 min to enhance crystallization. Reprinted with permission from [111]. Copyright 2021 American Chemical Society. (b) EL spectra (normalized to the guest emission peak intensity) collected initially (i.e., at t = 0) and after reaching the LT50 point of SOL or VAC EML devices. Reprinted with permission from [77]. Copyright 2020 American Chemical Society.

2.3.2 Chemical stability factors

While morphology seems to play a significant role in the lower stability of SOL OLEDs, chemical stability may also be playing a role. It should also be pointed out that differences in morphology may themselves lead to differences in chemical stability [112-114]. For example, in their studies of various solar-cell polymers, Mateker et al. observed a clear correlation between polymer packing density and its photo-stability. They also showed that the rate of degradation becomes slower upon increasing film density, and that, regardless of the choice of the materials, films with crystalline morphology generally exhibited a higher photo-stability [115]. One may therefore similarly expect the lower molecular packing density in SOL films to reduce their chemical stability.

SOL and VAC OLED films under prolonged excitation using UV irradiation were investigated to determine if the lower lifetime of SOL devices is primarily due to the aggregation in the films or if chemical degradation also contributed to this effect. The results showed that SOL film had more UV-induced chemical by-products formed under the irradiation conditions, indicating that chemical decomposition was faster relative to the VAC counterpart. Interestingly, the lower stability of SOL films was not due to any new (additional) chemical reactions or decomposition routes that occur in

SOL films, suggesting that the faster chemical decomposition of SOL films by the UV irradiation has its origins in the different morphological make-up of these systems which makes the molecules less chemically stable relative to those in their VAC counterparts. It is also found that the degradation rate depends on the choice of solvents used in the solution-coating process [47]. The changes in the stability with the type of solvent is due to the formation of different polymorphs [116]. More work must be done in this area to better understand the effect of chemical stability on shorter lifetime of SOL devices versus their VAC counterparts.

2.4 Conclusions

In summary, some of the work that has been done to date for elucidating the root causes of the lower EL stability of SOL OLEDs relative to their VAC counterparts was reviewed, addressing some of factors at play. These factors can generally be classified into extrinsic and intrinsic factors. The earlier involves factors that are *external* to the material(s) or layer(s) being coated, such as, contamination by impurities or solvent damage effects. The intrinsic factors, in contrast, involve phenomena that are *inherent* to the nature of the layer(s) produced by solution-coating such as differences in their morphologies or chemical stability that in turn negatively affect device stability. While the extrinsic factors, can generally be controlled via corrective measures, our understanding of the intrinsic factors seems to be more elusive. Among the intrinsic factors, morphology seems to play a major role as it affects several factors that directly affect stability, such as charge transport (and therefore charge balance), H $\rightarrow$ G energy transfer, and degradation by excitons. However, other intrinsic factors, especially the question of reduced chemical stability, need to be investigated further. The mini-review is intended to serve as an introduction to work done to-date on addressing the question of the causes of the lower stability of SOL OLEDs and to stimulate further work for the purpose of closing the existing knowledge gap in this area and surmounting this long standing challenge for the SOL OLEDs technology.

Chapter 3 - Research Objectives and Methodology

This chapter serves as a critical guide to the research objectives and methodology employed in this study, paving the way for a comprehensive understanding of the chosen research topic. Firstly, the research objectives are clearly defined, outlining the specific goals of the study. Furthermore, the methodology utilized in this study is thoroughly outlined, encompassing essential aspects such as material selection, device layout, fabrication process, and device characterization. By meticulously defining the research objectives and presenting a rigorous methodology, this chapter ensures utmost transparency, reliability, and validity throughout the research process, establishing a solid foundation for the subsequent findings.

3.1 Motivation & objectives

As previously discussed, SOL OLEDs have substantially shorter operational lifetimes compared to their VAC counterparts [21, 26, 29, 32-35]. The short lifetime is currently the main obstacle preventing the commercialization of low-cost OLEDs via solution-coating. While a number of studies have investigated degradation mechanisms in SOL OLEDs [36, 45-48] and identified excitons and polarons to be leading culprits, the root causes underlying the relatively faster degradation in these systems are still not clearly understood. Moreover, most of those investigations have focused on neat SOL layer systems comprised of only a single material. H:G systems, typical of those used in the EML of phosphorescent OLEDs, have not been adequately investigated.

In addition, these studies, have paid little attention to the role of guest molecules in the lower stability of SOL devices, focusing instead on the host materials. The role of guest molecules in the degradation process has been ignored despite observations that show that SOL H:G systems with the same host material but different guest materials can exhibit differences in their stability [21]. There is, therefore, a need to investigate the role of emitter guest materials in the faster EL degradation of SOL OLEDs relative to their VAC counterparts, and what underlying mechanisms may be involved in this case.

Furthermore, the means to enhance the stability of SOL OLEDs remains unknown. Lee et. al., demonstrated that OLEDs with EMLs deposited through solution-coating exhibited operational lifetimes of only around 1 hour. [33]. Therefore, it is imperative to investigate methods to extend the operational lifetimes of SOL OLEDs and overcome this long-standing challenge in SOL OLEDs technology.

To this end, the following research objectives will be addressed:

3.1.1 Investigating the root causes of the lower stability of SOL OLEDs relative to their VAC counterparts

    a. The role of $H \rightarrow G$ energy transfer in the lower EL stability of SOL versus VAC OLEDs:

        i. Investigating the intensity of host emission band in SOL versus VAC OLEDs

        ii. Investigating the effects of charges and excitons, separately and combined

        iii. Investigating the role of host excitons in device degradation

    b. The role of guest aggregation in the lower stability of SOL versus VAC OLEDs:

        i. Investigating the origin of new longer-wavelength bands, induced by the electrical driving, in SOL versus VAC OLEDs

        ii. Investigating the role of different morphologies in SOL versus VAC guest layers and its influence on faster guest aggregation in the former

        iii. Investigating the role of excitons, polarons or interactions in driving guest aggregation

    c. The effect of solvents and heat treatments on the lower stability of SOL OLEDs:

Investigating the root causes behind the different morphologies in SOL versus VAC guest layers

3.1.2 Exploring approaches to improve SOL device stability

    a.   Exploring EMLs with co-doped system:

              Investigating the effect of co-doped system on EL stability

    b.   Exploring TADF emitters:

              Investigating the effect of increasing guest concentration on EL stability

3.2 Methodology

3.2.1 Material selection

In this work, OLEDs with the following general structure are used: Anode (100 nm)/hole injection layer (HIL) (10 nm)/hole transport layer (HTL) (30 nm)/ light-emitting layer (EML) (20nm)/electron transport layer (ETL) (40 nm)/electron injection layer (EIL) (1 nm)/cathode (100 nm). Indium tin oxide (ITO), 1,4,5,8,9,11-hexaazatriphenylene hexacarbonitrile (HAT-CN), 9,9-Bis[4-[(4-ethenylphenyl)methoxy]phenyl]-N2,N7-di-1-naphthalenyl-N2,N7-diphenyl-9H-Fluorene-2,7-diamine (VB-FNPD), 1,3,5-tris(N-phenylbenzimidazol-2-yl)- benzene (TPBi), lithium fluoride (LiF), and aluminum (Al) are used for the anode, HIL, HTL, ETL, EIL and cathode, respectively. In all devices, HAT-CN and VB-FNPD are made by solution coating, while TPBi, LiF, and Al are made by vacuum deposition. 4,4′-Bis(carbazol-9-yl)biphenyl : Tris[2-(p-tolyl)pyridine]iridium(III) (CBP : Ir(mppy)$_3$) with 5% or 10% guest concentration (by weight), generally used as an EML, is fabricated by either solution-coating or vacuum-deposition. **Figure 3.1** depicts the main device structure used as a control in this work with its energy level diagram.

Since the main focus of this thesis is on EML, other martials are also selected as guests such as Tris[2-phenylpyridine]iridium(III) (Ir(ppy)$_3$), bis(2-phenylpyridine)(acetylacetonate)iridium

(Ir(ppy)$_2$(acac)), fac-Tris(2-(3-p-xylyl)phenyl)pyridine iridium(III) (TEG), bis(4-(9,9-dimethylacridin-10(9H)-yl)phenyl)methanone (DMAC-BP), and 9-[4-(4,6-diphenyl-1,3,5-triazin-2-yl)phenyl]-N,N,N′,N′-tetraphenyl-9H-carbazole-3,6-diamine (DACT-II). **Table 3.1** provides the chemical name, molecular structure, and HOMO and LUMO energy levels of the materials used in this thesis. All materials were purchased from EM Index and Luminescence Technology Corporation and used as received without further sublimation.
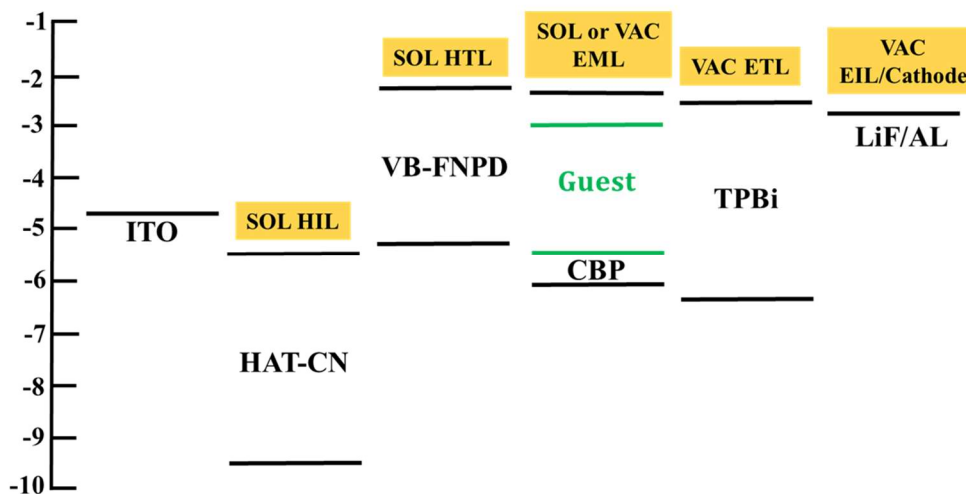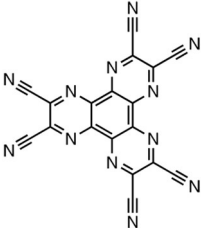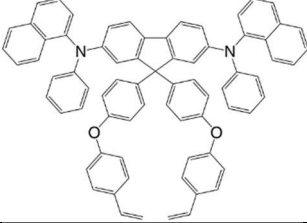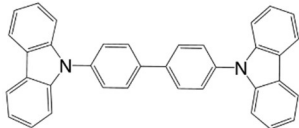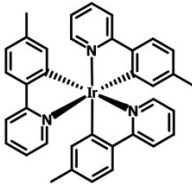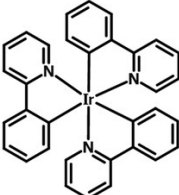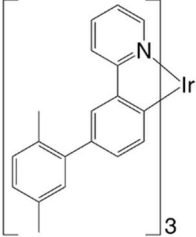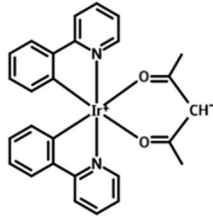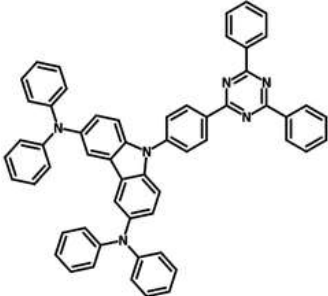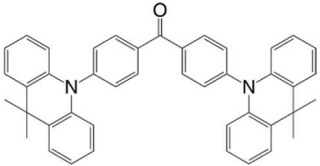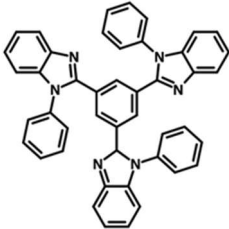
Figure 3.1. Energy level diagram of the control device in this thesis

Table 3.1. The chemical name, molecular structure, and HOMO and LUMO energy levels of the materials used in this thesis.

32

Chemical Name	Molecular structure	HOMO (eV)	LUNO (eV)	Functions in OLEDs
Dipyrazino[2,3-f:2',3'-h]quinoxaline-2,3,6,7,10,11-hexacarbonitrile **(HAT-CN)**		7.5	4.4	HIL
9,9-Bis[4-[(4-etheny lpheny l)methoxy]pheny l]-N2,N7-di-1-naphtha leny l-N2,N7-dipheny l-9H-F luorene-2,7-diamine **(VB-FNPD)**		5.3	2.3	HTL
4,4'-Bis(carbazol-9-yl)biphenyl **(CBP)**		6	2.9	HTL & host
Tris[2-(*p*-tolyl)pyridine]iridium(III) **(Ir(mppy)₃)**		5.6	3	dopant
Tris[2-phenylpyridine]iridium(III) **(Ir(ppy)₃)**		5.6	3	dopant
fac-Tris(2-(3-p-xylyl)phenyl)pyridine iridium(III) **(TEG)**		5.4	2.6	dopant

Bis[2-(2-pyridinyl-N)phenyl-C](acetylacetonato)iridium(III) **(Ir(ppy)₂(acac))**		5.6	3	dopant
9-[4-(4,6-diphenyl-1,3,5-triazin-2-yl)phenyl]-N,N,N′,N′-tetraphenyl-9H-carbazole-3,6-diamine **(DACT-II)**		5.5	3	dopant
bis(4-(9,9-dimethylacridin-10(9H)-yl)phenyl)methanone **(DMAC-BP)**		5.8	3.1	dopant
TPBi		6.7	2.7	ETL

3.2.2 Device layout

A top-down perspective schematic of a completed device is depicted in **Figure 3.2**, illustrating the area covered by the emissive and transport layers as well as the intersection of top and bottom electrodes which defines the OLED dimensions. Each OLED studied in this work has been fabricated on a 50.8 mm × 50.8 mm glass substrate with pre-patterned ITO electrodes with approximately 100 nm thickness and 20 Ω sq^{-1} resistivity. There are 7 ITO electrodes on two opposite sides of the substrate (14 in total) with a width of 2 mm used to define one dimension of the OLED area. Toward the edge of the substrate,

the width of each of those 14 ITO pads increases to 4 mm to improve the contact area with the test fixtures in the measurement systems. On either side of the sets of ITO electrodes are 7.4 mm thick ITO pads used as the counter electrode, bridged by a 100 nm thick layer of Al which defines the second dimension of the OLED. The overlap of the bottom ITO electrode and the Al top electrode results in OLEDs that are 2 mm × 2 mm. The emissive and transport layers are sandwiched between the two electrodes, with a thickness of approximately 100 nm. The rectangular feature in the ITO pad on the bottom left of the schematic is used to determine the orientation of the substrate.
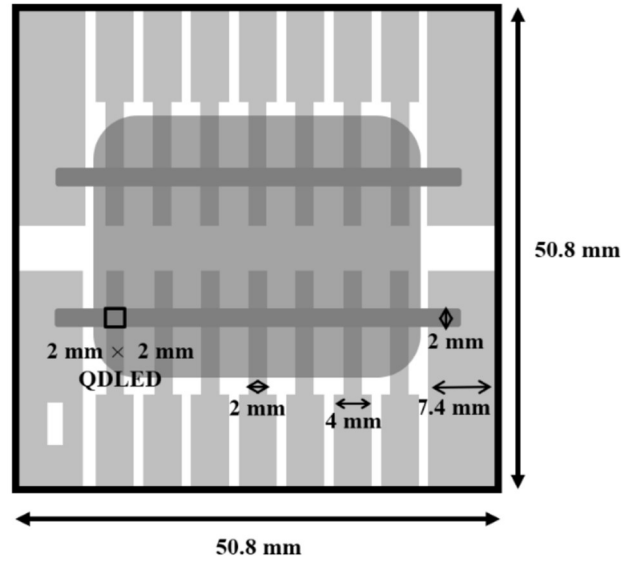
Figure 3.2. Schematic of the OLED substrate layout used in this work.

3.2.3 Fabrication Process

All devices were fabricated on pre-patterned ITO substrates (purchased from Kintec), cleaned, and sonicated sequentially with DI water, acetone, and isopropanol solutions before treating with O_2 plasma for 15 min. In all devices, the HIL and HTL were made by solution coating, and the ETL, EIL, and cathode were made by vacuum deposition. HAT-CN was dissolved in acetone (3mg mL^{-1}) and spin-coated on the substrates using a Laurell WS-400A-6NPP/LITE spin coater. The film was then baked at 130°C for 30 min. VB-FNPD dissolved in chlorobenzene was spin-coated and then baked at 100°C for 30 min to remove any residual solvent and again at 220°C for 1 hour to form a cross-linked HTL [117, 118]. EML was fabricated by either vacuum deposition or solution process. For SOL EML, the

precursor with a concentration of 10 mg mL^{-1} was spin-coated on the HTL and then baked at 60°C for 20 min. All solutions were filtered through a 0.22 μm polytetrafluoroethylene (PTFE) filter before spin-coating. Moreover, all solution processing and subsequent baking steps were carried out in a N$_2$ atmosphere inside a glovebox. ETLs, EILs, Al, and the VAC EMLs, were deposited at a rate of 0.2-2 Å s^{-1} in an Angstrom Engineering EvoVac thermal evaporation chamber at a base pressure of 5×10^{-6} Torr.

3.2.4 OLED Characterization

Once the OLED fabrication process is completed, the devices are kept in a nitrogen atmosphere during the electrical and optical measurements as well as storage to reduce the effects of ambient induced-degradation. Characterization of each set of devices generally encompasses current density-voltage-luminance (JVL) measurements, electroluminescence (EL) and photoluminescence (PL) spectral measurements, and EL stability measurements. Other characterization techniques such as transient photoluminescence (TRPL) spectroscopy are utilized to probe specific characteristics of the devices following the initial characterization measurements. Unless otherwise specified, all device tests are carried out in a test box under a N$_2$ gas atmosphere.

3.2.4.1 Current density-voltage-luminance characteristics

JVL measurements are performed by sweeping the driving voltage of the OLED from 0 V to 14 V by an Agilent 4155C semiconductor parameter analyzer to record the current at each step. The current density is calculated by dividing the measured current by OLED area (4 mm^2). The luminance is recorded by silicon photodiode connected to the semiconductor parameter analyzer to correlate each photocurrent value to the voltage step. Finally, the photocurrent is calibrated to a luminance value recorded at a driving current of 20 mA cm^{-2} by a Minolta Chroma Meter CS-100. The EQE of the OLEDs were calculated as outlined by Okamoto *et al*. assuming a Lambertian emission distribution [119].

3.2.4.2 Electroluminescence stability

EL lifetime measurements are conducted via a McScience M600 PLUS Lifetime Test System applying a constant current density of 20 mA cm^{-2} to the OLEDs while a silicon photodiode records the luminance of the devices as a function of testing time. The real luminance of the OLED over time is calibrated to the initial luminance as measured by a Minolta Chroma Meter CS-100. The driving voltage of the OLED is also recorded as a function of testing time. In order to measure the LT50 of a device, the test is terminated when the luminance of the OLED has reached 50% of its initial luminance value.

3.2.4.3 Electroluminescence spectroscopy

The EL emission spectra of the OLEDs are measured by an Ocean Optics QE65000 spectrometer with a range of 350-750 nm, collected via an optical fiber. The OLEDs are typically driven with a constant current density of 20 mA cm^{-2} unless otherwise specified. The light intensity measured by the spectrometer is normalized to the peak of interest which generally corresponds to the highest intensity peak to facilitate comparison between the different contributors to the EL spectrum.

3.2.4.4 Photoluminescence spectroscopy

The PL emission spectra of the OLEDs and other films are measured by an Ocean Optics QE65000 spectrometer with a range of 350-750 nm and collected via an optical fiber. PL is induced by illumination with a 200 W Hg-Xe lamp controlled with an Oriel 77200 monochromator to isolate certain peaks in the incident light emission spectrum. Generally, the Hg-Xe peaks near 330 nm and 365 nm are used in this work for the different absorption spectra of the materials used herein. The intensity of light measured by the spectrometer is then normalized to the peak of interest which generally corresponds to the highest intensity peak to facilitate comparison between the different contributors to the PL spectrum of the specimen.

3.2.4.5 Time-resolved transient photoluminescence spectroscopy

TRPL decay was measured with an Edinburgh Instruments FL920 spectrometer equipped with a 375 nm peak emission EPL375 picosecond pulsed laser diode. The laser diode optically excites the sample,

and the light emitted from the specimen at the target wavelength as a result of exciton recombination is measured as a function of time elapsed from the initial excitation. A material's TRPL characteristic is correlated to the materials' exciton lifetime. Therefore, this technique can be utilized to elucidate the exciton quenching processes in devices, or energy transfer characteristics between two materials. This measurement technique is carried out under ambient conditions.

3.2.4.6 UV photo-stability

Under electrical bias, charge carrier and exciton density and distribution all contribute to the degradation of OLEDs. However, the UV photostability of OLEDs has been measured in order to isolate the contribution of exciton-induced degradation to the devices from the contribution of charge carriers. Under UV irradiation, incident photons excite ground state electrons in the sample to form only singlet excitons. In these experiments, a 370 nm peak wavelength Analytik Jena UVL-18 handheld UV lamp with an irradiation power of 500 μW cm^{-2} is used as the excitation source. PL measurements of the specimen are measured by an Ocean Optics QE65000 spectrometer with a range of 350-750 nm and collected via an optical fiber over time. The peak emission of the specimen is normalized to the initial emission intensity to measure its change in intensity over time. Without the confounding factors of triplet excitons, charge carriers, and exciton-polaron interactions, the change in PL intensity over time can be attributed to the effects of singlet exciton formation and relaxation.

3.2.4.7 Surface morphology & roughness

A Veeco Nanoscope atomic force microscope (AFM) is used to characterize the surface morphology and roughness of deposited films. There are two characteristics of interest in the evaluation of roughness: peak-to-valley (R_{pv}) and root-mean-square (R_{rms}) roughness. R_{pv} represents the difference between the maximum and minimum heights in a given image whereas R_{rms} is the square root of the sum of squared film heights over the entire measured area. Both roughness values are useful in characterization of a film surface as the R_{pv} may result in localized shorts through the following layer and R_{rms} can be taken to represent the global film roughness and is the roughness value generally reported on in literature. In this work, AFM images are taken from a 5 μm × 5 μm area and roughness

values are taken from an average of at least 3 sample areas. This measurement technique is carried out under ambient conditions.

Chapter 4 - Host-to-Guest Energy Transfer and its Role in the Lower Stability of Solution-Coated Versus Vacuum-Deposited Phosphorescent OLEDs

In this chapter, the electrical aging behaviors of OLEDs comprising SOL versus VAC EMLs were investigated. These EMLs are made of the archetypical phosphorescent H:G material system CBP:Ir(mppy)$_3$. To facilitate a more accurate comparison and ensure that any differences between the behavior of the two groups of devices arise only from the differences in their EMLs with no contributions from confounding factors such as from changes to the underlying layers by the SOL EML solvent, a cross-linkable material is utilized in the HTL of all devices and tested for solvent stability first. EL and PL spectral measurements and TRPL measurements are used to compare between the degradation behaviors of SOL and VAC devices. In addition, hole-only devices are subjected to various stress scenarios in order to test for the roles of excitons and polarons in the degradation process. Moreover, double EML devices incorporating both SOL and VAC components are tested to glean additional insights into the role of host excitons concentration in device degradation. The results indicate that the faster degradation of SOL EML devices relative to their VAC EML counterparts under electrical stress is due – at least in part – to the less efficient H $\rightarrow$ G energy transfer in these systems. The less efficient H $\rightarrow$ G energy transfer of SOL OLEDs results in a greater host exciton concentration, escalating interactions between excitons and polarons which accelerates molecular aggregation.

4.1 Results and discussions

First, in order to test if the cross-linked VB-FNPD remains intact during the deposition of SOL EML, films with the structure of quartz/HAT-CN (10 nm)/VB-FNPD (30 nm) were fabricated and exposed to solvents. The solvent-exposure step was done by spin coating only solvent on the VB-FNPD surface in a way similar to that used in fabricating a SOL EML and was followed by annealing at 60°C for 20 min (similar to the annealing process of SOL EML). Chlorobenzene and toluene, being the most widely used solvents for SOL EML, were used for this purpose. **Figure 4.1(a)** depicts the UV−vis absorption spectra collected from the stacks before and after the solvent-exposure step. All spectra were essentially identical, showing that exposing the HIL/HTL stacks to the solvents does not affect their composition or structural integrity. Further, to also verify that the exposure to the solvent does not affect charge injection or transport properties of the ITO/HIL/HTL, devices of the following structure: ITO/HAT-CN/VB-FNPD/solvent-exposure/CBP:Ir(mppy)$_3$ 10% (30 nm)/TPBi/LiF/Al were fabricated and tested. In Device B and C, toluene and chlorobenzene were spin-coated on the VB-FNPD layer, respectively, followed by annealing at 60oC for 20 min. The EML, ETL, EIL and cathode were then deposited by vacuum deposition. A control device (Device A) with the same structure but without solvent-exposure process was also fabricated for comparison. **Figure 4.1(b)** and **(c)** depict the J–V–L characteristics and changes in luminance and driving voltage over time under continuous electrical driving at 20 mA cm^{-2} of the three devices. The J-V-L characteristics of all devices are almost identical, showing that the solvent exposure does not appreciably impact charge injection or transport in the ITO/HIL/HTL. Moreover, all devices exhibit an LT50 of 20 h (for an L$_0$ of 6000 cd m^{-2}). This corresponds to an LT50 of 420 h at an L$_0$ of 1000 cd m^{-2} using the lifetime scaling rule of L_0^nLT50=constant, where n is the acceleration factor of 1.7 commonly used for phosphorescent OLEDs [120]. Changes in driving voltage (the driving voltage for the device at a given time minus the initial driving voltage) versus time are also similar for all devices. These results prove that the solvent-exposure does not affect device performance or lifetime of the device, and establish the solvent resistance of the ITO/HAT-CN/VB-FNPD layers and interfaces for subsequent experiments.
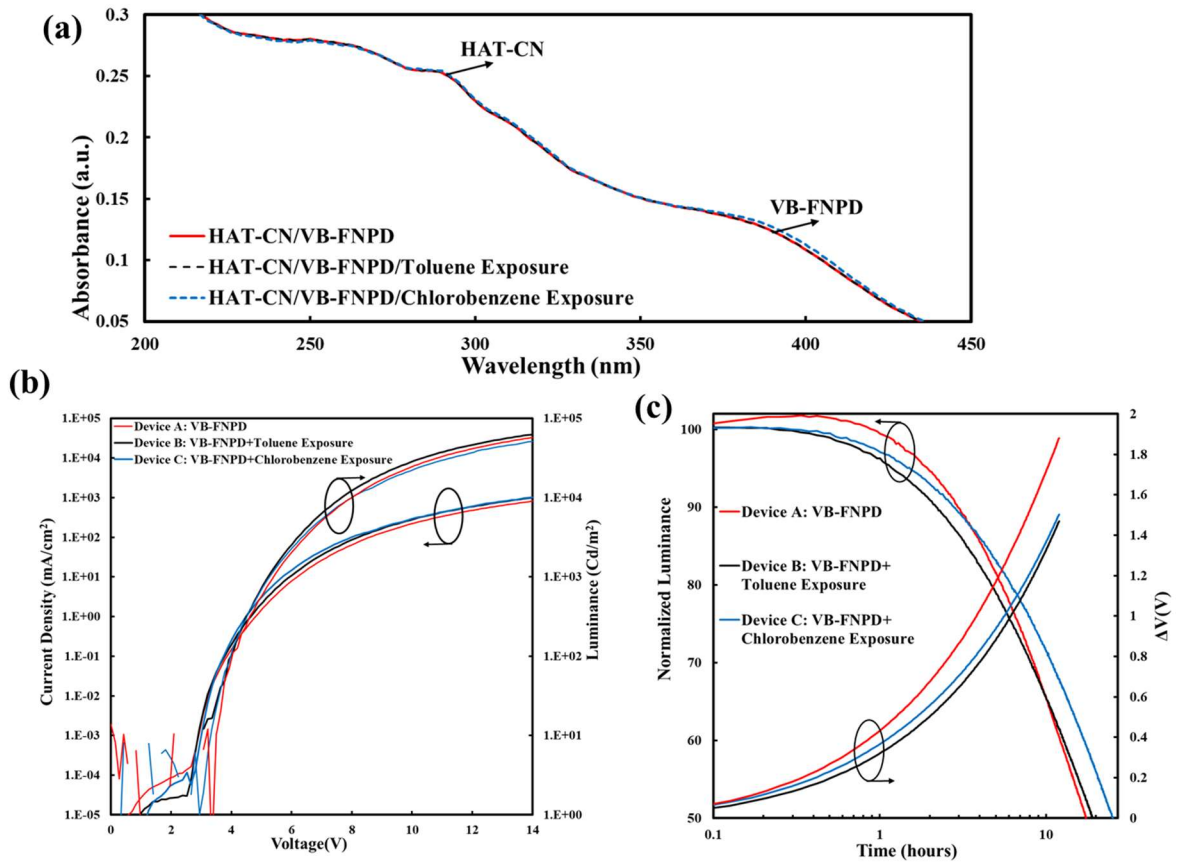
Figure 4.1. (a) UV−vis absorption spectra collected from HAT-CN/VB-FNPD films with or without solvent-exposure process. (b) Current density and luminance vs voltage characteristics, and (c) normalized luminance and change in driving voltage vs time characteristics of the devices with the structure of ITO/HAT-CN/VB-FNPD/VAC EML/TPBi/LiF/AL. In Device B and C, toluene and chlorobenzene were spin-coated on the VB-FNPD layer, respectively, while Device A was fabricated without solvent-exposure process.

Next, the performance of OLEDs with SOL versus VAC EMLs of the following structure: ITO/HAT-CN/VB-FNPD/EML/TPBi/LiF/Al were compared. **Figure 4.2(a)** depicts the J-V-L characteristics of these devices. Both devices show similar J-V-L characteristics, with the SOL EML device showing a slightly lower threshold voltage and a slightly higher current density at any given voltage. **Figure 4.2(b)** depicts the normalized luminance and change in driving voltage versus time trends of the devices while driven at a constant current density of 20 mA cm^{-2}. The LT50 of the VAC EML device is 20 h (for an L_0 of 6000 cd m^{-2}) which corresponds to an LT50 of 420 h at an L_0 of 1000 cd m^{-2}, whereas the LT50 of the SOL EML device is only 1 h (for an L_0 of 5000 cd m^{-2}) which corresponds to an LT50 of 16 h

at an L_0 of 1000 cd m^{-2}. The change in driving voltage versus time trends mirror the luminance trends, with the SOL EML device showing a faster increase in driving voltage over time. Since the possibility of any confounding effects in the other device layers have been eliminated, the distinctly different stability of the two devices must exclusively arise from differences in their EMLs as a result of the different fabrication processes.

Figure 4.2(c) depicts the EL spectra of the same devices initially (at t = 0 h) and after reaching the LT50 point. All spectra show the Ir(mppy)$_3$ characteristic emission band at 520 nm. A close comparison of the t = 0 h spectra shows that the SOL EML device spectrum has some emission at around 370-400 nm (evident from the elevated background level in this range) which coincides with CBP host emission band [36, 41, 121]. To help visualize the relative heights of the host bands, the spectra are normalized to the Ir(mppy)$_3$ band height and a logarithmic scale is used. The relative intensity of this emission increases after electrical driving in both devices. The increase is however larger in case of the SOL EML device, despite the shorter stress time (only 1 h in case of the SOL EML device versus 20 h in case of its VAC EML counterpart). Since the detection of host emission points to incomplete H $\rightarrow$ G energy transfer, the observations suggest that the energy transfer was initially somewhat less efficient in case of the SOL EML consistent with our previous findings from PL measurements on H:G systems [111], and, more importantly, that the energy transfer deteriorates much faster with electrical driving in case of SOL H:G systems.
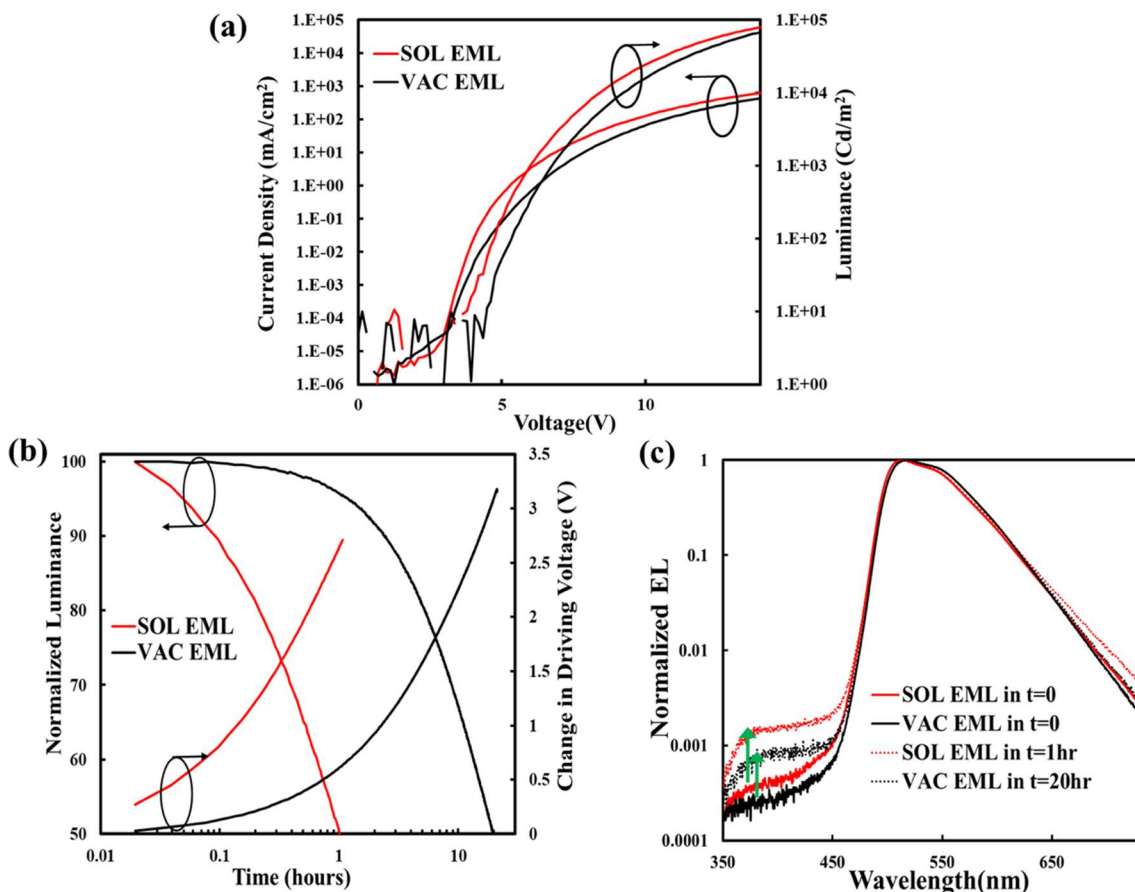
Figure 4.2. (a) Current density and luminance versus voltage characteristics, (b) normalized luminance and change in driving voltage versus time characteristics, and (c) EL spectra (normalized to the guest emission peak intensity) collected initially (i.e., at t=0) and after reaching the LT50 point of the devices with the structure of ITO/HAT-CN/VB-FNPD/EML/TPBi/LiF/Al. The EML was fabricated with either solution-coating or vacuum-deposition.

To explore this idea further, EL spectra collected from both devices at different time intervals during the electrical stress were examined. The normalized spectra are presented in **Figure 4.3(a)** and **(b)**. The non-normalized spectra are provided in **Figure 4.4** for reference and show the much faster decrease in the intensity of the main EL band (i.e. of Ir(mppy)$_3$) in the SOL EML device versus the VAC EML device, decreasing by 50% versus only by 10% after 1 hour of electrical stress, respectively. A comparison of the time evolution rates in **Figure 4.3(a)** and **(b)** shows that the relative intensity of the CBP emission band increases by 4 times in case of the SOL EML versus only 1.2 times in case of the VAC EML device after 1 hour of electrical stress.

44

In a well-dispersed H:G system, most host molecules will be located within a few angstroms from a guest molecule and can therefore transfer energy efficiently to the guest via Forster and Dexter processes. Any luminescence from the host molecules will therefore be suppressed. The appearance of a host luminescence band in the EL spectra indicates that energy transfer from the host to guest molecules is incomplete, as noted earlier, possibly due to some H-G phase separation and the formation of host-rich domains. A less efficient energy transfer in case of the SOL EML device compared to its VAC EML counterpart, despite using the same guest concentration, suggests that the SOL EML has a different molecular distribution or morphology, with more phase separation. Increasing the size or number of host-rich domains will make it more difficult for excited host molecules to transfer their excitation energy quickly to the guest molecules and will therefore be more susceptible to exciton-polaron-induced aggregation [39-41, 111], and hence to faster EL degradation. Such aggregation can further increase the H-G phase separation and contributes to the deterioration in H → G energy transfer reflected in the increase in the host emission band intensity over time when exposed to electrical stress.
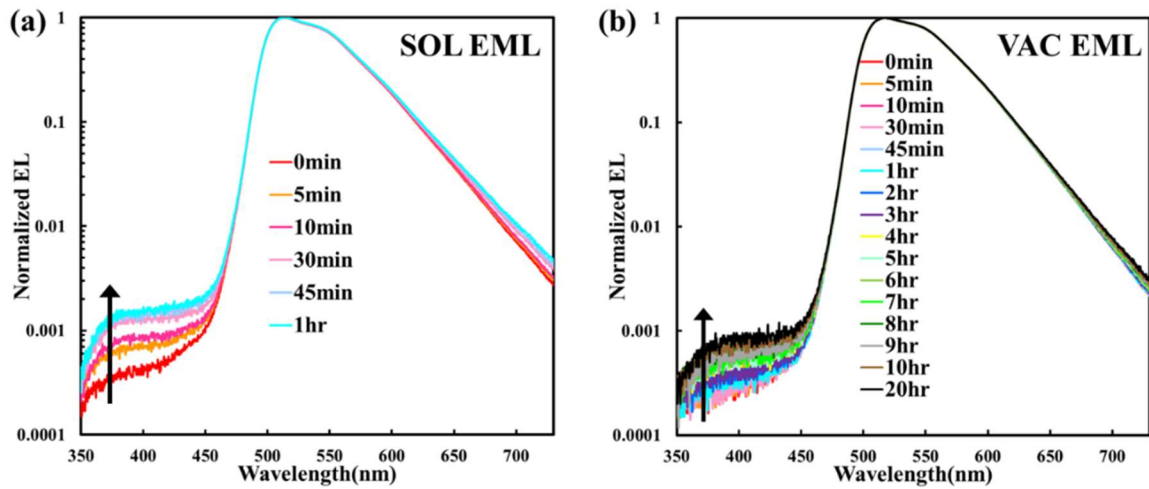
Figure 4.3. EL spectra (normalized to the guest emission peak intensity) of (a) SOL EML, and (b) VAC EML devices with the structure of ITO/HAT-CN/VB-FNPD/EML/TPBi/LiF/Al collected at different time intervals during the electrical stress at 20 mA cm^{-2}.
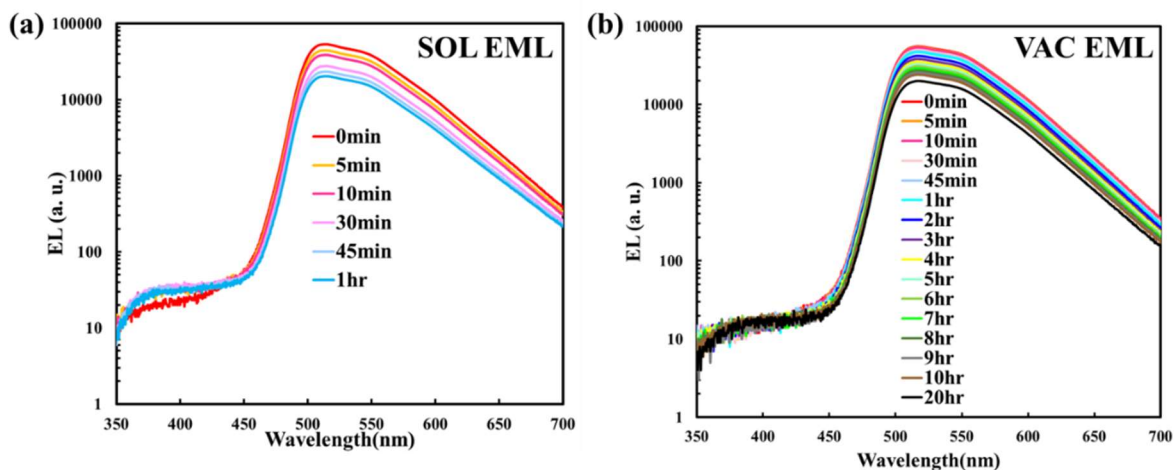
Figure 4.4. EL spectra (un-normalized) of (a) SOL EML, and (b) VAC EML devices with the structure of ITO/HAT-CN/VB-FNPD/EML/TPBi/LiF/AL collected at different time intervals during the electrical stress at 20 mA cm^{-2}.

Moreover, PL from the devices under 330 nm excitation were compared. **Figure 4.5(a)** depicts the PL spectra (normalized to the guest emission peak intensity) collected from the devices initially (at t = 0 h) and after reaching the LT50 point. The PL spectra show the same two bands as expected. The peak at 370-400 nm was however more pronounced than that of the EL spectra which can be attributed to fluorescence from the TPBi layer (TPBi fluorescence is in the 380 to 400 nm range [122]). More importantly, as can be seen, the PL spectra show the same trends as the EL spectra where the relative height of this peak is again found to increase after the electrical stress and the increase is higher in case of the SOL EML device, despite the shorter stress time. Since the TPBi layer is the same in both devices and is made by vacuum deposition, the differences in this band can be attributed to the CBP host emission.

The TRPL characteristics of devices were also tested. **Figure 4.5(b)** and **(c)** show the PL versus time at 400 nm and 520 nm (i.e., from the relaxation of the host CBP singlet excitons and the guest Ir(mppy)$_3$ triplet excitons), respectively, collected from the devices initially and after reaching the LT50 point. The CBP fluorescence decay from the pristine SOL EML device (at t=0) exhibits a slower decay rate relative to its VAC EML counterpart, pointing to a longer exciton lifetime in case of the SOL EML, consistent with less efficient H → G energy transfer. The PL decay rate becomes slower after the electrical stress in both SOL and VAC devices, pointing to an increase in host exciton lifetime in both

cases. The increase is however more significant in case of the SOL EML device. This observation is consistent with the results in **Figures 4.2** and **4.3** and suggest that H → G energy transfer is less efficient in case of SOL EML device reflected in longer lifetime of CBP exciton. In contrast, Ir(mppy)$_3$ phosphorescence decay rate becomes faster after the electrical stress in case of SOL EML device compared to VAC EML one, although both devices have the same decay rate initially. The decrease in guest exciton lifetime with electrical stress points to the formation of additional pathways by which excitons can now lose their energy nonradiatively, and is fully consistent with the occurrence of molecular aggregation. Due to increased intermolecular interactions in aggregate morphologies, new quenching pathways become efficient and compete with the radiative phosphorescence process.
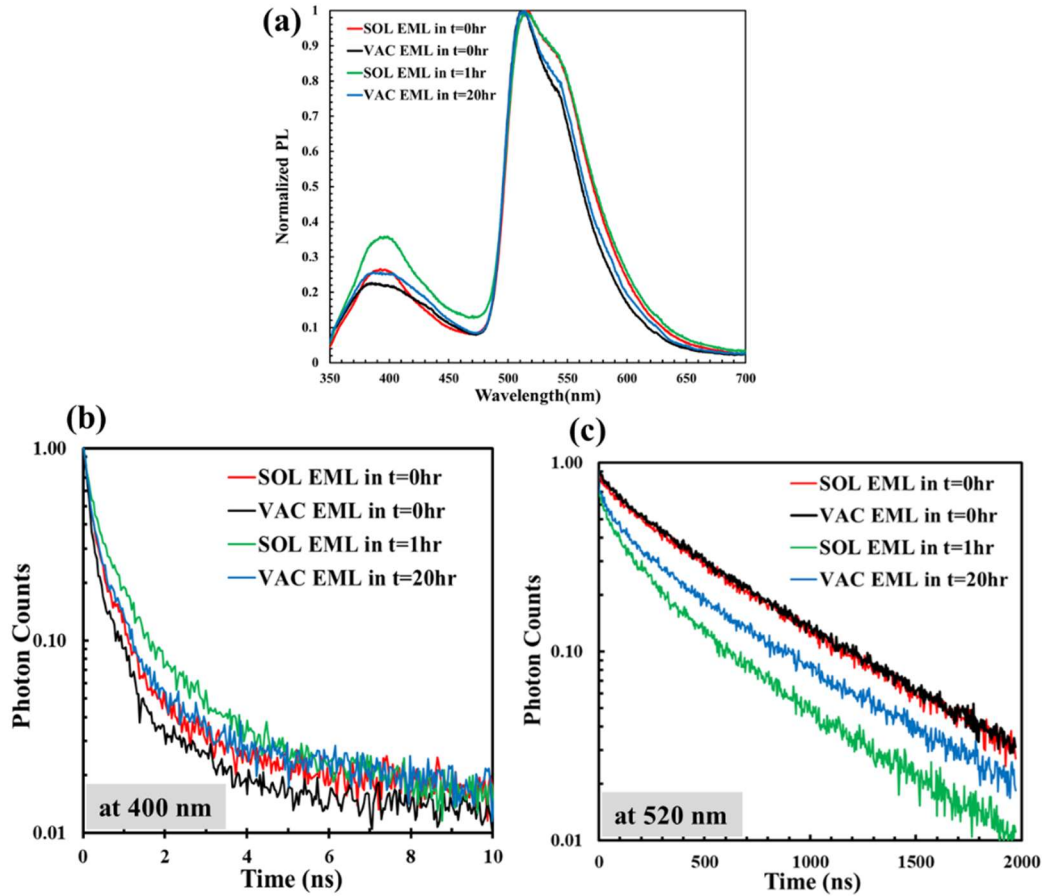
Figure 4.5. (a) PL spectra collected under 330 nm excitation, TRPL characteristics collected (b) at 400 nm (i.e., from the relaxation of CBP singlet excitons), and (c) at 520 nm (i.e., from the relaxation of Ir(mppy)$_3$ triplet excitons) of the devices with the structure of ITO/HAT-CN/VB-FNPD/EML/TPBi/LiF/Al initially and after reaching the LT50 point. The EML was fabricated with either solution-coating or vacuum-deposition.

47

In order to understand if interactions between excitons and polarons play a role in the faster degradation of SOL EML devices, the changes in the electrical characteristics of the EMLs in unipolar (hole-only) devices under different stress scenarios were studied. Unlike in bipolar devices where electrical bias inevitably also produces excitons and therefore makes it difficult to distinguish if the changes by the electrical stress are induced by the charge carriers (i.e. polarons) or excitons, the use of unipolar devices decouples the two stress factors because electrical bias does not produce excitons in this case. Any changes in the material under electrical bias must therefore be the result of polaron stress. Optical excitation can be used to produce excitons in the material and thus to study the effect of exciton stress alone (in the absence of electrical bias) or in combination with polaron stress (with an electrical bias). Therefore, two groups of devices with the following structure are fabricated: ITO/HAT-CN (10nm)/VB-FNPD (30nm)/CBP:Ir(mppy)$_3$ 10% (30nm) /MoO$_3$ (10nm)/Al (100nm). The device structure is depicted in **Figure 4.6(a)**. The CBP:Ir(mppy)$_3$ layer was made by solution-coating in one group and by vacuum deposition in the other. Under forward bias (i.e., the ITO is positively biased relative to the Al), the injection of electrons from Al is blocked by the presence of the MoO3 layer, and therefore the flow of current occurs almost exclusively via holes that get injected from the ITO contact and collected at the Al contact rendering the transport unipolar. **Figure 4.6(b)** shows the J-V characteristics of the devices. The SOL CBP:Ir(mppy)$_3$ device again shows a higher current density at any given voltage in comparison to its VAC counterpart. These devices were put through three stress scenarios successively: (1) electric current flow only, under a forward bias to sustain a flow of current density 20 mA cm^{-2}; (2) irradiation by UV light only, at 360 nm of power density 2.3 mW cm^{-2}; (3) electric current flow and irradiation together (i.e. with scenarios (1) and (2) applied simultaneously). Because these hole-only devices do not emit light, changes in the driving voltage (Vd), (i.e. the voltage needed to maintain a current flow of 20 mA cm^{-2}) in the devices, are used as an indicator of degradative changes in the materials. **Figure 4.6(c)** shows the changes in driving voltage (ΔV), defined as Vd at any given time minus Vd at time zero. The flow of current alone or irradiation alone does not bring about any appreciable increase in the Vd, reflected in the negligible change in ΔV. However, when devices are subjected to UV irradiation and current flow simultaneously, a rapid increase in Vd is observed, which was also much faster in case of the SOL CBP:Ir(mppy)$_3$ device. This increase demonstrates that the coexistence of polarons and excitons (which in this case will be mostly singlets since they are generated by optical excitation) leads to changes in the material that result in a deterioration in charge transport. This observation indicates that interactions between the two species

play an influential role in accelerating material degradation, possibly through exciton-polaron-induced aggregation, a process in which singlets, which are inevitably created on the host material during normal device operation, can play a leading role [35, 38, 39, 59]. The polarons change the dipole moment of the molecules, providing a driving force for molecules to achieve certain preferential orientations, whereas excitons provide sufficient energy to facilitate this movement or reorientation. Therefore, only when subjected to conditions where both excitons and polarons are present in high concentrations, host and/or guest material molecules may undergo morphological reorganization or aggregation in order to reach more energetically favorable states. In this context, SOL H:G systems are more susceptible to these morphological changes due to their known lower molecular packing density [100] and the longer residence time of excitons on the host molecules arising from the less efficient H → G energy transfer which leads to a higher concentration of residual excitons on the host.
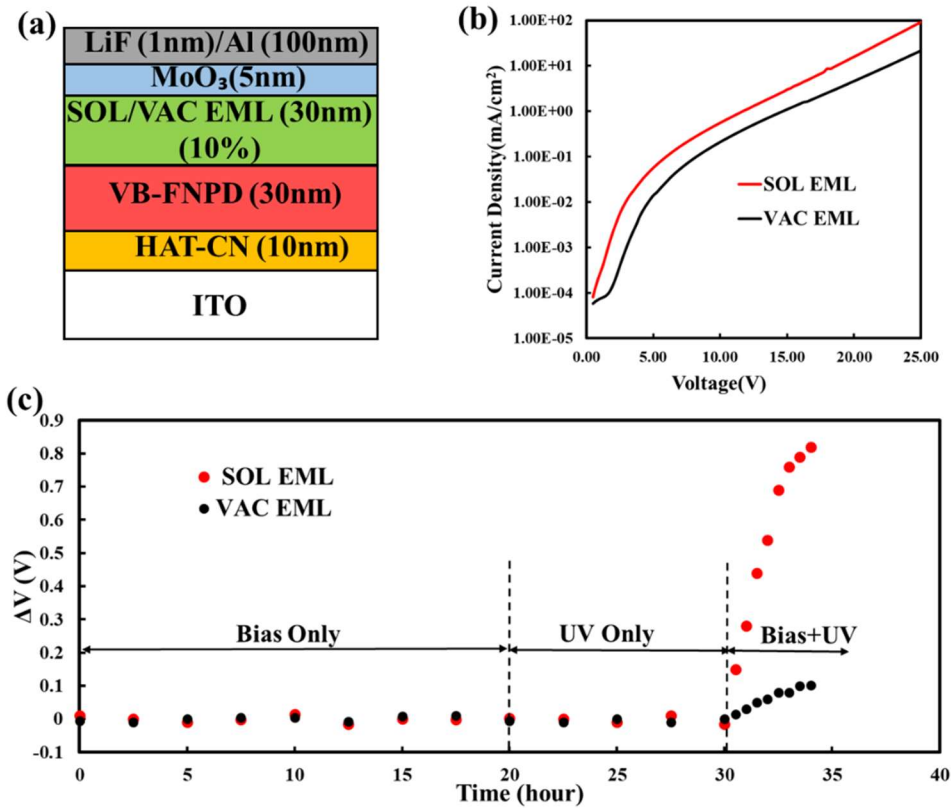
Figure 4.6. (a) Hole-only devices of structure ITO/HAT-CN/VB-FNPD/EML/MoO$_3$/AL. The EML fabricated with either solution-coating or vacuum-deposition. (b) Current density versus voltage characteristics. (c) Changes in V$_d$ (ΔV) driven by a current of density 20 mA cm^{-2} in the devices versus time, during which these devices are subjected to scenarios bias only, light only, and bias and light together, successively.

To investigate if the lower EL stability of SOL EML device indeed correlates with a higher CBP exciton concentration, four different devices with double EMLs comprising SOL and VAC components (SOL+VAC) were fabricated and tested. The general device structure is shown in **Figure 4.7(a)** and consists of: ITO/HAT-CN/VB-FNPD/SOL EML (20nm)/VAC EML(10nm)/TPBi/LiF/Al. All devices had the same Ir(mppy)$_3$ concentration in the SOL EML (10%) but different concentrations in the VAC EML (0.2%, 2%, 5% or 10%). **Figure 4.7(b)** and **(c)** show the J-V-L characteristics and normalized luminance and change in driving voltage versus time trends of these devices, respectively. For comparison, the characteristics of the single layer SOL and VAC EML devices (from **Figure 4.2**) are included in these graphs. (Note that the EML thickness and guest concentration were 30 nm and 10%, respectively, in the single EML devices). The similar J-V-L characteristics of all the double EML (SOL+VAC) devices suggest that charge injection and transport in all four devices is similar. However, as **Figure 4.7(c)** shows, the devices show significant differences in stability, exhibiting LT50 values of 2 h, 4 h, 8 h, and 8 h, for the 0.2%, 2% or 5%, and 10% Ir(mppy)$_3$ concentration in the VAC EML component, respectively. L_0 in the four devices was very similar, around 5000 cd m^{-2}. These LT50 values correspond to 30 h, 62 h, 125 h, and 125 h for a L_0 of 1000 cd m^{-2}, respectively. As mentioned above, the LT50 of the single layer VAC and SOL EML devices are 420 h and 16 h at a L_0 of 1000 cd m^{-2}, respectively. It is notable that driving voltage versus time trends are similar in all four SOL+VAC devices, and similar to that of the single SOL EML device. Considering that an increase in the driving voltage in an OLED during electrical driving usually arises from the buildup of charges at inter-layer interfaces [38], the observed increase in driving voltage may arise due to the buildup of charges at the HTL/EML interface which occurs faster when the EML is made by solution-coating. It is also possible that it arises from the buildup of charges in the EML bulk.

Figure 4.7(d) depicts the normalized EL spectra collected from the SOL+VAC devices initially (at t = 0 h) and after electrical driving at 20 mA cm^{-2} for 8 hours (t = 8 h). The differences between the spectra show that light emission does not originate exclusively in the SOL EML, indicating that the VAC EML participates in the EL process. The CBP band, which can be attributed to incomplete H → G energy transfer, is present in the EL spectra of devices with the 0.2 and 2% Ir(mppy)$_3$ in the VAC EML component due to their low guest concentration. This band is not present in either the 5% or 10% devices, signaling that H → G energy transfer becomes almost complete as the guest concentration reaches 5% in VAC H:G systems. There is a correlation between the intensity of this band (which scales with the concentration of residual host excitons that do not get transferred to the guest) and a lower

device stability, where devices with increasingly higher residual concentrations of host excitons (i.e. the 5%, 2%, and 0.2% devices, in this order) exhibit sequentially shorter LT50 values. The notably similar LT50 values of 5% and 10% devices is also consistent with this model since the concentration of residual host excitons was also similar in these devices as inferred from their almost identical EL spectra at t = 0 h. The relative intensity of the CBP band once again increases after electrical driving in all devices, pointing to faster H-G phase separation under the electrical stress. The increase is greater when the guest concentration in the VAC EML component decreases, which can again be attributed to the increased exciton-polaron-induced aggregation as H → G energy transfer decreases and the concentration of residual excitons on the host increases. The less efficient H → G energy transfer in SOL H:G systems therefore appears to play a leading role in the lower stability of solution-coated OLEDs.
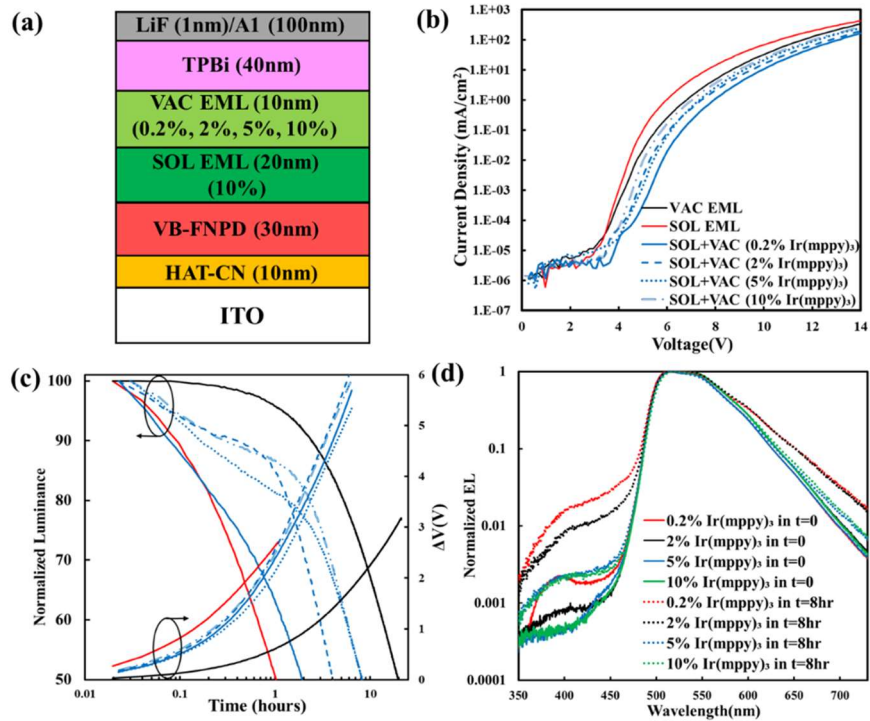
Figure 4.7. (a) SOL+VAC EML devices of structure ITO/HAT-CN/VB-FNPD/SOL EML/VAC EML/TPBi/LiF/Al. (b) Current density versus voltage characteristics, (c) normalized luminance and change in driving voltage versus time characteristics, (d) EL spectra (normalized to the guest emission peak intensity) collected before and after 8 h continuous electrical driving at 20 mA cm^{-2} of the SOL+VAC EML devices where the Ir(mppy)$_3$ concentration in VAC EML part varies from 0.2% to 10%. SOL and VAC EML devices are shown in the graphs too.

51

Seeing from the double EML devices that 5% guest concentration is sufficient for complete H → G energy transfer in a VAC EML component, the stability of single layer VAC EML devices with these concentrations was next investigated. The results are presented in **Figure 4.8(a)**. Both VAC EML devices exhibit similar stability despite the different guest concentration as expected, exhibiting LT50 of 33 h and 20 h for the 5% and 10% VAC EMLs, respectively (at L_0 of 4500 and 6000 cd m^{-2}, respectively), which corresponds to LT50 of 425 h and 420 h at a L_0 of 1000 cd m^{-2}. In addition, as seen from **Figure 4.8(b)**, both devices show that with decreasing Ir(mppy)$_3$ concentrations from 10% to 5%, CBP emission peak, which reflects the efficiency of the H → G energy transfer in the EML, does not change, indicating that 5% guest concentration is sufficient for complete H → G energy transfer in VAC EMLs. Note that the small shoulder at ≈460 nm arises from VB-FNPD emission [118], which increases when the guest concentration decreases and its (the guest's) role in facilitating hole injection and transport into the EML diminishes causing a shift of the electron-hole recombination zone towards the HTL.

The stability of single layer SOL EML devices with 5% and 10% guest concentrations was also compared. The results are presented in **Figure 4.8(c)**, showing very similar stability trends. The LT50 of SOL EML devices with 5% and 10% Ir(mppy)$_3$ concentrations are 1.5 h and 1 h for a L_0 of 3500 and 5000 cd m^{-2}, respectively, which corresponds to a LT50 of 16 h and 14 h at a L_0 of 1000 cd m^{-2}. Although at first glance this may seem unexpected considering that H → G energy transfer is incomplete in the SOL H:G and therefore reducing the guest concentration from 10% to 5% would be expected to further reduce the energy transfer, an examination of the EL spectra of these EMLs (**Figure 4.8(d)**) reveals that the relative intensity of the CBP band is comparable in both SOL EML devices despite the different guest concentrations, indicating they both have comparable H → G energy transfer. This observation suggests that the less efficient H → G energy transfer in SOL H:G systems may be rooted in solubility factors that limit the dispersion of guest molecules and reduce intermixing between the host and the guest in layers fabricated by solution coating. It is noted that attempts to increase guest concentration beyond 10% were inhibited by solubility issues in the formulation stage, indicating that solubility limitations of the guest in the host may indeed be underlying the poor H → G energy transfer in the solid H:G films made by solution coating.
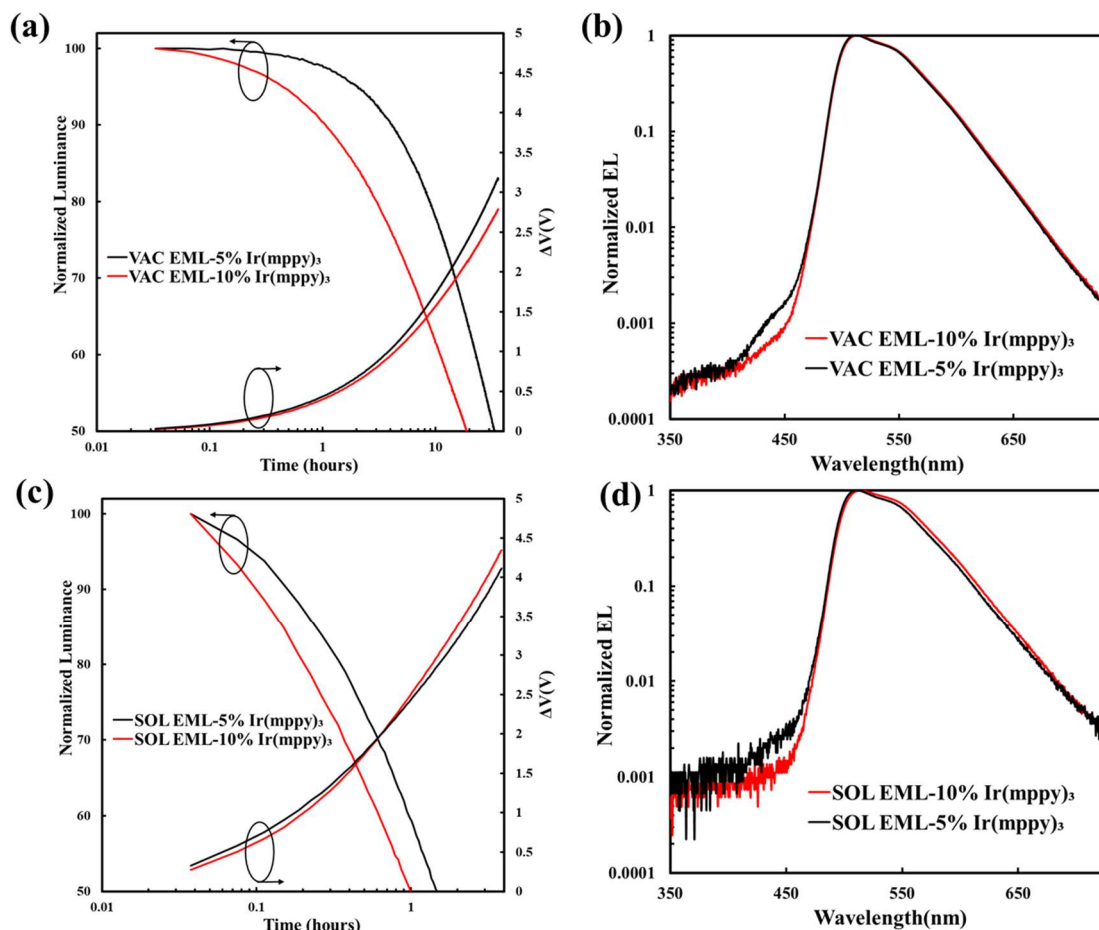
Figure 4.8. Normalized luminance and change in driving voltage versus time characteristics of (a) SOL EML devices, and (c) VAC EML devices. EL spectra (normalized to the guest emission peak intensity) collected from fresh (b) SOL EML devices, and (d) VAC EML devices. 5% and 10% Ir(mppy)$_3$ concentrations were used as the guest.

4.2 Conclusion

The root causes of the lower stability of SOL H:G systems compared to their VAC counterparts were investigated. The results indicate that the faster degradation of SOL EML devices under electrical bias is due – at least in part – to less efficient H → G energy transfer. Poor H → G energy transfer causes the concentration of exciton on the host to be greater which accelerates device degradation through increased exciton-polaron-induced aggregation. This initial inefficient H → G energy transfer leads to

53

further increases H-G phase separation and further decreases the H $\rightarrow$ G energy transfer efficiency. Solubility limitations in case of the SOL system could be the source of this reduced energy transfer. These findings bring to light one of the fundamental causes of the lower stability of SOL OLEDs.

Chapter 5 - Role of Guest Materials in the Lower Stability of Solution-Coated versus Vacuum-Deposited Phosphorescent OLEDs

In this chapter, EL degradation behavior of OLEDs with EMLs made of H:G systems fabricated by solution-coating was compared to counterparts with VAC EMLs. In order to investigate and determine the reproducibility of the observations, and ensure that they are not specific to one guest material, three different guest materials (but the same host material) are used in the EMLs of these devices. The guest materials are selected to have comparable band-gaps in order to ensure that any differences in the observations between the devices arise exclusively from the choice of the fabrication process of the EML (i.e., solution-coating or vacuum-deposition) and are not confounded by influences from differences in their band-gaps which can also affect the degradation behavior [40]. The same materials and device structures are used in both cases, limiting the difference to only the fabrication method of the EMLs. The results show that EL degradation in the devices due to electrical stress is always accompanied with changes in their EL spectra, corresponding to the appearance of new bands at longer-wavelengths. The bands are associated with emission from guest aggregation. The intensity of these new bands is always much stronger in the case of SOL EML devices, suggesting that guest aggregation is faster in them in comparison to the VAC ones. The differences in behavior arise from the different morphological structures, likely as a result of using solvents in the solution-coating process. In addition, further investigations have revealed that guest materials in SOL devices are more prone to molecular aggregation by exciton–polaron interactions compared with their VAC counterparts. This aggregation behavior appears to be–at least in part–behind SOL devices experiencing faster EL degradation than occurs in VAC ones.

5.1 Results and Discussion

The EL stability of OLEDs utilizing various guest emitters doped into the CBP, which is used as a host material was first tested. The structure of the devices is ITO/HAT-CN(10nm)/VB-FNPD(30nm)/CBP:guest(20nm) (5 wt%)/TPBi(40nm)/LiF(1 nm)/Al(100 nm). **Figure 5.1** depicts changes in luminance over time under continuous electrical driving at 20 mA cm^{-2} of the devices. **Table 5.1** also summarizes the key device performance data including initial luminescence (L_0), LT50 at L_0. The presented data represents the average values from measurements on 9 different samples in each case. Typical variation ranges for each are also included. The table also shows the LT50 at 1000 cd m^{-2} obtained using the lifetime scaling rule of $L_0^n LT50$=constant. In this formula, n=1.7 and represents the acceleration factor commonly used for phosphorescent OLEDs [120]. Using Ir(mppy)$_3$, Ir(ppy)$_2$acac, and TEG, the LT50 at 1000 cd m^{-2} of VAC devices is 425 h, 300 h, and 310 h, respectively, and SOL EML devices is 16 h, 9 h, and 7 h, respectively.

Clearly, the LT50 values of the VAC EML devices are much longer than their SOL EML counterparts despite the same materials being used in both cases which is in agreement with previous reports [35, 36, 47, 111]. To ensure that the lower stability is exclusively associated with differences in the EMLs and not due to confounding factors such as solvent damage of the HTL when coating the SOL EMLs, the effect of subjecting VB-FNPD to the chlorobenzene, used in coating the EMLs, was tested. Therefore, two devices with the following structure were fabricated and tested: ITO/HAT-CN/VB-FNPD/solvent-exposure/CBP:Ir(mppy)$_3$ (10 wt%)/TPBi/LiF/Al where EMLs were made by vacuum-deposition in both devices. In Device A, chlorobenzene was spin-coated on the VB-FNPD layer, followed by annealing for 15 min at 60°C (similar to the annealing process of the SOL EML). The remaining layers were then deposited by vacuum deposition. A control device (Device B) with the same structure but without the solvent-exposure step was also fabricated for comparison. **Figure 5.2** depicts the steps followed in fabricating these devices. The results show the J–V–L characteristics of both devices to be almost identical, indicating that the solvent exposure does not appreciably impact charge injection or transport in the ITO/HIL/HTL. Moreover, both devices exhibit an LT50 of about 20 h (for an L_0 of 6000 cd m^{-2}). These results prove that the solvent-exposure does not affect device performance or lifetime, and establish the solvent-resistance of the ITO/HAT-CN/VB-FNPD layers and interfaces for subsequent experiments [123].

Previous works showed that increasing the guest concentration can lead to increased stability due to enhanced host-to-guest energy transfer and thus reduced exciton stress in the wide band gap host

materials [40, 41]. Therefore, the EL stability of a similar set of devices with 10 wt% guest concentration was also tested and compared . The results for these devices are also presented in **Figure 5.1** and **Table 5.1**. Using 10 wt% Ir(mppy)$_3$, Ir(ppy)$_2$acac, and TEG, the LT50 at 1000 cd m^{-2} of VAC EML devices are 420 h, 300 h, and 300 h, respectively, and SOL EML devices are 14 h, 11 h, and 8 h, respectively.

Although it was expected that increasing the guest concentrations would lead to a longer LT50, this effect upon increasing the concentration from 5 wt% to 10 wt% was not observed. Conversely, it led to a significant decrease in EL lifetime in case of the VAC devices, and a little effect in case of the SOL devices, as the results show. The decrease in the VAC EML devices' lifetimes may be attributed to the aggregation in phosphorescent guest molecules which reduces their intermixing and dispersion in the host matrix. Thus, host excitons could not transfer their energy to the guests [39]. Despite the decrease, the lifetimes of the VAC EL devices were still significantly longer than those of the SOL devices. The fact that the SOL EML devices lifetimes were still much shorter and did not change appreciably upon increasing guest concentration suggests that they may already be somewhat aggregated even at the lower concentration.
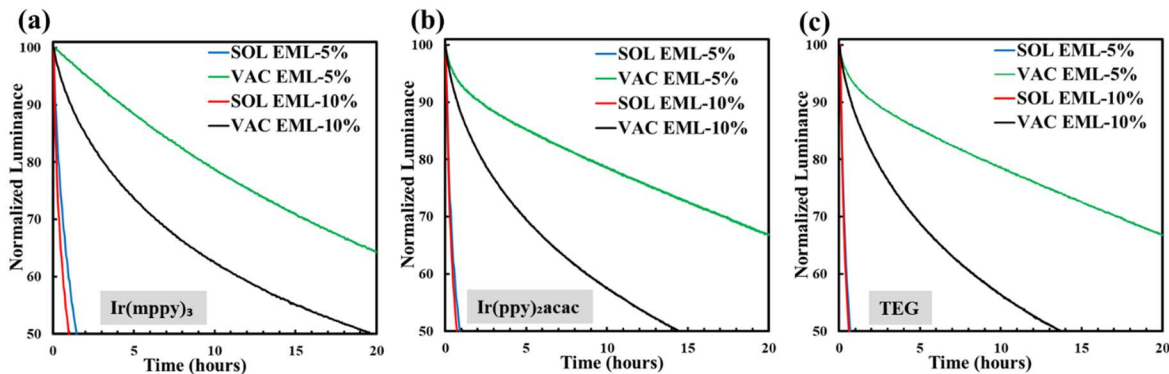
Figure 5.1. Changes in EL intensity (normalized to initial values) versus time of SOL and VAC EML devices containing 5 wt% or 10 wt% (a) Ir(mppy)$_3$, (b) Ir(ppy)$_2$acac, and (c) TEG. The devices are continuously driven by a current density of 20 mA cm^{-2}.
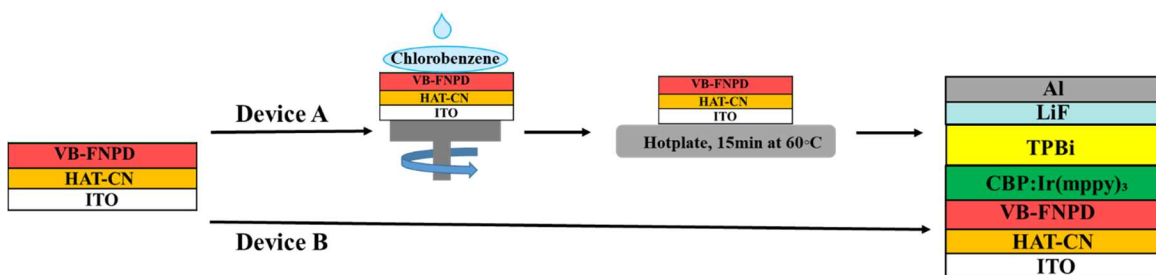
Figure 5.2. Schematic illustrations of the device fabrication sequence including the solvent exposure process.

Table 5.1. EL performance parameters of the OLEDs with the EMLs described in the text

	L_0* (Cd m^{-2})		LT50 at L_0 (h)		L50 at 1000 Cd m^{-2} (h)	
	SOL EML	VAC EML	SOL EML	VAC EML	SOL EML	VAC EML
5% Ir(mppy)₃	3500	4500	1.5	33	16	425
5% Ir(ppy)₂acac	3900	4400	0.9	24	9	300
5% TEG	3800	3800	0.7	32	7	310
10% Ir(mppy)₃	5000	6000	1	20	14	420
10% Ir(ppy)₂acac	4500	6000	0.9	14.5	11	300
10% TEG	4600	6100	0.6	13.5	8	300

*The numbers are rounded to the nearest hundred.

In order to investigate whether the guest aggregation may indeed be playing a role in the faster degradation of SOL EML devices relative to their VAC counterparts, the EL spectra of the same SOL and VAC devices with the 10 wt% guest concentration at various stages of electrical aging were examined. **Figure 5.3** presented the EL spectra collected initially and after electrical driving at 20 mA cm^{-2} for certain periods of time. The inset shows the spectral differences between the EL spectra collected after the electrical driving relative to the initial spectra, obtained by mathematically subtracting the EL spectra after electrical driving from the initial one. The measured CIE coordinates of these devices initially and after reaching the LT50 point are also included in **Table 5.2**. As can be clearly seen in **Figure 5.3**, the differences correspond to the appearance of new emission bands at longer wavelengths that are similar for the SOL and VAC devices with any given guest but varied from one guest to another. Interestingly, the intensity of the bands is much stronger in the case of SOL EML devices compared with their VAC EML counterparts over time. For example, in the case of the SOL EML device with Ir(mppy)₃ after 1 h electrical driving, a new band with a peak at 560 nm appears while

in its VAC EML counterpart, the same band with comparable intensity emerges after 70 h electrical driving. In the case of the SOL EML device with Ir(ppy)$_2$acac, two new bands with the peaks of 550 nm and 600 nm appear, and with TEG a new band with a peak of 550 nm appears after 1 h electrical driving whereas in the case of VAC EML devices, although the same bands are observed after 20 h, their intensity is too low.

The appearance of longer-wavelength bands could be the result of molecular aggregation in either the host or the guest molecules under the electrical stress [40, 124]. However, the peak wavelengths of the new bands in the insets of **Figure 5.3** do not correspond to CBP aggregate band [40]. Moreover, the fact that the peak wavelengths of the new bands vary with the different guest materials suggests they cannot be from the host which is constant in all cases. The observation therefore suggests that the new bands must arise from guest aggregates. The higher intensity of these new bands in the case of SOL EML devices relative to their VAC counterparts over time indicates that guest aggregation is much faster in the former. One can expect the guest aggregation to lead to less efficient host-to-guest energy transfer, which may, in turn lead to shorter device lifetime [123].
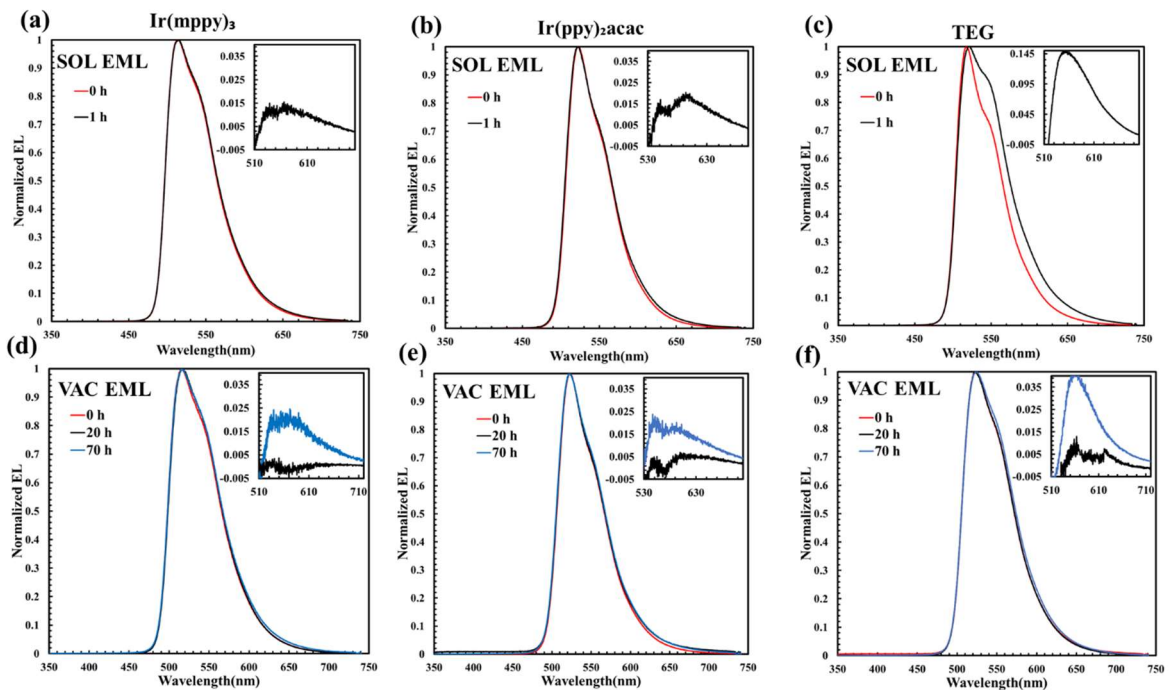
Figure 5.3. EL spectra (normalized to the peak intensities) of SOL EML devices containing (a) Ir(mppy)₃, (b) Ir(ppy)₂acac, and (c) TEG, and of VAC EML devices containing (d) Ir(mppy)₃, (e) Ir(ppy)₂acac, and (f) TEG collected before and after electrical driving at 20 mA cm⁻² for the given periods of time. The guest concentrations is 10 wt% in all cases. The insets show the mathematically calculated differences between the final and the initial spectra in each case.

Table 5.2. CIE Coordinates of SOL and VAC EML devices containing 10 wt% Ir(mppy)₃, Ir(ppy)₂acac, or TEG initially (at t = 0 h) and after reaching the LT50 point (i.e. after about 1 h and 20 h of electrical driving for the SOL EML and VAC EML devices, respectively).

		CIE color coordinates (x,y) initially	CIE color coordinates (x,y) after reaching LT50 point
SOL Devices	**10% Ir(mppy)₃**	0.290, 0.623	0.302, 0.609
	10% Ir(ppy)₂acac	0.305, 0.645	0.320, 0.630
	10% TEG	0.302. 0.645	0.330. 0.605
VAC Devices	**10% Ir(mppy)₃**	0.295, 0.628	0.296, 0.628
	10% Ir(ppy)₂acac	0.309, 0.643	0.311, 0.641
	10% TEG	0.312, 0.640	0.315, 0.635

To further verify the origin of these new bands, the effect of varying the guest concentration was also tested. **Figure 5.4** shows the normalized EL spectra collected from the fresh devices with Ir(mppy)$_3$, Ir(ppy)$_2$acac, or TEG with 5 wt% and 10 wt% concentrations. The differences between the EL spectra collected from the devices with 10 wt% guest relative to those from the devices with 5 wt% guest are shown in the insets. As can be seen, the spectral differences are similar to those observed in the insets of **Figure 5.3**. The differences between 10 wt% and 5 wt% can be explained in terms of the decreasing intermolecular separation between the guest molecules and thus increased intermolecular interactions. Therefore, it follows that the new bands in **Figure 5.3** must be associated with guest aggregation. Interestingly, the intensity of these bands in SOL EML devices is somewhat higher relative to their VAC counterparts, indicating that they must have a different molecular distribution or morphology initially. This may be a factor in their different susceptibility to guest aggregation.

It is noted that there is also ≈10–20 nm difference in the peak positions of the bands in the insets of **Figure 5.4** versus **Figure 5.3**. This can be attributed to micro-cavity effects associated with small shifts in the location of the e–h recombination zone relative to the reflective Al electrode when the guest concentration is changed [125].
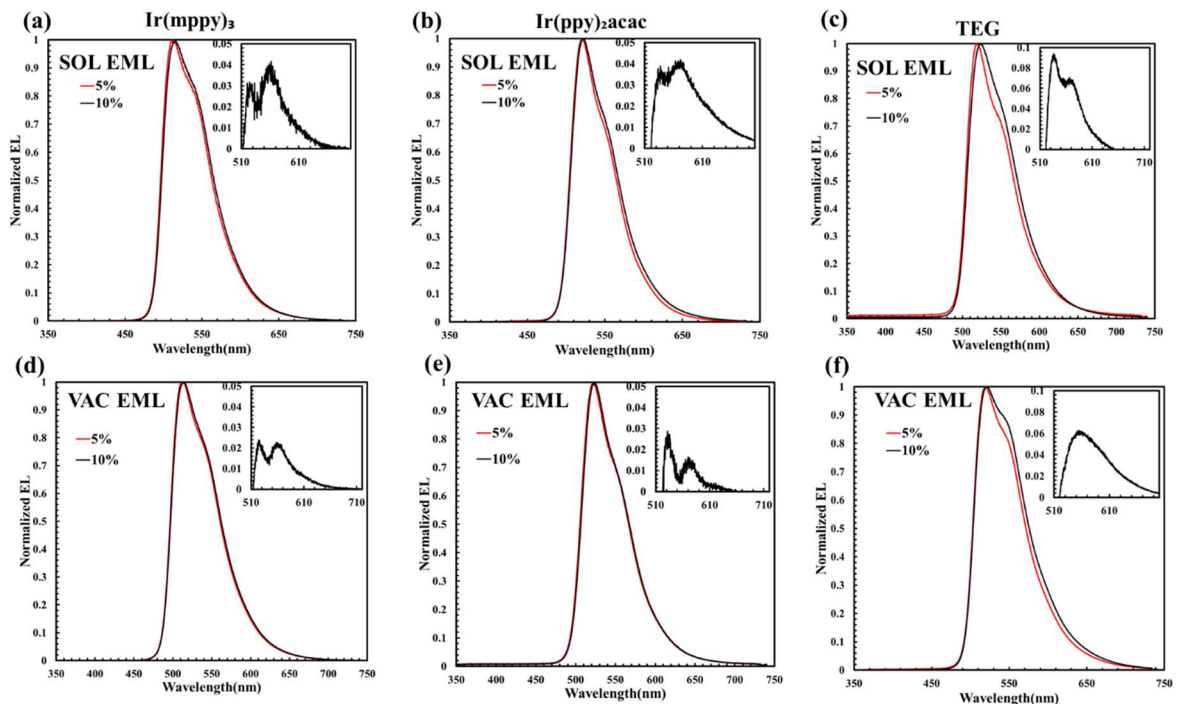
Figure 5.4. Normalized EL spectra collected from fresh SOL EML devices containing (a) Ir(mppy)$_3$, (b) Ir(ppy)$_2$acac, and (c) TEG, and VAC EML devices containing (d) Ir(mppy)$_3$, (e) Ir(ppy)$_2$acac, and (f) TEG with concentrations of 5 wt% and 10 wt%. The insets show mathematically calculated differences between the spectra collected from the 10 wt% versus the 5 wt% guest concentration devices.

The TRPL characteristics of the devices with the 10 wt% guest concentrations initially and after reaching the LT50 points (i.e., after about 1 h in the case of the SOL EML devices and about 20 h in the case of their VAC EML counterparts) were also tested. **Figure 5.5** shows TRPL characteristics of devices at 520 nm (i.e., from the relaxation of the guest triplet excitons) collected under pulsed excitation at 380 nm. All devices show reduced exciton lifetime after degradation, evident in the faster relaxation rate of the excitons. More importantly, decay rate becomes much faster in the case of SOL EML devices relative to their VAC EML counterparts, despite their comparable decay rates initially. This observation indicates that more exciton-quenching channels are introduced in the EMLs after degradation. This phenomenon is consistent with increased intermolecular interactions in morphologies with increased aggregation which leads to the new quenching pathways becoming more efficient and competitive with the radiative phosphorescence process.

From the above results, the conclusion can be drawn that the guest molecules aggregate under electrical stress in both SOL and VAC EML devices, however, the aggregation is faster in the case of the SOL EML devices. Such aggregation must be associated with differences in the morphologies of the SOL versus VAC layers. Solution-coating may produce film morphologies with some initial phase separation containing guest-rich and guest-deficient domains, with electrical stress driving further aggregation and phase separation. The phase separation reduces the ability of excited host molecules to lose their excitation energy, in turn making them more prone to exciton-induced degradation and aggregation [123, 126].
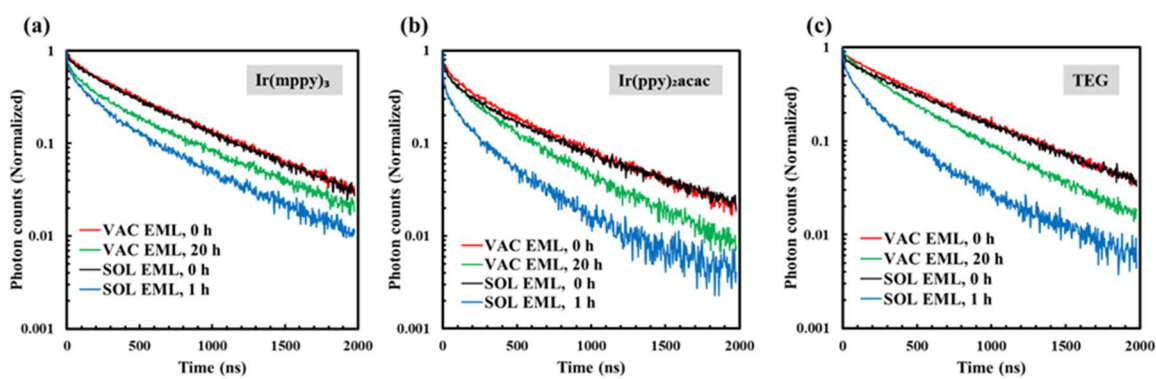
Figure 5.5. TRPL characteristics collected at 520 nm (i.e., from the relaxation of guest triplet excitons) of SOL and VAC EML devices with 10 wt% (a) Ir(mppy)$_3$, (b) Ir(ppy)$_2$acac, and (c) TEG, initially and after electrical driving at 20 mA cm^{-2} for certain periods of time. The data and **Figure 5.5(a)** reprinted with permission from [123]. Copyright 2021 American Chemical Society.

To investigate the possibility that guest materials may attain different morphologies in SOL and VAC layers and their influence in the faster guest aggregation in the former, the surface topography and roughness of the neat layers of the guest molecules were also measured using AFM. Since in a H:G system, the morphology is dominated by the host, neat layers of the guest molecules were used here in order to be able to distinguish and test the effect of the fabrication process on the guest molecules specifically. Films with the structure of ITO/HAT-CN(10nm)/VB-FNPD(30nm)/Ir(mppy)$_3$, Ir(ppy)$_2$acac, or TEG (20 nm) were therefore fabricated, where the neat guest layers were made by either vacuum-deposition or solution-coating. AFM images are shown in **Figure 5.6**. As can be seen, the images reveal very different topologies of the SOL versus VAC guest layers in each case, with the SOL layers showing less homogenous morphologies and a lot of pinholes. The surface roughness (Rms)

was also higher in the case of SOL films (for Ir(mppy)$_3$, Ir(ppy)$_2$acac, and TEG, the R$_{rms}$ of SOL films is 3.74 nm, 3.59 nm and 2.24 nm TEG, respectively, and VAC films is 1.72 nm, 1.55 nm, and 1.64 nm, respectively). The higher roughness suggests increased molecular aggregation in the SOL films [127]. These results clearly show that the fabrication process strongly influences the morphology of the guest materials, and produces a morphological disposition that increases their susceptibility to morphological changes and aggregation later. Interestingly, the results also show that morphology of the films varied depending on the guests especially in the case of SOL films.
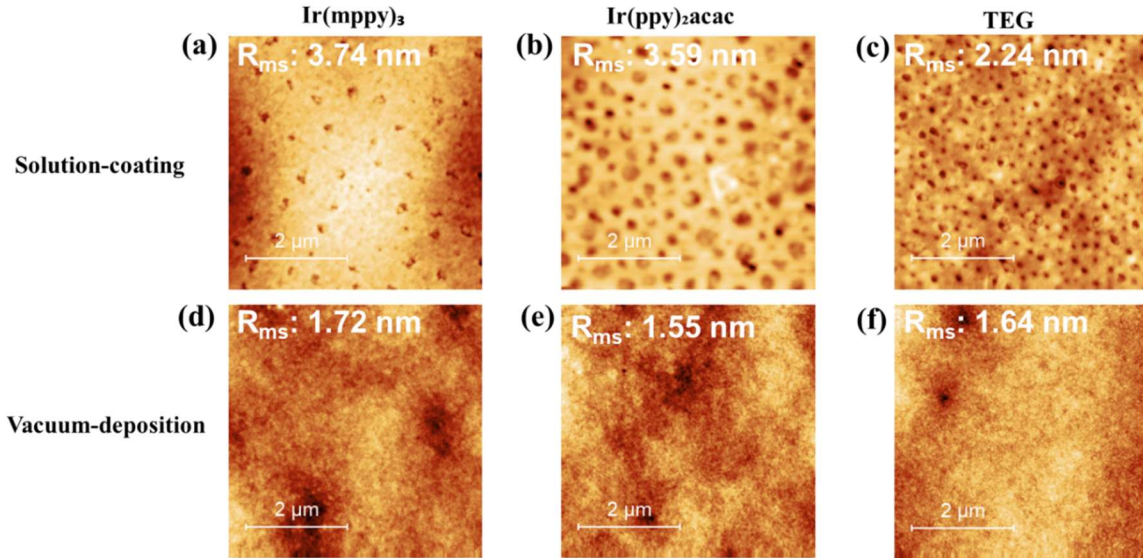
Figure 5.6. AFM images of SOL neat films of (a) Ir(mppy)$_3$, (b) Ir(ppy)$_2$acac, and (c) TEG, and VAC neat films of (d) Ir(mppy)$_3$, (e) Ir(ppy)$_2$acac, and (f) TEG.

To identify the root causes behind the different morphologies in the case of SOL EML devices compared with their VAC counterparts, an investigation was conducted to examine the effects of solvent and baking treatments, both of which are integral to any solution coating process, on the morphology of the EML and the subsequent impact on device performance. To understand the effect of these factors irrespective of any other factors in the solution-coating process, their effects on EMLs that were coated by vacuum deposition were studied. For studying the effect of the solvent, these VAC EMLs were exposed to chlorobenzene, the same solvent used in the SOL EML formulation, by mounting the test samples on the lid of a sealed container that also contains chlorobenzene such that the samples get exposed to only the solvent vapors (without immersion in the solvent itself) as

illustrated in **Figure 5.7**. Three test devices were fabricated and tested. In all three devices, ITO/HAT-CN(10 nm)/VB-FNPD(30 nm)/CBP:Ir(mppy)$_3$(20 nm) layers were first made. In the first device, denoted "Solvent+Bake", the EML was exposed to the chlorobenzene for 10 s, and then subsequently baked at 60°C for 15 min to remove any residual solvent that may have been absorbed by the EML during the 10s exposure time. This process therefore simulates to a large extent the effect of the solvent that SOL EMLs experience. In the second device, denoted "Bake", the substrate was only baked at 60°C for 15 min. The third device, denoted "Control" remained untreated. Afterward, the deposition of subsequent layers (TPBi(40 nm)/LiF(1 nm)/Al(100 nm)) was resumed. **Figure 5.7** illustrates the fabrication steps of devices.

Figure 5.8(a) depicts the J–V–L characteristics of the three devices. The J-V-L characteristics of all devices are almost identical, showing that neither the solvent exposure nor the baking, separately or combined, appreciably impacts charge injection or transport. **Figure 5.8(b)** shows changes in luminance and driving voltage over time under continuous electrical driving at 20 mA cm^{-2}. The LT50 of the Solvent+Bake, Bake, and Control devices are 4 h, 19 h, and 20 h (for an L_0 of 6000 cd m^{-2}) which corresponds to an LT50 of 84 h, 400h, and 420 h at an L_0 of 1000 cd m^{-2}, respectively. These results show that device lifetime decreases dramatically with the solvent treatment whereas the baking alone has almost no effect. The changes in the driving voltage versus time trends mirror the luminance trends, with the Solvent+Bake device showing a faster increase in the driving voltage over time. Since the HIL and HTL are not affected by the solvent and/or baking as was established earlier, the distinctly different stability of the Solvent+Bake device compared to the Control and Bake devices must exclusively arise from differences in their EMLs, caused by the solvent exposure.

Figure 5.8(c), **(d)**, and **(e)** depict the EL spectra of the Solvent+Bake, Bake, and Control devices, respectively, measured initially (at t = 0 h) and again after 20 h of electrical driving. Once again, the insets show the differences between the EL spectra collected after the electrical driving relative to the initial one. The Solvent+Bake device shows a new band at 560 nm attributed to the Ir(mppy)$_3$ aggregation band whereas the Control and Bake devices do not show such discernible band after 20 h. These results indicate that the EML in the Solvent+Bake device is particularly susceptible to guest aggregation, similar to SOL EML devices. Since exposure to solvent vapor would increase the mobility of molecules [128], it cab be concluded that the solvent affects the morphology of the VAC EML making it become more similar to that of the SOL EML and facilitating guest aggregation. These results convincingly show not only that SOL and VAC EML devices have different morphologies, and that

SOL EML morphology influences their increased susceptibility to guest aggregation, but also that the solvent used in solution-coating plays a significant role in this phenomenon. The effects of solvent and backing treatments on the devices containing Ir(ppy)$_2$acac or TEG were similarly studied. The data from these devices is provided in the **Figure 5.9** and **Figure 5.10**, respectively. As can be seen, they also exhibit the same behavior with the Solvent+Bake devices again exhibiting significantly lower stability and higher guest aggregation bands in comparison to the Control and Bake devices in all cases.

the effects of solvent and baking treatments on the morphology of neat layers of Ir(mppy)$_3$, Ir(ppy)$_2$acac, and TEG were also measured using AFM. AFM images showed that the solvent brings about an increase in the surface roughness (changing from 1.72 nm to 2.17 nm, 1.55nm to 2.76 nm, and 1.64 nm to 1.96 nm for Ir(mppy)$_3$, Ir(ppy)$_2$acac, and TEG, respectively) whereas the baking has no such effect.
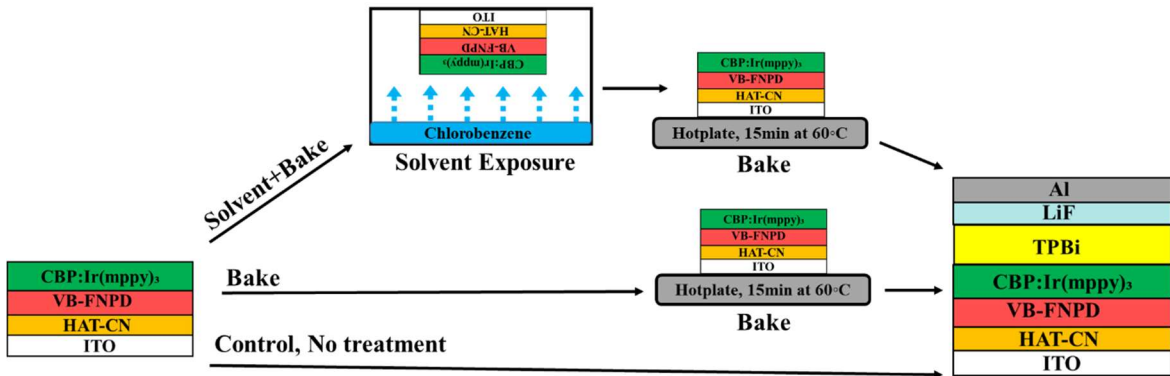
Figure 5.7. Schematic illustrations of the fabrication sequence of the Solvent+Bake, Bake, and Control devices.
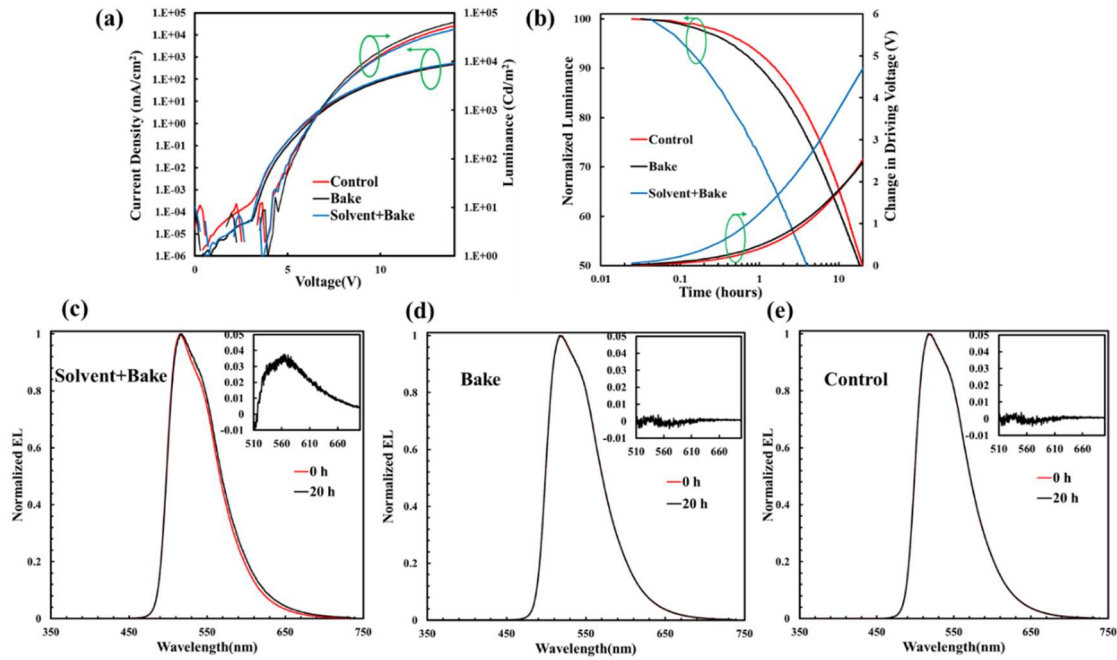
Figure 5.8. (a) Current density and luminance versus voltage characteristics, and (b) normalized luminance and change in driving voltage versus time characteristics of Solvent+Bake, Bake, and Control devices. EL spectra (normalized to the guest emission peak intensity) collected initially (i.e., at t = 0) and after 20 h of electrical aging of the (c) Solvent+Bake, (d) Bake, and (e) Control devices containing 10 wt% Ir(mppy)$_3$. The insets show the mathematically calculated differences between the final and the initial spectra in each case.
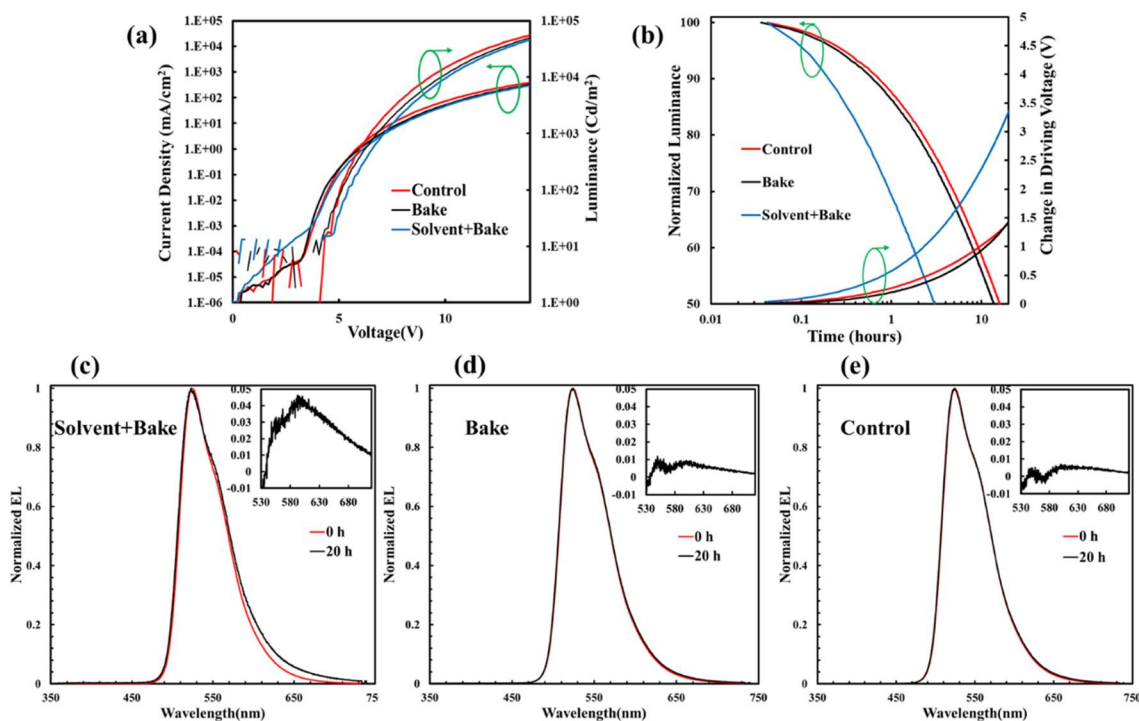
Figure 5.9. (a) Current density and luminance versus voltage characteristics, and (b) normalized luminance and change in driving voltage versus time characteristics of Solvent+Bake, Bake, and Control devices. EL spectra (normalized to the guest emission peak intensity) collected initially (i.e., at t = 0) and after 20 h of electrical aging of the (c) Solvent+Bake, (d) Bake, and (e) Control devices containing 10 wt% Ir(ppy)$_2$acac. The insets show the mathematically calculated differences between the final and the initial spectra in each case.
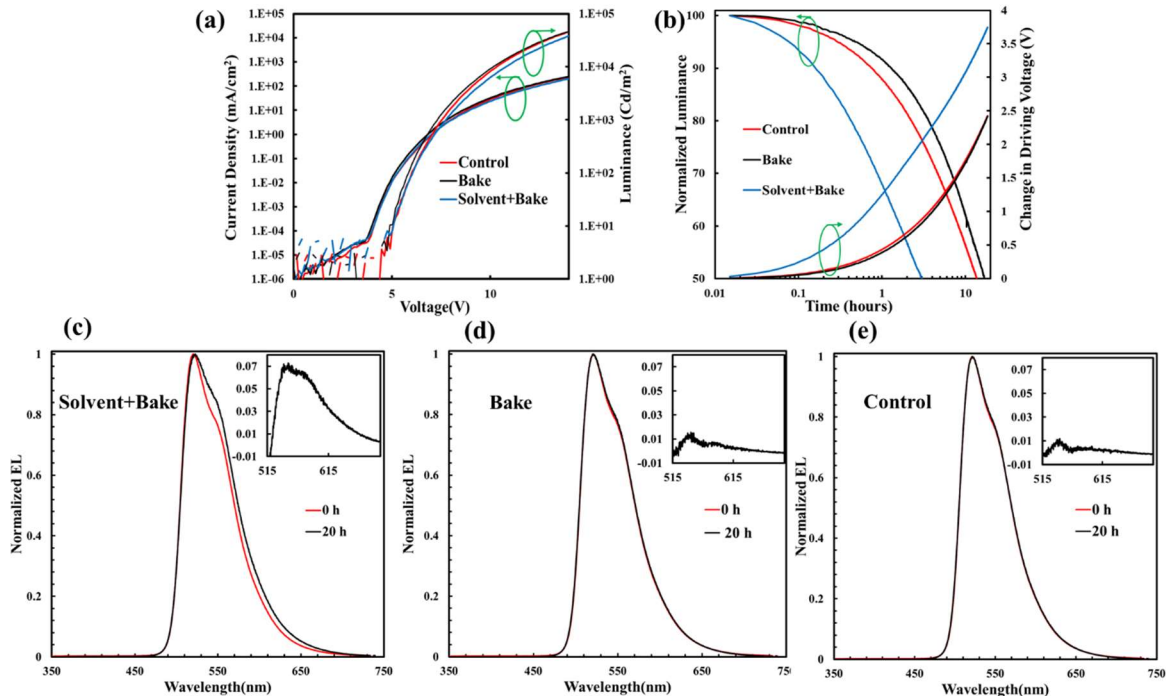
Figure 5.10. (a) Current density and luminance versus voltage characteristics, and (b) normalized luminance and change in driving voltage versus time characteristics of Solvent+Bake, Bake, and Control devices. EL spectra (normalized to the guest emission peak intensity) collected initially (i.e., at t = 0) and after 20 h of electrical aging of the (c) Solvent+Bake, (d) Bake, and (e) Control devices containing 10 wt% TEG. The insets show the mathematically calculated differences between the final and the initial spectra in each case

Seeing that exposing VAC EMLs to the solvent leads to a significant reduction in device stability and accelerates the appearance of guest aggregation bands, making them more similar to SOL EMLs, the effects of the solvent and backing treatments on the TRPL characteristics of VAC EML devices were also measured. Results from these TRPL measurements, comparing the PL decay rates at 520nm of the Solvent+Bake and Control devices, are presented in **Figure 5.11**. Quite remarkably, the PL decay rate in the Solvent+Bake devices was very similar to that of the SOL EML devices (shown in **Figure 5.5**), suggesting that aggregation had indeed occurred with the solvent treatment. The TRPL characteristics of the Bake devices were also tested and they were found to be very similar to those of the Control devices.

69

The results clearly reveal that exposing the guest materials to solvents can speed up their aggregation, a phenomenon that would lead to non-complete host-to-guest energy transfer and decreased EL stability under electrical stress.
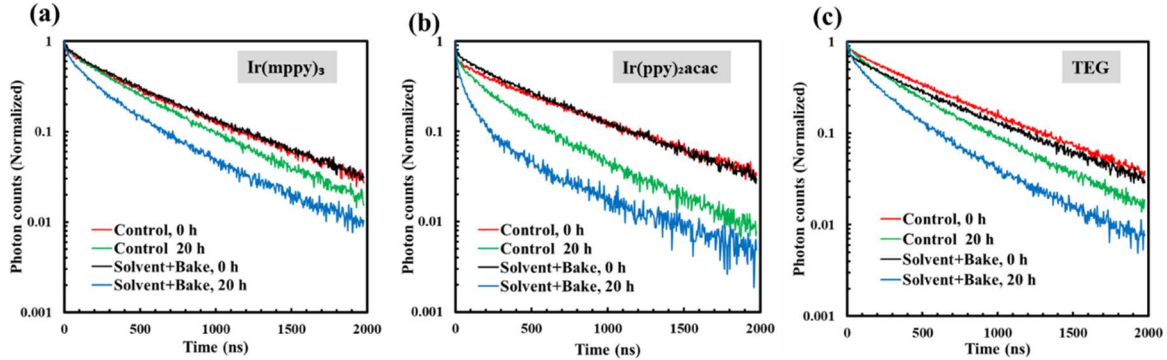
Figure 5.11. TRPL characteristics collected at 520 nm of Solnent+Bake and Control devices with (a) Ir(mppy)$_3$, (b) Ir(ppy)$_2$acac, and (c) TEG initially and after 20 h electrical driving at 20 mA cm^{-2}.

Finding that SOL EML devices are more susceptible to guest aggregation under electric stress than their VAC EML counterparts, and that the behavior arises from differences in morphology likely caused by the use of solvent in the case SOL devices, the question about whether excitons, polarons or interactions between them play the leading role in driving this aggregation arises.

Therefore, the changes in the EL spectra of SOL and VAC EML devices were studied using a neat layer of Ir(mppy)$_3$ as an EML–selected as a representative of the three guest materials used here because of its wide use. The layers were incorporated in unipolar (hole-only) devices of the structure ITO/HAT-CN(10 nm)/VB-FNPD(30 nm)/Ir(mppy)$_3$(2 nm)/TPBi(5 nm)/MoO$_3$(10 nm)/Al(100 nm), where the Ir(mppy)$_3$ layer was made by either solution-coating or vacuum-deposition. Under forward bias (i.e., the Al is negatively biased relative to the ITO), the MoO$_3$ layer blocks the injection of electrons from Al, and therefore the flow of current occurs almost entirely by means of holes that get injected from the ITO contact and collected at the Al contact. The use of unipolar devices allows studying the effect of polarons in the absence of excitons since the unipolar nature of the current does not allow for exciton formation by the electrical stress. Optical excitation can however be used to produce excitons, and thus allow to study their effects separately or in combination with polarons. Hole-only (as opposed to

electron-only) unipolar devices were selected because of the known more detrimental effect of positive polarons on these materials [40].

The devices were subjected to one of three stress scenarios: (1) electric current flow, under a forward bias to sustain a current flow of density$\approx$20 mA cm^{-2}, denoted by "Bias only"; (2) irradiation by UV light, at 360 nm of power density$\approx$2.3 mW cm^{-2}, denoted by "UV only"; or (3) electric current flow and irradiation together (i.e., scenarios (1) and (2) applied simultaneously), denoted by "Bias+UV". Also, a control device was kept in the dark to be used as a reference, denoted by "Control". After about 3 h under the above conditions, the Al electrode was peeled off using scotch tape in a N$_2$ atmosphere. Since the adhesion of inorganic/inorganic interfaces is much stronger than that of organic/inorganic interfaces [129], the 10 nm MoO$_3$ layer would also be peeled off with the Al layer. After that, another 10 nm of TPBi followed by LiF and Al were deposited, thereby converting the unipolar devices into bipolar devices capable of producing EL [39]. The process is illustrated in **Figure 5.12(a)**.

Figure **5.12(b)** and **5.12(c)** present the normalized EL spectra collected from these devices, with the SOL and VAC EMLs, respectively. The insets display the differences between the spectra of devices subjected to the UV only, Bias only, or Bias+UV relative to the Control one. As **Figure 5.12(b)** shows, the SOL EML devices show spectral differences that correspond to the appearance of a new band at $\approx$560-570 nm for all stress scenarios. This band is also similar to that seen in **Figure 5.3**. Therefore, it can be attributed to the Ir(mppy)$_3$ aggregation. In contrast, the VAC EML devices show no such features in their spectra.

Also, the band height was much higher in the EL spectrum of the SOL EML device subjected to the Bias+UV, pointing to more significant guest aggregation relative to those subjected to the UV only or Bias only. This observation indicates that the coexistence of polarons and excitons accelerates guest aggregation, possibly due to exciton-polaron interactions, similar to those observed in the OLED systems and often inferred to as exciton-polaron-induced aggregation (EPIA). In this regard, the presence of excitons provides thermal energy (via non-radiative pathways) to molecules which facilitate their movement and reorientation, whereas the presence of polarons increases columbic interactions between the molecules providing an additional driving force for aggregation. Therefore, the coexistence of excitons and polarons speeds up the aggregation of the guest materials.
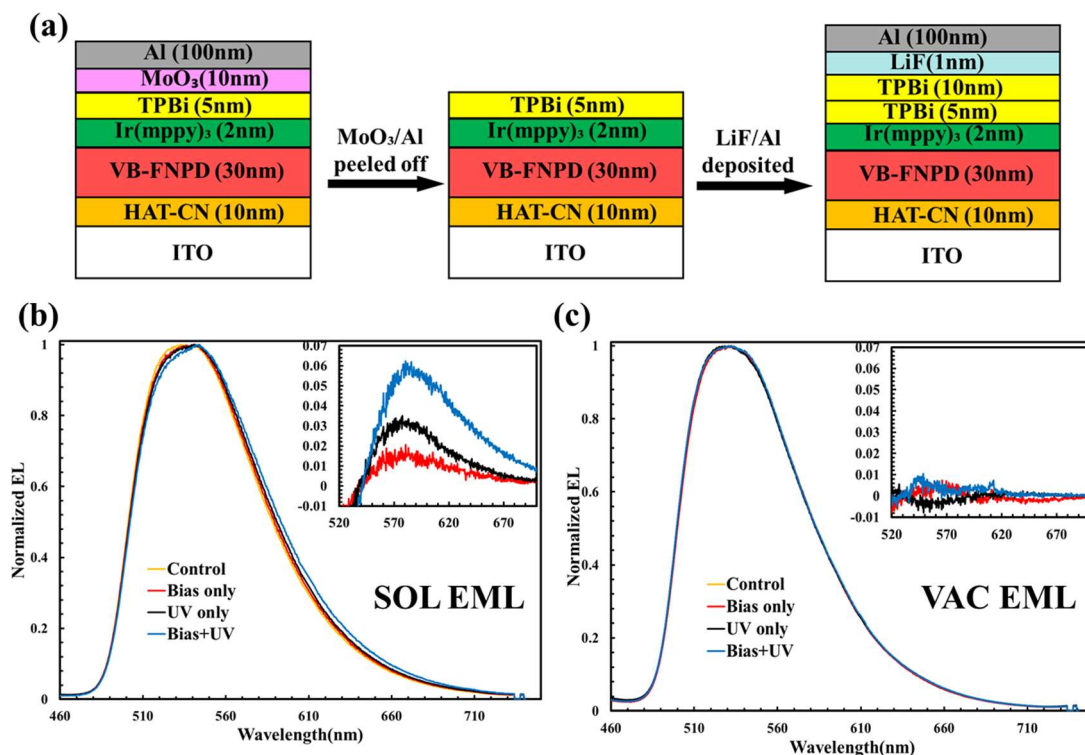
Figure 5.12. (a) Illustration of replacing the top electrode with an electron-injecting cathode, in which hole-only devices are converted into bipolar devices. Normalized EL spectra of (b) SOL, and (c) VAC devices collected from bipolar devices. The insets display the mathematically calculated differences between the spectra of devices subjected to the UV only, Bias only, or Bias+UV relative to the Control one.

5.2 Conclusions

In conclusion, the EL degradation mechanisms of devices made by solution-coating and vacuum-deposition containing various phosphorescent guests, widely used in OLEDs, were studied. Results show that the aggregation of the guest materials plays a dominant role in the lower electroluminescence stability of SOL devices. The solvent used in the solution-coating process leaves a morphological deposition that seems to be the main cause of the higher propensity of the guest materials for aggregation. The aggregation is also found to be driven by excitons and accelerated by the presence of polarons likely due to exciton-polaron interactions. The results uncover one of the main causes of the lower EL stability of phosphorescent OLEDs made by solution-coating relative to those made by

vacuum-deposition and reveal the importance of adopting new molecular designs that make them less susceptible to aggregation for the development of SOL OLEDs with high performance.

Chapter 6 - Exploring Approaches to Improve SOL Device Stability

As mentioned earlier, SOL H:G systems exhibit a lower EL stability relative to their VAC counterparts, and this behavior is associated with a lower H $\rightarrow$ G energy transfer efficiency in the former [77]. The observations suggest that the less efficient H $\rightarrow$ G energy transfer in SOL H:G systems may be rooted in limited dispersion of guest molecules and reduced intermixing between the host and the guest in layers fabricated by solution-coating.

Increasing the guest concentration can potentially enhance H $\rightarrow$ G energy transfer and thus reduce exciton stress in the wide band gap host materials [40, 41]. However, in the case of SOL H:G systems, increasing the phosphorescence emitter concentrations beyond 10 wt. % is inhibited by solubility issues in the formulation stage [77]. Moreover, guest aggregation occurs more rapidly in H:G systems with 10 wt. % phosphorescent guest concentration compared to those with 5 wt. % concentration, which shows that even at the 10 wt. % concentration, the phosphorescent guest molecules tend to aggregate to some extent [39].

In this chapter, two approaches are introduced with the objective of increasing guest concentrations and promoting their intermixing between host molecules while preventing guest aggregation: the co-doped system and the utilization of thermally-activated delayed fluorescence (TADF) emitters. The co-doped system involves employing two phosphorescent emitters with similar energy bandgaps as molecular spacer for each other, instead of using a single emitter. This approach may inhibit fast guest aggregation in SOL devices leading to a more efficient H $\rightarrow$ G energy transfer and subsequently improving EL stability. On the other hand, TADF emitters possess the advantageous characteristic of being able to be incorporated into the EML at relatively high concentrations. Therefore, utilizing TADF emitters in SOL H:G systems holds promise for enhancing H $\rightarrow$ G energy transfer and improving the operational stability of the devices.

Results from investigations of the co-doping approach are presented in section 6.1, whereas results from the use of TADF emitters are presented in section 6.2.

6.1 Improvement in the stability of SOL OLED using co-doped system

In H:G systems, guest molecules have a tendency to cluster or coalesce, forming larger aggregates or domains within the EML. This aggregation can lead to various issues such as reduced H → G energy transfer efficiency, altered emission properties, and decreased device stability. It is particularly problematic in SOL H:G systems where guest molecules exhibit a notably faster aggregation rate compared to their VAC counterparts.

To mitigate guest aggregation, the co-doped system is introduced, in which two phosphorescent emitters with comparable energy bandgaps are simultaneously co-doped into the host material. The presence of two emitters prevents rapid guest aggregation by maintaining spatial separation and hindering their close proximity, allowing for improved intermixing between the host and guest molecules. As a result, the H → G energy transfer efficiency is enhanced, leading to a more stable OLED device.

In this work, Ir(mppy)$_3$ and Ir(ppy)$_3$ emitters are co-doped into CBP host. The results show that the intensity of guest aggregation emission bands is much stronger in the case of devices with the single dopant compared with their co-doped counterparts, indicating that guest aggregation occurs much faster in the former. In addition, the results indicate that the LT50 of devices with the co-doped system is 3× longer than devices with the single dopant while the same concentrations are used in both cases.

6.1.1 Results and discussions

First, OLEDs utilizing 5% and 10% Ir(mppy)$_3$ doped into CBP (denoted as H:G 5% and H:G 10%, respectively) were fabricated to evaluate the effect of increasing the guest concentrations on the stability of the devices with the single dopant. The structure of the devices is ITO/HATCN/VB-FNPD/CBP:Ir(mppy)$_3$ (5 or 10 wt%)/TPBi/LiF/Al. **Figure 6.1(a)** exhibits the J-V-L characteristics of fabricated OLEDs, where H:G 10% device shows both a lower threshold voltage and leakage current compared with H:G 5% device. The lower threshold voltage of the former may be attributed to better hole injection from HTL into the increased guest molecules because of a lower energy offset between the HOMO of HTL and guest martials compared to the host material. Moreover, the lower leakage current of H:G 10% OLED suggests that the increased guest concentration leads to more effective hole

injection into the EML, causing radiative recombination within the emission layer and, in turn, preventing electron leakage through the HTL.

The EQE vs current density characteristics of the OLEDs are shown in **Figure 6.1(b)**. The maximum EQE (EQE_{max}) values of H:G 10% and H:G 5% are 7.3% and 4.5%, respectively. The higher EQE of the H:G 10% OLED may be associated with its better hole injection into the EML, resulting in improved charge balance and, consequently, better device efficiency.

Figures 6.1(c) and **(d)** depict the normalized luminance and change in driving voltage versus time trends of the devices, respectively, while driven at a constant current density of 20 mA cm^{-2}. The LT50 of H:G 5% and H:G 10% is 1.5 h and 1 h, respectively. The change in driving voltage versus time trends mirrors the luminance trends, with the H:G 10% device showing a faster increase in driving voltage over time.

Our initial expectation was that increasing the guest concentrations from 5% to 10% would result in a longer LT50 due to more efficient H $\rightarrow$ G energy transfer in the latter. However, the results showed a decrease in the EL lifetime of devices with increasing guest concentration. The decrease in the lifetime can be attributed to the aggregation of phosphorescent guest molecules, which reduces their intermixing and dispersion in the host matrix. This phenomenon hinders the energy transfer from the host to the guest, resulting in the observed outcome [39].

Figure 6.1. (a) Current density and luminance vs voltage characteristics, (b) EQE vs current density characteristics, (c) normalized luminance vs time and (d) changes in driving voltage vs time of H:G 5% and H:G 10% OLEDs. The luminescence is measured while driving the OLEDs at a 20 mA cm^{-2} current density.

To investigate whether guest aggregation plays a role in the shorter EL stability of the H:G 10% device relative to H:G 5% device, the EL spectra of the devices were examined initially (at t = 0 h) and after reaching the LT50 point. **Figures 6.2 (a)** and **(b)** show the EL spectra of the H:G 5% and H:G 10% OLEDs, respectively. The inset displays the spectral differences between the EL spectra collected after the electrical driving relative to the initial spectra. As can be seen, the differences correspond to the emergence of new bands at longer wavelengths which is attributed to Ir(mppy)$_3$ aggregation bands [130]. The intensity of the bands is much stronger in the H:G 10% device compared to the H:G 5% device, despite the shorter stress time (1 h for the H:G 10% device versus 1.5 h for the H:G 5%

77

counterpart). This indicates that guest aggregation occurs much faster in the former. The faster aggregation of the guest molecules leads to less efficient H → G energy transfer, which, in turn leads to a shorter device lifetime [123].
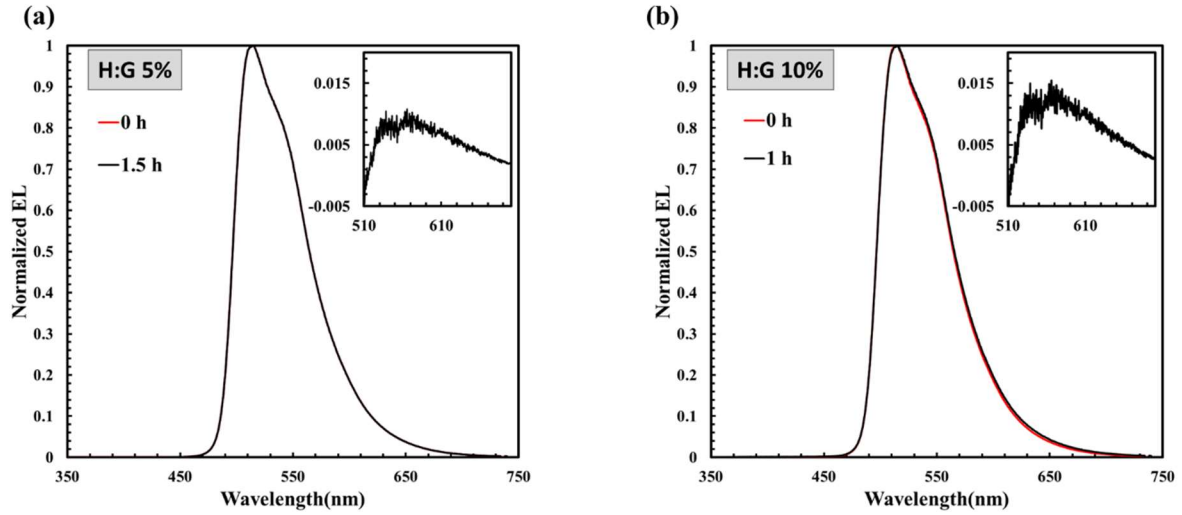
Figure 6.2. (a) EL spectra (normalized to the peak intensities) of (a) H:G 5%, and (b) H:G 10% OLEDs collected before and after electrical driving at 20 mA cm^{-2}. The insets show the mathematically calculated differences between the final and the initial spectra in each case.

To utilize high concentrations while avoiding guest aggregation, Ir(mppy)$_3$ and Ir(ppy)$_3$ were co-doped into CBP to form a Host:2Guest EML. In this system, Ir(mppy)$_3$ and Ir(ppy)$_3$ molecules act as molecular spacers for each other, preventing guest aggregation. Additionally, because Ir(mppy)$_3$ and Ir(ppy)$_3$ have comparable energy band gap, energy transfer from one guest to another one is inefficient, and as a result, H → G energy transfer can occur to either of them. Two groups of devices with the structure of ITO/HATCN/VB-FNPD/CBP:Ir(mppy)$_3$:Ir(ppy)$_3$/TPBi/LiF/Al were fabricated, where the concentration of guests was 5 wt% in one group (denoted as H:2G 5%) and 10 wt% in another group (denoted as H:2G 10%).

Figure 6.3 (a) exhibits the J-V-L characteristics of the fabricated OLEDs, where the H:2G 10% device shows both lower threshold voltage and leakage current compared with the H:2G 5% device, which is consistent with the J-V characteristics of the H:G 5% and H:G 10% OLEDs, observed in **Figure 6.1(a)**. The EQE vs current density characteristics of the OLEDs are shown in **Figure 6.3 (b)**.

The EQE$_{max}$ values of the H:2G 10% and H:2G 5% devices are 7.8% and 4.8%, respectively. The higher EQE of the H:2G 10% OLED may be associated with its better hole injection into the EML, which is consistent with the above results.

Figures 6.3 (c) and (d) depict the normalized luminance and changes in driving voltage versus time trends of the devices, respectively, while driven at a constant current density of 20 mA cm^{-2}. The LT50 of the H:2G 5% and H:G 10% devices is 2.2 h and 3 h, respectively, and the changes in driving voltage versus time trends for both devices are almost the same. Interestingly, the LT50 of the H:2G 10% device is 3× longer than that of the H:G 10%, despite both devices having the same guest concentration and EQE. The increased stability observed in the co-doped system can be attributed to the fact that Ir(mppy)$_3$ and Ir(ppy)$_3$ act as the molecular spacers for each other, preventing guest aggregation and leading to better dispersion of the guest molecules within the host matrix. This, in turn, results in more efficient H → G energy transfer and better EL stability.
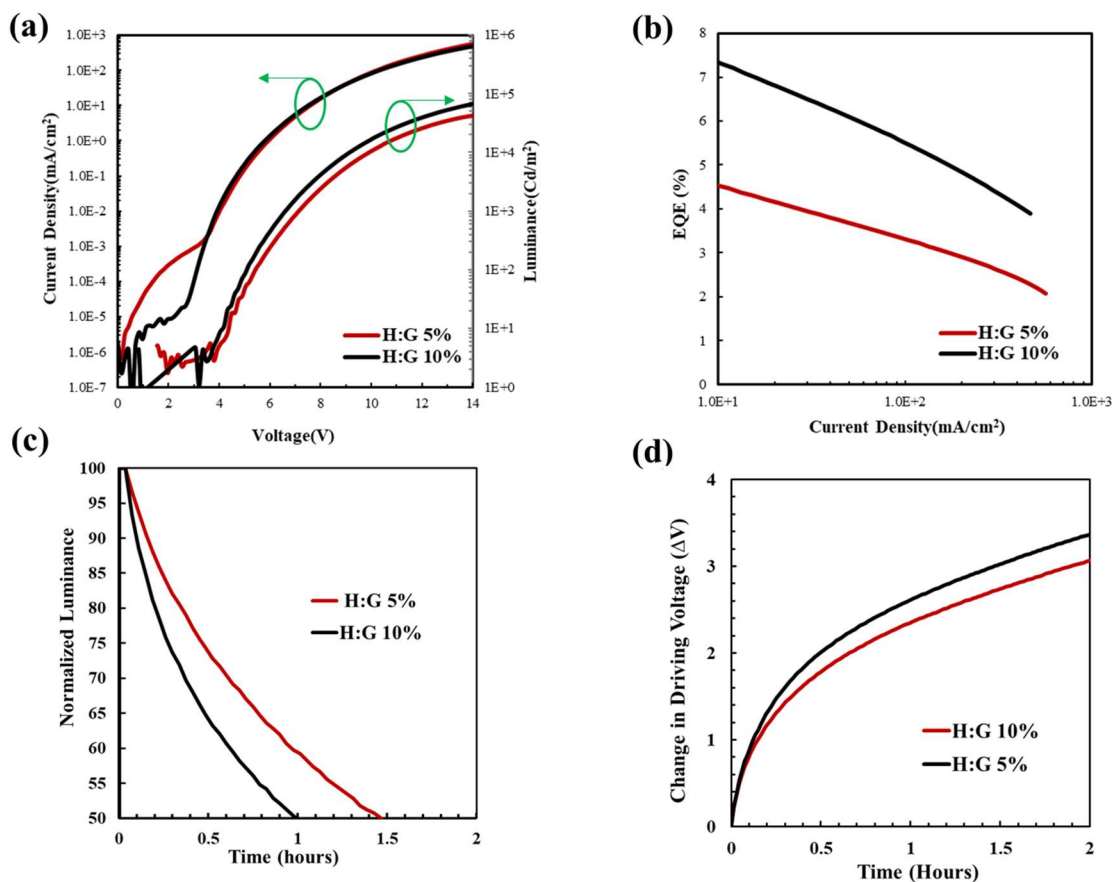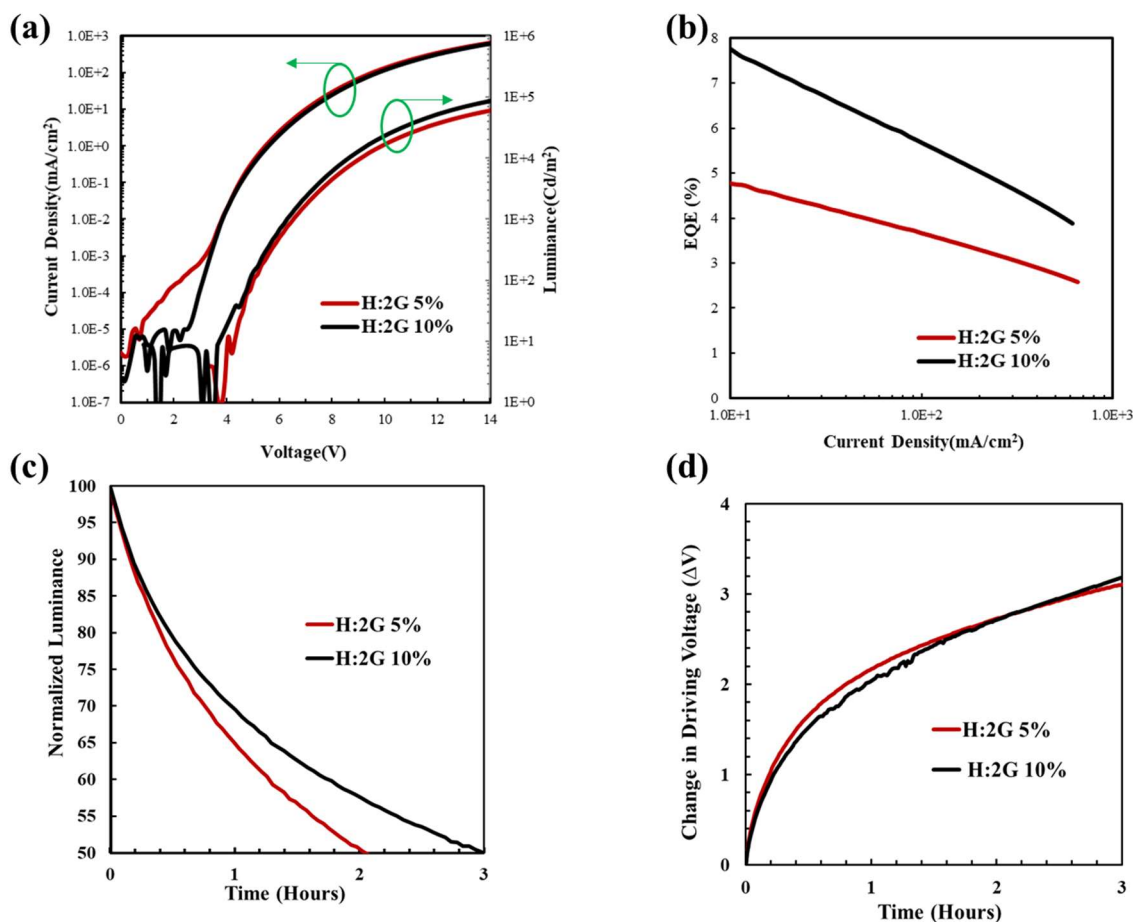
Figure 6.3. (a) Current density and luminance vs voltage characteristics, (b) EQE vs current density characteristics, (c) normalized luminance vs time and (d) changes in driving voltage vs time of H:2G 5% and H:2G 10% OLEDs. The luminescence is measured while driving the OLEDs at a 20 mA cm^{-2} current density.

To further explore this idea, the EL spectra of the H:2G 10% OLED collected at different time intervals during the electrical stress were examined, as shown in **Figure 6.4**. As seen, the intensity of the guest aggregation bands is lower in the case of the H:2G 10% device compared to its H:G 10% counterpart over time, indicating that the use of two dopants instead of one indeed reduces guest aggregation. For example, after 1 hour of electrical driving, the intensity of the guest aggregation band with a peak at 560 nm in the H:2G 10% device is three times lower than that in the H:G 10% device. The lower intensity of guest aggregation bands in the H:2G 10% suggests that it is less susceptible to

aggregation of the phosphorescent guests. On the other hand, faster guest aggregation in the H:G 10% OLED leads to less efficient H → G energy transfer, which, in turn, results in a shorter device lifetime.
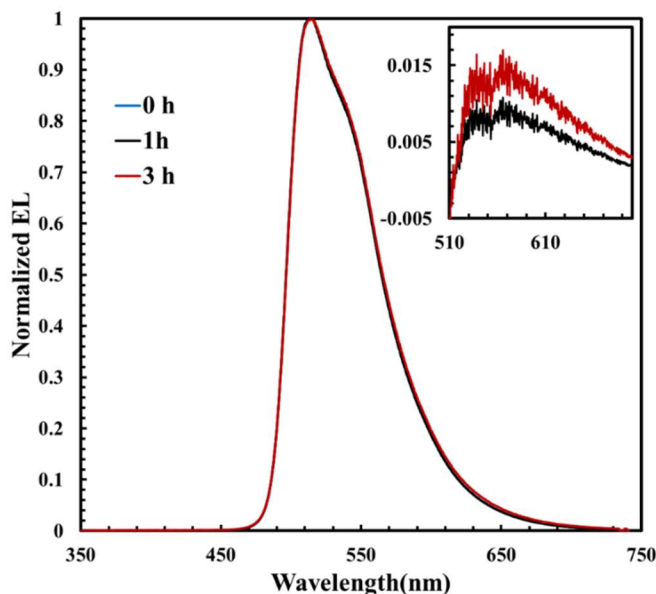
Figure 6.4. EL spectra (normalized to the peak intensities) of H:2G 10% OLED collected at different time intervals during the electrical driving at 20 mA cm^{-2}. The insets show the mathematically calculated differences between the final and the initial spectra in each case.

6.2 Improvement in the stability of SOL OLEDs using TADF emitters

Phosphorescent emitters often contain heavy metals, such as iridium or platinum, as the central atoms responsible for their phosphorescence properties. These metal-centered complexes are typically larger and more structurally complex compared to organic molecules. These structures can facilitate intermolecular interactions, such as metal-metal or π-π stacking interactions, which may lead to aggregation when emitters come into close proximity. Moreover, the presence of heavy metals can result in lower solubility in common organic solvents, making it challenging to achieve high concentrations of phosphorescent emitters in solution. It was found that increasing the phosphorescence emitter concentrations beyond 10 wt. % is inhibited by solubility issues in the formulation stage [77].

On the other hand, TADF emitters are predominantly organic materials. Organic materials generally exhibit greater solubility in common organic solvents compared to heavy metal-based phosphorescent

emitters. The improved solubility of TADF emitters in organic solvents allows for their incorporation into the EML of OLEDs at relatively high concentrations. Therefore, utilizing TADF emitters in SOL H:G systems holds promise in term of enhancing H → G energy transfer and improving operational stability.

In this study, two different TADF emitters, DACT-II and DMAC-BP, were doped into CBP to form H:G system. The results showed that increasing guest concentration from 10 wt. % to 30 wt. % in H:G systems leads to more efficient H → G energy transfer, and in turn, leads to a longer LT50. However, continuing to increase the guest concentration to 50 wt. % results in a deterioration of H → G energy transfer and leads to a lower device stability.

6.2.1 Results and Discussion

Figure 6.5(a) shows the J-V-L characteristics of fabricated OLEDs using the DACT-II emitter at different concentrations. By increasing the guest concentration from 10 wt. % to 30 wt. %, the current density increases at any given voltage. However, when continuing to increase the doping concentration to 50 wt. %, the current density decreases. The EQE vs current density characteristics follow the same trend, with the concentration of 30 wt. % yielding the highest EQE_{max}, as shown in **Figure 6.5(b)**.

The higher current density and EQE observed in devices with the doping concentration of 30 wt. % compared to devices with 10 wt. % doping concentration can be attributed to improved hole injection from the HTL into the increased guest molecules. However, when the doping concentration is further increased to 50 wt.%, the EQE_{max} decreases, possibly due to aggregation in the guest molecules, leading to reduced dispersion within the host matrix [130].

The effects of increasing the guest concentration on the J-V-L and EQE vs current density characteristics of devices containing DMAC-BP were also studied, as depicted in **Figures 6.5(c)** and **(d)**, respectively. As shown, similar trends were observed, with devices having a 30 wt. % doping concentration again exhibiting higher current density and EQE_{max} compared to the other devices.
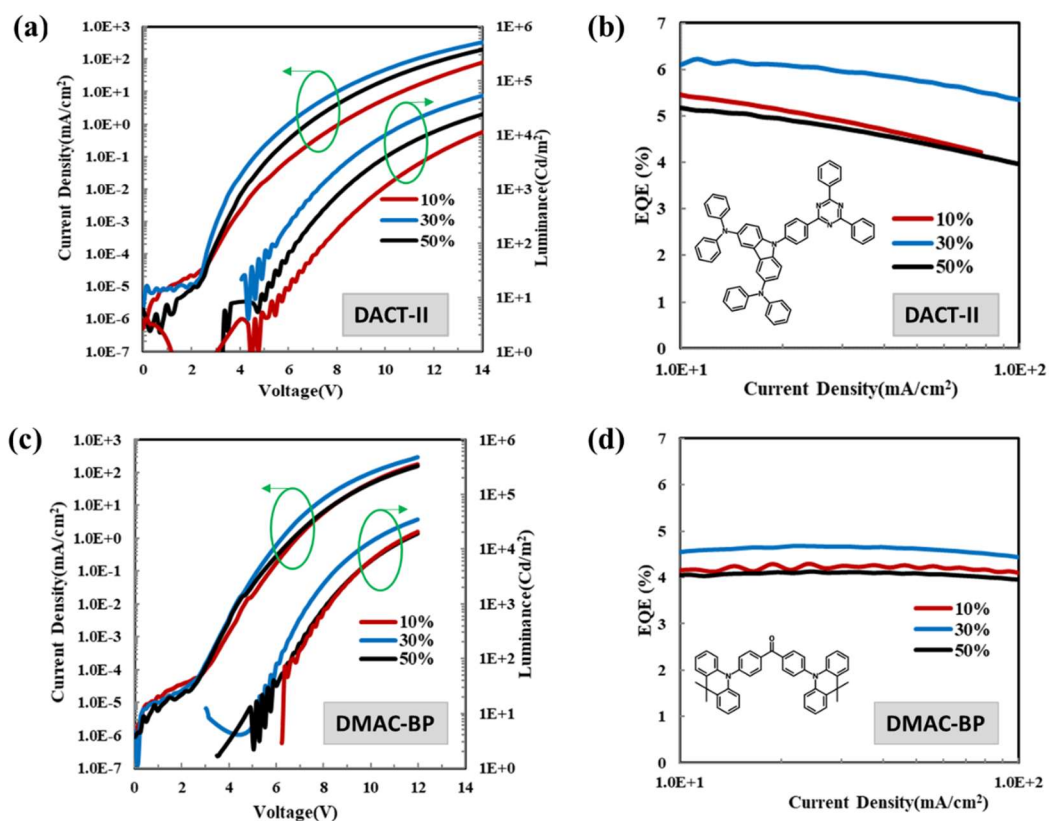
Figure 6.5. Current density and luminance vs voltage characteristics of devices with different concentrations of (a) DACT-II, and (c) DMAC-BP. EQE vs current density characteristics of devices with different concentrations of (b) DACT-II, and (d) DMAC-BP

Figure 6.6 depicts the changes in luminance over time under continuous electrical driving at 20 mA cm^{-2} for the devices. Additionally, **Table 6.1** summarizes the key performance data of the devices including L_0, LT50 at L_0, and LT50 at 100 cd m^{-2}, obtained using the lifetime scaling rule of L_0^nLT50=constant. In this formula, n represents the acceleration factor of 1.7, commonly used for TADF OLEDs [120]. The LT50s at 100 cd m^{-2} for devices with 10 wt. %, 20 wt. %, and 30 wt. % DACT-II concentrations are 212 h, 1530 h, and 478 h, respectively. Similarly, the LT50s at 100 cd m^{-2} for devices with 10 wt. %, 20 wt. %, and 30 wt. % DMAC-BP concentrations are 126 h, 614 h, and 208 h, respectively.

The results demonstrate that increasing the DACT-II (DMAC-BP) concentration from 10 wt. % to 30 wt. %, leads to a 7× (5×) increase in LT50 at 100 cd m^{-2}. However, further increasing the doping concentrations to 50 wt. % results in a decrease in LT50. Since any confounding effects in the other device layers have been eliminated, the varying stability of the devices must be solely attributed to the differences in their EMLs arising from the different doping concentrations.
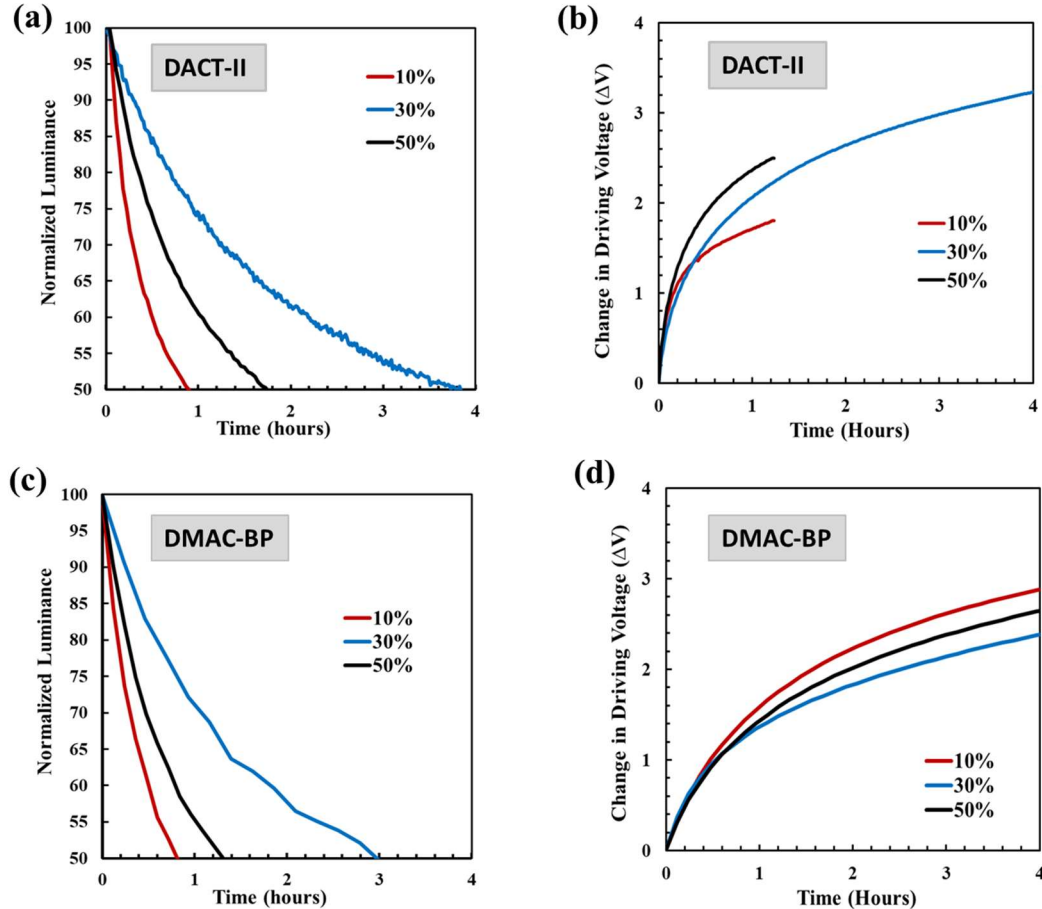
Figure 6.6 (a) Normalized luminance vs time of devices with different concentrations of (a) DACT-II and (c) DMAC-BP. Changes in driving voltage vs time of devices with different concentrations of (b) DACT-II and (d) DMAC-BP. The luminescence is measured while driving the OLEDs at a 20 mA cm^{-2} current density.

Table 6.1. EL performance parameters of the OLEDs with the EMLs described in the text.

	L_0^* (Cd m^{-2})		LT50 at L_0 (h)		L50 at 100 Cd m^{-2} (h)	
	DACT-II	DMAC-BP	DACT-II	DMAC-BP	DACT-II	DMAC-BP
10%	3500	2500	0.8	0.84	212	126
30%	4400	3000	3.9	3	1530	614
50%	3500	2600	1.8	1.3	478	208

*The numbers are rounded to the nearest hundred.

Figures 6.7(a) and **(b)** depict the EL spectra of the devices with different concentrations of DACT-II and DMAC-BP, respectively, at t = 0 h. A close comparison of the spectra shows that all spectra have some emission at around 370-400 nm which corresponds to the CBP host emission band [36, 41, 121]. To better visualize the relative heights of the host bands, the spectra are normalized to the guest band height, and a logarithmic scale is used. The relative intensity of this emission decreases upon increasing guest concentrations from 10 wt. % to 30 wt. %, while a further increase in the guest concentration to 50 wt. % leads to an increase in the intensity of the CBP host emission band.

Figures. 6.7(c) and **(d)** present the EL spectra of the same devices with DACT-II and DMAC-BP, respectively, after reaching the LT50 point. The relative intensity of CBP emission increases in all devices after electrical driving, the increase is however lower in the devices with 30 wt. % guest concentration, despite the longer stress time (3.9 h for the DACT-II device and 3 h for the DMAC-BP device).

In a well-dispersed H:G system, most host molecules are located within a few angstroms from a guest molecule, enabling efficient energy transfer from the host to the guest through Forster and Dexter processes. As a result, any luminescence originating from the host molecules is suppressed. The detection of the host emission band in the EL spectra points to incomplete H → G energy transfer. Since the intensity of the host emission band was lower in devices with 30 wt. % doping concentration compared to their 10 wt. % counterparts, this observation suggests that the energy transfer is more efficient in the former. This can be attributed to the fact that increasing the guest concentration will make it easier for excited host molecules to transfer their excitation energy quickly to the guest molecules, located within a few angstroms from the host molecules [39-41, 111].

Although we expected that increasing the guest concentrations would result in a higher efficient of H → G energy transfer, the increase in guest concentration from 30 wt. % to 50 wt. % surprisingly

leads to an increase in CBP band intensity, indicating a decrease in H → G energy transfer. This can be attributed to the aggregation of guest molecules at high concentrations, which reduces their intermixing within the host matrix. Thus, host excitons are unable to transfer their energy to the guests effectively [39].

We noted that there is also ≈10–20 nm difference between the peak positions by changing the guest concentrations, as seen in **Figure 6.7.** This disparity may perhaps be due to possible shifts in the location of the e–h recombination zone toward the cathode (yet still within the CBP:guest layer) upon changing the guest concentration [125].

Our results revealed that increasing the guest concentration from 10 wt. % to 30 wt. % in the H:G system leads to a more efficient H → G energy transfer, resulting in a longer LT50 of the devices. This observation highlights the importance of optimizing guest concentration in TADF emitters to enhance overall device performance.
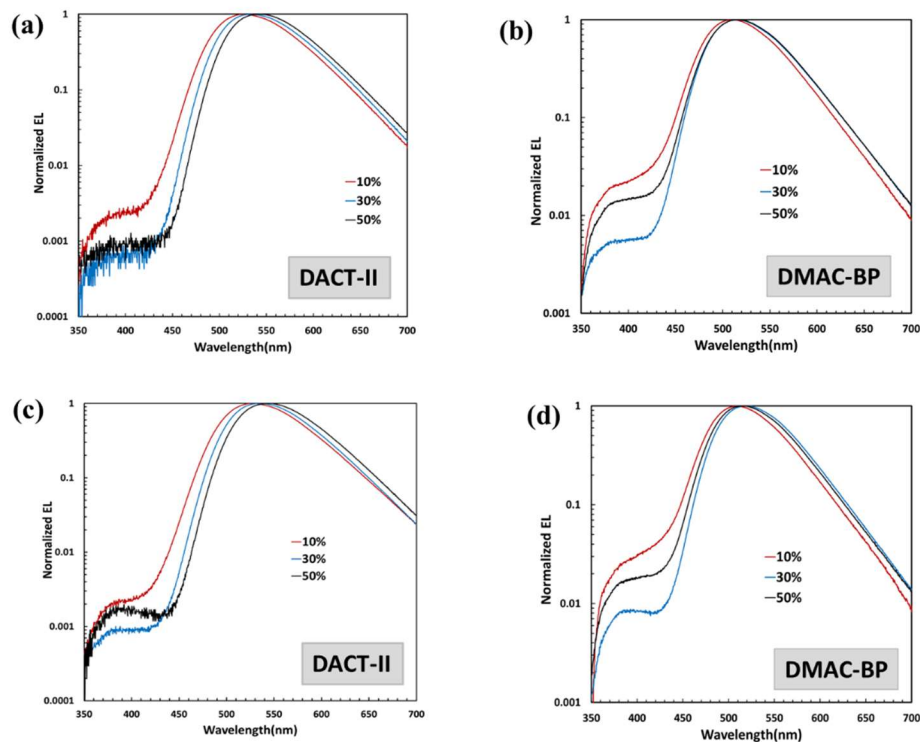
Figure 6.7. EL spectra (normalized to the guest emission peak intensity) collected at t=0 of the devices with different concentrations of (a) DACT-II and (b) DMAC-BP, and after reaching the LT50 point of the devices with different concentrations of (c) DACT-II and (d) DMAC-BP.

6.3 Conclusion

This chapter has been divided into two parts. The first part investigated a new approach for enhancing the EL stability of SOL phosphorescent OLEDs through the utilization of a co-doped system. The EL characteristics of the devices revealed that guest aggregation emission bands are significantly stronger in devices with single dopants, suggesting faster guest aggregation in those devices. Furthermore, the results demonstrated that the LT50 of devices with the co-doped system is 3× longer than devices with single dopants, despite using the same guest concentrations in both cases. Therefore, employing the co-doped system effectively mitigates fast guest aggregation in SOL devices, leading to enhanced H → G energy transfer and improved EL stability.

The second part of the chapter focused on examining the impact of increasing guest concentration on the H → G energy transfer and EL stability. To explore this, two different TADF emitters, which can be doped into the EML at a relatively high concentration compared to phosphorescence emitters, were doped to the host material to form EMLs. Our results revealed that increasing the guest concentration from 10 wt. % to 30 wt. % in the H:G system results in a more efficient H → G energy transfer, leading to a longer LT50 for the devices. However, further increasing the guest concentration to 50 wt. % leads to a deterioration in H → G energy transfer and ultimately reduces device stability. This study underscores the significance of optimizing guest concentration in TADF emitters to enhance device performance.

Overall, these findings indicate limited success in addressing the low EL stability issue of SOL OLEDs. Therefore there is a need to explore new molecular designs for guest materials that render them less susceptible to aggregation and effectively tackle the stability challenges.

Chapter 7 - Summary and Future Work

7.1 Summary of main conclusions

The main objective of this research was twofold: (i) to understand the role H → G energy transfer and guest materials in the lower stability of SOL versus VAC phosphorescent OLEDs, and (ii) to explore approaches to enhance the stability of SOL devices. The main findings of this study can be summarized as follows:

In chapter 4, the root causes of the lower stability of SOL H:G systems compared to their VAC counterparts were investigated. The results indicated that the faster degradation of SOL EML devices under electrical bias can be attributed – at least in part – to less efficient H → G energy transfer. Poor H → G energy transfer causes the concentration of exciton on the host to be greater which accelerates device degradation through increased exciton-polaron-induced aggregation. This initial inefficient H → G energy transfer leads to further increases H-G phase separation and further decreases the H → G energy transfer efficiency. Solubility limitations in case of the SOL system could be the source of this reduced energy transfer.

In chapter 5, the EL degradation mechanisms of devices made by solution-coating and vacuum-deposition containing various phosphorescent guests were studied. Results showed that the aggregation of the guest materials plays a key role in the lower electroluminescence stability of SOL devices. The solvent used in the solution-coating process leaves a morphological deposition that seems to be the main cause of the higher susceptibility of the guest materials to aggregation. The aggregation was also found to be driven by excitons and accelerated by the presence of polarons likely due to exciton-polaron interactions.

In chapter 6, two approaches were introduced, aimed at increasing guest concentrations and promoting their intermixing between host molecules while preventing guest aggregation: the co-doped system and the utilization of TADF emitters. In co-doped system two phosphorescent emitters with the same energy bandgaps were employed as molecular spacer for each other, deviating from the

conventional use of a single emitter. This approach effectively inhibited fast guest aggregation in SOL devices, leading to a more efficient H → G energy transfer and consequently improved EL stability. Specifically, Ir(mppy)$_3$ and Ir(ppy)$_3$ were co-doped into CBP to form a H:2G EML. The EL characteristics of the devices revealed that guest aggregation emission bands were significantly stronger in devices with single dopants, indicating a faster occurrence of guest aggregation in those devices. Moreover, the results demonstrated that devices with the co-doped system exhibited a 3× longer LT50 compared to devices with single dopants, despite using the same guest concentrations in both cases.

Additionally, the incorporation of TADF emitters into the EML offered the advantage of accommodating relatively high concentrations. Consequently, incorporating TADF emitters into SOL H:G systems exhibited promising outcomes in terms of enhancing H → G energy transfer and improving operational stability. The results showed that increasing the guest concentration from 10 wt.% to 30 wt.% in the H:G system resulted in a more efficient H → G energy transfer, leading to a longer LT50 for the devices.

7.2 Future work

This section outlines recommendations for future studies based on the conclusions and major findings derived from this work.

First, this work has revealed that in SOL H:G systems, solution-coating may produce film morphologies with some initial host and guest phase separation into guest-rich and guest-deficient domains, and guest aggregation accelerates the formation of guest-deficient domains. Consequently, it is more difficult for excited host molecules in these domains to lose their excitation energy as quickly, in turn making them more susceptible to exciton-induced degradation and aggregation. Therefore, it is necessary to adopt new molecular designs for guest materials that make them less susceptible to aggregation for the development of SOL OLEDs with high performance. Future studies can focus on designing and synthesizing novel guest materials with improved stability and reduced aggregation tendencies. This can involve exploring different molecular structures, functional groups, or chemical modifications to enhance the performance of SOL OLEDs. For instance, guest materials incorporating a tert-butyl group can be considered. The presence of a bulky tert-butyl group prevents π-π stacking in the materials, resulting in similar energy gap (i.e. HOMO/LUMO levels) between the molecules in the solution and the solid state. Incorporating materials with a tert-butyl group as guests can effectively

reduce molecular aggregation and mitigate the phase separation issues that contribute to the lower stability of SOL OLEDs compared to VAC counterparts.

Second, the findings indicated that co-doped system approach shows promise in inhibiting guest aggregation and improving H → G energy transfer. Further exploration of co-doped systems can be conducted to explore different combinations of co-doped emitters and optimize their concentrations, aiming to achieve better stability and performance in SOL devices. This can involve studying different phosphorescent emitters with similar energy bandgaps and evaluating their synergistic effects when used as molecular spacers for each other. By fine-tuning the doping concentrations, it may be possible to maximize the inhibitory effect on guest aggregation and improve the efficiency of H → G energy transfer, ultimately leading to superior stability and performance in SOL devices.

Furthermore, as demonstrated in this study, the utilization of TADF emitters in SOL H:G systems has shown potential for enhancing energy transfer and operational stability. Future research can concentrate on evaluating a broader range of TADF emitters, investigating their synthesis, characterization, and performance in SOL OLEDs. This comprehensive investigation can yield valuable insights into the underlying mechanisms governing their efficacy and assess their applicability for practical device implementations. By exploring various TADF emitters, their molecular structures, and their interactions within the EML, a deeper understanding can be gained, paving the way for the development of advanced SOL OLEDs with improved stability and performance.

References

[1]   M. Pope, H. P. Kallmann, and P. Magnante, "Electroluminescence in organic crystals," *The Journal of Chemical Physics,* vol. 38, no. 8, pp. 2042-2043, 1963.

[2]   P. Vincett, W. Barlow, R. Hann, and G. Roberts, "Electrical conduction and low voltage blue electroluminescence in vacuum-deposited organic films," *Thin solid films,* vol. 94, no. 2, pp. 171-183, 1982.

[3]   C. W. Tang and S. A. VanSlyke, "Organic electroluminescent diodes," *Applied physics letters,* vol. 51, no. 12, pp. 913-915, 1987.

[4]   D. J. Gaspar and E. Polikarpov, *OLED fundamentals: materials, devices, and processing of organic light-emitting diodes*. CRC press, 2015.

[5]   S. Tse, C. Cheung, and S. So, "Charge transport and injection in amorphous organic semiconductors," in *Organic Electronics*: CRC Press, 2009, pp. 75-124.

[6]   A. Dey, A. Singh, D. Das, and P. K. Iyer, "Organic semiconductors: a new future of nanodevices and applications," *Thin Film Structures in Energy Applications,* pp. 97-128, 2015.

[7]   J. A. Barltrop and J. D. Coyle, *Principles of photochemistry*. Wiley, 1978.

[8]   Y. Tao *et al.*, "Thermally activated delayed fluorescence materials towards the breakthrough of organoelectronics," *Advanced materials,* vol. 26, no. 47, pp. 7931-7958, 2014.

[9]   C. T. Ernest, *High-resolution studies of the A1A2-X1A1 electronic transition of formaldehyde: Spectroscopy and photochemistry*. University of Miami, 2011.

[10]   G. Hong *et al.*, "A brief history of OLEDs—emitter development and industry milestones," *Advanced Materials,* vol. 33, no. 9, p. 2005630, 2021.

[11]   C. Adachi *et al.*, "Organic light-emitting diodes (OLEDs): materials, photophysics, and device physics," in *Organic Electronics Materials and Devices*: Springer, 2015, pp. 43-73.

[12]   K. H. Kim and J. J. Kim, "Origin and Control of Orientation of Phosphorescent and TADF Dyes for High-Efficiency OLEDs," *Advanced Materials,* vol. 30, no. 42, p. 1705600, 2018.

[13]   H. Inoue *et al.*, "Deep-blue phosphorescent organic light-emitting diode with external quantum efficiency over 30% using novel Ir complex," in *Organic Light Emitting Materials and Devices XX*, 2016, vol. 9941, p. 994127: International Society for Optics and Photonics.

[14]   L. Xiao *et al.*, "Recent progresses on materials for electrophosphorescent organic light-emitting devices," *Advanced Materials,* vol. 23, no. 8, pp. 926-952, 2011.

[15]   H. Kaji *et al.*, "Purely organic electroluminescent material realizing 100% conversion from electricity to light," *Nature communications,* vol. 6, no. 1, pp. 1-8, 2015.

[16]   C. K. Moon, K. Suzuki, K. Shizu, C. Adachi, H. Kaji, and J. J. Kim, "Combined inter-and intramolecular charge-transfer processes for highly efficient fluorescent organic light-emitting diodes with reduced triplet exciton quenching," *Advanced Materials,* vol. 29, no. 17, p. 1606448, 2017.

[17]   T. A. Lin *et al.*, "Sky-blue organic light emitting diode with 37% external quantum efficiency using thermally activated delayed fluorescence from spiroacridine-triazine hybrid," *Advanced Materials,* vol. 28, no. 32, pp. 6976-6983, 2016.

[18]   D. P.-K. Tsang, T. Matsushima, and C. Adachi, "Operational stability enhancement in organic light-emitting diodes with ultrathin Liq interlayers," *Scientific reports,* vol. 6, no. 1, pp. 1-10, 2016.

[19] T. Kamata, H. Sasabe, M. Igarashi, and J. Kido, "A novel sterically bulky hole transporter to remarkably improve the lifetime of thermally activated delayed fluorescent OLEDs at high brightness," *Chemistry–A European Journal,* vol. 24, no. 18, pp. 4590-4596, 2018.

[20] S. R. Forrest, "The path to ubiquitous and low-cost organic electronic appliances on plastic," *nature,* vol. 428, no. 6986, pp. 911-918, 2004.

[21] L. Duan *et al.*, "Solution processable small molecules for organic light-emitting diodes," *Journal of Materials Chemistry,* vol. 20, no. 31, pp. 6392-6407, 2010.

[22] J. H. Kwon, R. Pode, H. D. Kim, and H. K. Chung, "High-performance organic light-emitting diode displays," *Applications of Organic and Printed Electronics: A Technology-Enabled Revolution,* pp. 57-81, 2013.

[23] M. C. Petty, *Molecular electronics: from principles to practice*. John Wiley & Sons, 2008.

[24] N. C. Greenham, R. H. Friend, and D. D. Bradley, "Angular dependence of the emission from a conjugated polymer light-emitting diode: implications for efficiency calculations," *Advanced Materials,* vol. 6, no. 6, pp. 491-494, 1994.

[25] S. Chen, J. Yu, Y. Jiang, R. Chen, and T. K. Ho, *Active-matrix organic light-emitting display technologies*. Bentham Science Publishers, 2015.

[26] T.-H. Han, M.-R. Choi, C.-W. Jeon, Y.-H. Kim, S.-K. Kwon, and T.-W. Lee, "Ultrahigh-efficiency solution-processed simplified small-molecule organic light-emitting diodes using universal host materials," *Science advances,* vol. 2, no. 10, p. e1601428, 2016.

[27] J.-H. Jou *et al.*, "High-efficiency blue organic light-emitting diodes using a 3, 5-di (9H-carbazol-9-yl) tetraphenylsilane host via a solution-process," *Journal of Materials Chemistry,* vol. 20, no. 38, pp. 8411-8416, 2010.

[28] C. W. Lee, K. S. Yook, and J. Y. Lee, "Synthesis and device application of hybrid host materials of carbazole and benzofuran for high efficiency solution processed blue phosphorescent organic light-emitting diodes," *Organic Electronics,* vol. 14, no. 3, pp. 1009-1014, 2013.

[29] K. S. Yook and J. Y. Lee, "Solution processed deep blue phosphorescent organic light-emitting diodes with over 20% external quantum efficiency," *Organic Electronics,* vol. 12, no. 10, pp. 1711-1715, 2011.

[30] K. S. Yook and J. Y. Lee, "Small molecule host materials for solution processed phosphorescent organic light-emitting diodes," *Advanced Materials,* vol. 26, no. 25, pp. 4218-4233, 2014.

[31] Y. J. Cho, B. D. Chin, S. K. Jeon, and J. Y. Lee, "20% External Quantum Efficiency in Solution-Processed Blue Thermally Activated Delayed Fluorescent Devices," *Advanced Functional Materials,* vol. 25, no. 43, pp. 6786-6792, 2015.

[32] M. Cai, T. Xiao, E. Hellerich, Y. Chen, R. Shinar, and J. Shinar, "High-efficiency solution-processed small molecule electrophosphorescent organic light-emitting diodes," *Advanced Materials,* vol. 23, no. 31, pp. 3590-3596, 2011.

[33] T. W. Lee *et al.*, "Characteristics of solution-processed small-molecule organic films and light-emitting diodes compared with their vacuum-deposited counterparts," *Advanced Functional Materials,* vol. 19, no. 10, pp. 1625-1630, 2009.

[34] B. Zhang *et al.*, "High-efficiency single emissive layer white organic light-emitting diodes based on solution-processed dendritic host and new orange-emitting iridium complex," *Advanced Materials,* vol. 24, no. 14, pp. 1873-1877, 2012.

[35] Y. J. Cho, Y. Zhang, H. Yu, and H. Aziz, "The Root Causes of the Limited Stability of Solution-Coated Small-Molecule Organic Light-Emitting Devices: Faster Host Aggregation by Exciton–Polaron Interactions," *Advanced Functional Materials,* vol. 26, no. 47, pp. 8662-8669, 2016.

[36] Y. J. Cho, S. Taylor, and H. Aziz, "Increased electromer formation and charge trapping in solution-processed versus vacuum-deposited small molecule host materials of organic light-emitting devices," *ACS applied materials & interfaces,* vol. 9, no. 46, pp. 40564-40572, 2017.

[37] S. Stolz, Y. Zhang, U. Lemmer, G. Hernandez-Sosa, and H. Aziz, "Degradation mechanisms in organic light-emitting diodes with polyethylenimine as a solution-processed electron injection layer," *ACS applied materials & interfaces,* vol. 9, no. 3, pp. 2776-2785, 2017.

[38] Q. Wang and H. Aziz, "Degradation of organic/organic interfaces in organic light-emitting devices due to polaron–exciton interactions," *ACS applied materials & interfaces,* vol. 5, no. 17, pp. 8733-8739, 2013.

[39] Q. Wang and H. Aziz, "Exciton–Polaron-Induced Aggregation of Organic Electroluminescent Materials: A Major Degradation Mechanism in Wide-Bandgap Phosphorescent and Fluorescent Organic Light-Emitting Devices," *Advanced Optical Materials,* vol. 3, no. 7, pp. 967-975, 2015.

[40] Q. Wang, B. Sun, and H. Aziz, "Exciton–polaron-induced aggregation of wide-bandgap materials and its implication on the electroluminescence stability of phosphorescent organic light-emitting devices," *Advanced Functional Materials,* vol. 24, no. 20, pp. 2975-2985, 2014.

[41] Y. Zhang and H. Aziz, "Influence of the guest on aggregation of the host by exciton–polaron interactions and its effects on the stability of phosphorescent organic light-emitting devices," *ACS applied materials & interfaces,* vol. 8, no. 22, pp. 14088-14095, 2016.

[42] N. C. Giebink *et al.*, "Intrinsic luminance loss in phosphorescent small-molecule organic light emitting devices due to bimolecular annihilation reactions," *Journal of Applied Physics,* vol. 103, no. 4, p. 044509, 2008.

[43] S. Kim *et al.*, "Degradation of blue-phosphorescent organic light-emitting devices involves exciton-induced generation of polaron pair within emitting layers," *Nature communications,* vol. 9, no. 1, pp. 1-11, 2018.

[44] J.-M. Kim, C.-H. Lee, and J.-J. Kim, "Mobility balance in the light-emitting layer governs the polaron accumulation and operational stability of organic light-emitting diodes," *Applied Physics Letters,* vol. 111, no. 20, p. 203301, 2017.

[45] S. Feng *et al.*, "A comparison study of the organic small molecular thin films prepared by solution process and vacuum deposition: roughness, hydrophilicity, absorption, photoluminescence, density, mobility, and electroluminescence," *The Journal of Physical Chemistry C,* vol. 115, no. 29, pp. 14278-14284, 2011.

[46] X. Xing *et al.*, "Essential differences of organic films at the molecular level via vacuum deposition and solution processes for organic light-emitting diodes," *The Journal of Physical Chemistry C,* vol. 117, no. 48, pp. 25405-25408, 2013.

[47] Y. J. Cho and H. Aziz, "Root causes of the limited electroluminescence stability of organic light-emitting devices made by solution-coating," *ACS applied materials & interfaces,* vol. 10, no. 21, pp. 18113-18122, 2018.

[48] S. Liu, C. Peng, A. Cruz, Y. Chen, and F. So, "Degradation study of organic light-emitting diodes with solution-processed small molecule phosphorescent emitting layers," *Journal of Materials Chemistry C,* vol. 4, no. 37, pp. 8696-8703, 2016.

[49] D. Kondakov, W. Lenhart, and W. Nichols, "Operational degradation of organic light-emitting diodes: Mechanism and identification of chemical products," *Journal of Applied Physics,* vol. 101, no. 2, p. 024512, 2007.

[50] S. Sudheendran Swayamprabha *et al.*, "Approaches for long lifetime organic light emitting diodes," *Advanced Science,* vol. 8, no. 1, p. 2002254, 2021.

[51] P. Burrows and S. Forrest, "Electroluminescence from trap-limited current transport in vacuum deposited organic light emitting devices," *Applied Physics Letters,* vol. 64, no. 17, pp. 2285-2287, 1994.

[52] P. Burrows, V. Bulovic, S. Forrest, L. S. Sapochak, D. McCarty, and M. Thompson, "Reliability and degradation of organic light emitting devices," *applied physics letters,* vol. 65, no. 23, pp. 2922-2924, 1994.

[53] H. Aziz, Z. D. Popovic, N.-X. Hu, A.-M. Hor, and G. Xu, "Degradation mechanism of small molecule-based organic light-emitting devices," *Science,* vol. 283, no. 5409, pp. 1900-1902, 1999.

[54] N. C. Giebink, B. D'Andrade, M. Weaver, J. Brown, and S. Forrest, "Direct evidence for degradation of polaron excited states in organic light emitting diodes," *Journal of Applied Physics,* vol. 105, no. 12, p. 124514, 2009.

[55] Y. Luo, H. Aziz, G. Xu, and Z. D. Popovic, "Electron-induced quenching of excitons in luminescent materials," *Chemistry of materials,* vol. 19, no. 9, pp. 2288-2291, 2007.

[56] M. Matsumura, A. Ito, and Y. Miyamae, "Accumulation of positive charges in organic light-emitting diodes with a double-layer structure," *Applied physics letters,* vol. 75, no. 8, pp. 1042-1044, 1999.

[57] D. Y. Kondakov, J. R. Sandifer, C. W. Tang, and R. H. Young, "Nonradiative recombination centers and electrical aging of organic light-emitting diodes: Direct connection between accumulation of trapped charge and luminance loss," *Journal of applied physics,* vol. 93, no. 2, pp. 1108-1119, 2003.

[58] D. Kondakov, "Direct observation of deep electron traps in aged organic light emitting diodes," *Journal of applied physics,* vol. 97, no. 2, p. 024503, 2005.

[59] Q. Wang and H. Aziz, "The different influence of singlet and triplet excitons in the degradation of phosphorescent organic light-emitting devices due to exciton–polaron-induced aggregation of host materials," *Organic Electronics,* vol. 26, pp. 464-470, 2015.

[60] L. J. Rothberg and A. J. Lovinger, "Status of and prospects for organic electroluminescence," *Journal of Materials Research,* vol. 11, no. 12, pp. 3174-3187, 1996.

[61] S.-C. Dong, L. Xu, and C. W. Tang, "Chemical degradation mechanism of TAPC as hole transport layer in blue phosphorescent OLED," *Organic Electronics,* vol. 42, pp. 379-386, 2017.

[62] Q. Lin *et al.*, "Cadmium-free quantum dots based violet light-emitting diodes: High-efficiency and brightness via optimization of organic hole transport layers," *Organic Electronics,* vol. 25, pp. 178-183, 2015.

[63] L. Zheng *et al.*, "Solution-processed blue quantum-dot light-emitting diodes based on double hole transport layers: Charge injection balance, solvent erosion control and performance improvement," *Superlattices and Microstructures,* vol. 140, p. 106460, 2020.

[64] L. Lan *et al.*, "Preparation of efficient quantum dot light-emitting diodes by balancing charge injection and sensitizing emitting layer with phosphorescent dye," *Journal of Materials Chemistry C,* vol. 7, no. 19, pp. 5755-5763, 2019.

[65] F. Huang, Y.-J. Cheng, Y. Zhang, M. S. Liu, and A. K.-Y. Jen, "Crosslinkable hole-transporting materials for solution processed polymer light-emitting diodes," *Journal of Materials Chemistry,* vol. 18, no. 38, pp. 4495-4509, 2008.

[66] A. Köhnen, N. Riegel, J. H. W. Kremer, H. Lademann, D. C. Müller, and K. Meerholz, "The simple way to solution-processed multilayer OLEDs–layered block-copolymer networks by living cationic polymerization," *Advanced Materials,* vol. 21, no. 8, pp. 879-884, 2009.

[67] M. C. Gather, A. Koehnen, A. Falcou, H. Becker, and K. Meerholz, "Solution-processed full-color polymer organic light-emitting diode displays fabricated by direct photolithography," *Advanced Functional Materials,* vol. 17, no. 2, pp. 191-200, 2007.

[68] N. Rehmann, D. Hertel, K. Meerholz, H. Becker, and S. Heun, "Highly efficient solution-processed phosphorescent multilayer organic light-emitting diodes based on small-molecule hosts," *Applied Physics Letters,* vol. 91, no. 10, p. 103507, 2007.

[69] G. Liaptsis and K. Meerholz, "Crosslinkable TAPC-based hole-transport materials for solution-processed organic light-emitting diodes with reduced efficiency roll-off," *Advanced Functional Materials,* vol. 23, no. 3, pp. 359-365, 2013.

[70] G. Liaptsis, D. Hertel, and K. Meerholz, "Solution processed organic double light-emitting layer diode based on cross-linkable small molecular systems," *Angewandte Chemie,* vol. 125, no. 36, pp. 9742-9746, 2013.

[71] S. Wang, H. Zhang, B. Zhang, Z. Xie, and W.-Y. Wong, "Towards high-power-efficiency solution-processed OLEDs: Material and device perspectives," *Materials Science and Engineering: R: Reports,* vol. 140, p. 100547, 2020.

[72] M. S. Liu *et al.*, "Thermally cross-linkable hole-transporting materials for improving hole injection in multilayer blue-emitting phosphorescent polymer light-emitting diodes," *Macromolecules,* vol. 41, no. 24, pp. 9570-9580, 2008.

[73] Y. H. Niu *et al.*, "Crosslinkable Hole-Transport Layer on Conducting Polymer for High-Efficiency White Polymer Light-Emitting Diodes," *Advanced Materials,* vol. 19, no. 2, pp. 300-304, 2007.

[74] S. Ho, S. Liu, Y. Chen, and F. So, "Review of recent progress in multilayer solution-processed organic light-emitting diodes," *Journal of Photonics for Energy,* vol. 5, no. 1, p. 057611, 2015.

[75] S.-W. Chao *et al.*, "Cross-linkable hole transporting layers boost operational stability of high-performance quantum dot light-emitting device," *Organic Electronics,* vol. 71, pp. 206-211, 2019.

[76] C. Xiang *et al.*, "Phosphorescent organic light emitting diodes with a cross-linkable hole transporting material," *Organic Electronics,* vol. 15, no. 7, pp. 1702-1706, 2014.

[77] F. Samaeifar, H. Yu, T. Davidson-Hall, M. Sadeghianlemraski, D. S. Chung, and H. Aziz, "Host-to-Guest Energy Transfer and Its Role in the Lower Stability of Solution-Coated versus Vacuum-Deposited Phosphorescent OLEDs," *The Journal of Physical Chemistry C,* vol. 125, no. 36, pp. 20094-20103, 2021.

[78] N. Aizawa *et al.*, "Solution-processed multilayer small-molecule light-emitting devices with high-efficiency white-light emission," *Nature communications,* vol. 5, no. 1, pp. 1-7, 2014.

[79] X. Gong, S. Wang, D. Moses, G. C. Bazan, and A. J. Heeger, "Multilayer polymer light-emitting diodes: white-light emission with high efficiency," *Advanced Materials,* vol. 17, no. 17, pp. 2053-2058, 2005.

[80] T. Ye, S. Shao, J. Chen, L. Wang, and D. Ma, "Efficient phosphorescent polymer yellow-light-emitting diodes based on solution-processed small molecular electron transporting layer," *ACS applied materials & interfaces,* vol. 3, no. 2, pp. 410-416, 2011.

[81] C. M. Hansen, *Hansen solubility parameters: a user's handbook*. CRC press, 2007.

[82] Y. Fujii, H. Atarashi, M. Hino, T. Nagamura, and K. Tanaka, "Interfacial width in polymer bilayer films prepared by double-spin-coating and flotation methods," *ACS applied materials & interfaces,* vol. 1, no. 9, pp. 1856-1859, 2009.

[83] H. Yu and H. Aziz, "The negative effect of toluene on poly (3, 4-ethylenedioxythiophene)-poly (styrenesulfonate)(PEDOT: PSS) hole injection layer and its role in reducing the stability of solution-coated organic light-emitting devices," *Synthetic Metals,* vol. 273, p. 116704, 2021.

[84]   Q. Wang *et al.*, "Modifying organic/metal interface via solvent treatment to improve electron injection in organic light emitting diodes," *Organic Electronics,* vol. 12, no. 11, pp. 1858-1863, 2011.

[85]   Q. Wang *et al.*, "Solvent treatment as an efficient anode modification method to improve device performance of polymer light-emitting diodes," *Organic electronics,* vol. 14, no. 2, pp. 548-553, 2013.

[86]   D.-J. Yun *et al.*, "Study on the disparate transition behaviors of the electrical/physical properties in PEDOT: PSS film depending on solvent species under a follow-up solution-treatment process," *Nanotechnology,* vol. 27, no. 16, p. 165706, 2016.

[87]   T. Davidson-Hall and H. Aziz, "Significant enhancement in quantum dot light-emitting device stability via a cascading hole transport layer," *ACS applied materials & interfaces,* vol. 12, no. 14, pp. 16782-16791, 2020.

[88]   S. C. Xia, R. C. Kwong, V. I. Adamovich, M. S. Weaver, and J. J. Brown, "OLED device operational lifetime: Insights and challenges," in *2007 IEEE International Reliability Physics Symposium Proceedings. 45th Annual*, 2007, pp. 253-257: IEEE.

[89]   P. Kaur, V. Karar, and N. Marriwala, "Study of effect of environmental factors on organic light emitting diode (OLED) displays: a review," *IOSR J. Electron. Commun. Eng,* vol. 1, no. 01, pp. 84-89, 2016.

[90]   H. Fujimoto *et al.*, "Influence of vacuum chamber impurities on the lifetime of organic light-emitting diodes," *Scientific reports,* vol. 6, no. 1, pp. 1-9, 2016.

[91]   H. Fujimoto *et al.*, "Killer impurities in vacuum chamber that affect the lifetime of organic light-emitting diodes," *Applied Physics Letters,* vol. 116, no. 14, p. 143301, 2020.

[92]   H. Aziz and Z. D. Popovic, "Degradation phenomena in small-molecule organic light-emitting devices," *Chemistry of Materials,* vol. 16, no. 23, pp. 4522-4532, 2004.

[93]   G. Baldacchini, T. Baldacchini, A. Pace, and R. B. Pode, "Emission intensity and degradation processes of Alq3 films," *Electrochemical and Solid State Letters,* vol. 8, no. 10, p. J24, 2005.

[94]   J. E. Knox, M. D. Halls, H. P. Hratchian, and H. B. Schlegel, "Chemical failure modes of AlQ3-based OLEDs: AlQ3 hydrolysis," *Physical Chemistry Chemical Physics,* vol. 8, no. 12, pp. 1371-1377, 2006.

[95]   D. W. Gotthold, "14. Vapor Deposition Methods and Technologies," *OLED Fundamentals: Materials, Devices, and Processing of Organic Light-Emitting Diodes,* p. 365, 2015.

[96]   A. Oostra, "Towards Self-Healing Organic Electronics," University of Groningen, 2016.

[97]   A. J. Oostra, P. W. Blom, and J. J. Michels, "Prevention of short circuits in solution-processed OLED devices," *Organic Electronics,* vol. 15, no. 6, pp. 1166-1172, 2014.

[98]   H. Becker, I. Bach, M. Holbach, J. Schwaiger, and H. Spreitzer, "5.1: Purity of OLED-Materials and the Implication on DevicePerformance," in *SID Symposium Digest of Technical Papers*, 2010, vol. 41, no. 1, pp. 39-42: Wiley Online Library.

[99]   H. Kim, Y. Byun, R. R. Das, B.-K. Choi, and P.-S. Ahn, "Small molecule based and solution processed highly efficient red electrophosphorescent organic light emitting devices," *Applied Physics Letters,* vol. 91, no. 9, p. 093512, 2007.

[100]   M. Shibata, Y. Sakai, and D. Yokoyama, "Advantages and disadvantages of vacuum-deposited and spin-coated amorphous organic semiconductor films for organic light-emitting diodes," *Journal of Materials Chemistry C,* vol. 3, no. 42, pp. 11178-11191, 2015.

[101]   S. Tokito, H. Tanaka, K. Noda, A. Okada, and Y. Taga, "Thermal stability in oligomeric triphenylamine/tris (8-quinolinolato) aluminum electroluminescent devices," *Applied physics letters,* vol. 70, no. 15, pp. 1929-1931, 1997.

[102] Y. Shirota and H. Kageyama, "Charge carrier transporting molecular materials and their applications in devices," *Chemical reviews,* vol. 107, no. 4, pp. 953-1010, 2007.

[103] D. Yokoyama, "Molecular orientation in small-molecule organic light-emitting diodes," *Journal of Materials Chemistry,* vol. 21, no. 48, pp. 19187-19202, 2011.

[104] M. Ishihara, K. Okumoto, and Y. Shirota, "Effects of the method of preparation of organic thin films and chemical doping on charge injection from electrodes," in *Organic Light-Emitting Materials and Devices VII*, 2004, vol. 5214, pp. 133-140: International Society for Optics and Photonics.

[105] K. M. Kuznetsov *et al.*, "Eu (tta) 3 DPPZ-based organic light-emitting diodes: spin-coating vs vacuum-deposition," *Dalton Transactions,* 2021.

[106] Z. Wang, Y. Lou, S. Naka, and H. Okada, "Direct comparison of solution-and vacuum-processed small molecular organic light-emitting devices with a mixed single layer," *ACS applied materials & interfaces,* vol. 3, no. 7, pp. 2496-2503, 2011.

[107] Z. Wang, Y. Lou, S. Naka, and H. Okada, "Highly simplified small molecular phosphorescent organic light emitting devices with a solution-processed single layer," *AIP Advances,* vol. 1, no. 3, p. 032130, 2011.

[108] C. W. Lee and J. Y. Lee, "High Quantum Efficiency in Solution and Vacuum Processed Blue Phosphorescent Organic Light Emitting Diodes Using a Novel Benzofuropyridine-Based Bipolar Host Material," *Advanced Materials,* vol. 25, no. 4, pp. 596-600, 2013.

[109] G. Mao *et al.*, "Considerable improvement in the stability of solution processed small molecule OLED by annealing," *Applied surface science,* vol. 257, no. 17, pp. 7394-7398, 2011.

[110] D. K. Mangalore, P. W. Blom, and G.-J. A. Wetzelaer, "Hole-transport comparison between solution-processed and vacuum-deposited organic semiconductors," *APL Materials,* vol. 7, no. 1, p. 011105, 2019.

[111] H. Yu and H. Aziz, "Differences in Photoluminescence Stability and Host-to-Guest Energy Transfer in Solution-Coated Versus Vacuum-Deposited Electroluminescent Host: Guest Small-Molecule Materials," *The Journal of Physical Chemistry C,* vol. 124, no. 21, pp. 11701-11707, 2020.

[112] E. Ito, H. Ito, H. Kang, T. Hayashi, M. Hara, and J. Noh, "Influence of surface morphology and substrate on thermal stability and desorption behavior of octanethiol self-assembled monolayers: Cu, Ag, and Au," *The Journal of Physical Chemistry C,* vol. 116, no. 33, pp. 17586-17593, 2012.

[113] A. Ahmadi and T. Wu, "Electrocatalytic reduction of nitrobenzene using TiO2 nanotube electrodes with different morphologies: Kinetics, mechanism, and degradation pathways," *Chemical Engineering Journal,* vol. 374, pp. 1241-1252, 2019.

[114] X. Geng *et al.*, "Electrosprayed polydopamine membrane: Surface morphology, chemical stability and separation performance study," *Separation and Purification Technology,* vol. 244, p. 116857, 2020.

[115] W. R. Mateker *et al.*, "Molecular packing and arrangement govern the photo-oxidative stability of organic photovoltaic materials," *Chemistry of Materials,* vol. 27, no. 18, pp. 6345-6353, 2015.

[116] C. J. Gleason, J. M. Cox, I. M. Walton, and J. B. Benedict, "Polymorphism and the influence of crystal structure on the luminescence of the opto-electronic material 4, 4′-bis (9-carbazolyl) biphenyl," *CrystEngComm,* vol. 16, no. 33, pp. 7621-7625, 2014.

[117] B. S. Du *et al.*, "Os (II) Based Green to Red Phosphors: A Great Prospect for Solution-Processed, Highly Efficient Organic Light-Emitting Diodes," *Advanced Functional Materials,* vol. 22, no. 16, pp. 3491-3499, 2012.

[118] C.-Y. Lin *et al.*, "A thermally cured 9, 9-diarylfluorene-based triaryldiamine polymer displaying high hole mobility and remarkable ambient stability," *Journal of Materials Chemistry,* vol. 19, no. 22, pp. 3618-3623, 2009.

[119] S. Okamoto, K. Tanaka, Y. Izumi, H. Adachi, T. Yamaji, and T. Suzuki, "Simple measurement of quantum efficiency in organic electroluminescent devices," *Japanese journal of applied physics,* vol. 40, no. 7B, p. L783, 2001.

[120] J.-H. Lee *et al.*, "Blue organic light-emitting diodes: current status, challenges, and future outlook," *Journal of Materials Chemistry C,* vol. 7, no. 20, pp. 5874-5888, 2019.

[121] H. Yu, Y. Zhang, Y. J. Cho, and H. Aziz, "Exciton-induced degradation of carbazole-based host materials and its role in the electroluminescence spectral changes in phosphorescent organic light emitting devices with electrical aging," *ACS Applied Materials & Interfaces,* vol. 9, no. 16, pp. 14145-14152, 2017.

[122] A. K. Bansal *et al.*, "In situ formation and photo patterning of emissive quantum dots in small organic molecules," *Nanoscale,* vol. 7, no. 25, pp. 11163-11172, 2015.

[123] F. Samaeifar, H. Yu, T. Davidson-Hall, M. Sadeghianlemraski, D. S. Chung, and H. Aziz, "Host-to-Guest Energy Transfer and Its Role in the Lower Stability of Solution-Coated versus Vacuum-Deposited Phosphorescent OLEDs," *The Journal of Physical Chemistry C,* 2021.

[124] Q. Wang, Y. Luo, and H. Aziz, "Evidence of intermolecular species formation with electrical aging in anthracene-based blue organic light-emitting devices," *Journal of Applied Physics,* vol. 107, no. 8, p. 084506, 2010.

[125] D. Song, S. Zhao, Y. Luo, and H. Aziz, "Causes of efficiency roll-off in phosphorescent organic light emitting devices: Triplet-triplet annihilation versus triplet-polaron quenching," *Applied Physics Letters,* vol. 97, no. 24, p. 268, 2010.

[126] H. Yu and H. Aziz, "Direct Observation of Exciton-Induced Molecular Aggregation in Organic Small-Molecule Electroluminescent Materials," *The Journal of Physical Chemistry C,* vol. 123, no. 26, pp. 16424-16429, 2019.

[127] W. Li *et al.*, "Improving the performance of solution-processed small molecule OLEDs via micro-aggregation formed by an alcohol additive incorporation," *Organic Electronics,* vol. 64, pp. 252-258, 2019.

[128] Y. Kajiyama, K. Kajiyama, and H. Aziz, "Maskless RGB color patterning of vacuum-deposited small molecule OLED displays by diffusion of luminescent dopant molecules," *Optics express,* vol. 23, no. 13, pp. 16650-16661, 2015.

[129] T. Tong *et al.*, "Adhesion in organic electronic structures," *Journal of Applied Physics,* vol. 106, no. 8, p. 083708, 2009.

[130] F. Samaeifar and H. Aziz, "Role of Guest Materials in the Lower Stability of Solution-Coated versus Vacuum-Deposited Phosphorescent OLEDs," *ACS Applied Materials & Interfaces,* vol. 14, no. 6, pp. 8199-8208, 2022.